Solar Physics
DOI: 10.1007/•••••-•••-•••-••••-•

Fine Structure of Metric Type-IV Radio Bursts Observed with the ARTEMIS-IV Radio–Spectrograph: Association with Flares and Coronal Mass Ejections

C. Bouratzis[1], A. Hillaris[1], C. E. Alissandrakis[2], P. Preka-Papadema[1], X. Moussas[1], C. Caroubalos[2], P. Tsitsipis[3], A. Kontogeorgos[3]

© Springer ••••

Abstract Fine structures embedded in type-IV burst continua may be used as diagnostics of the magnetic field restructuring and the corresponding energy release associated with the low corona development of flare/CME events. A catalog of 36 type-IV bursts observed with the SAO receiver of the ARTEMIS-IV solar radio-spectrograph in the 450–270 MHz range at high cadence (0.01 sec) was compiled; the fine structures were classified into five basic classes with two or more sub-classes each. The time of fine structure emission was compared with the injection of energetic electrons as evidenced by HXR and microwave emission, the SXR light-curves and the CME onset time. Our results indicate a very good temporal association between energy release episodes and pulsations, spikes, narrow-band bursts of the type-III family and zebra bursts. Of the remaining categories, the featureless broadband continuum starts near the time of the first energy release, between the CME onset and the SXR peak, but extends for several tens of minutes after that, covering almost the full extent of the flare–CME event. The intermediate drift bursts, fibers in their majority, mostly follow the first energy release but have a wider distribution, compared to other fine structures.

Keywords: Radio Bursts, Dynamic Spectrum, Meter-Wavelengths and Longer, Association with Flares, Coronal Mass Ejections

arXiv:1406.1202v1 [astro-ph.SR] 4 Jun 2014

1. Introduction

Solar metric radio bursts provide a unique diagnostic of the development of flare/CME events in the low corona; their onset and evolution coincides with

[1] University of Athens,GR-15784 Athens, Greece
[2] University of Ioannina, GR-45110 Ioannina, Greece
[3] Technological Educational Institute of Lamia, 35100 Lamia

an extended opening of the magnetic field, accompanied by energetic-particle acceleration and injection into interplanetary space as well as shocks (e.g. review by Pick and Vilmer, 2008). Their signatures at metric–decimetric and longer waves trace disturbances propagating from the low corona to interplanetary space.

The complexity of the above mentioned processes is reflected in a diversity of forms in dynamic spectra, which exhibit a variety of fine structures in time and frequency; these are characterized by a wide range in period, bandwidth, amplitude, temporal and spatial signatures. The fine structures may be used for the detailed study of the magnetic field restructuring and the corresponding energy release associated with solar flare/CME events (e.g. reviews by Benz, 2003; Nindos and Aurass, 2007). A number of morphological taxonomy schemes, mostly in the microwaves and the decimetric frequency range, have been presented (Bernold, 1980; Slottje, 1981; Guedel and Benz, 1988; Allaart *et al.*, 1990; Isliker and Benz, 1994; Jiřička *et al.*, 2001; Fu *et al.*, 2004) of which the most recent are also the most comprehensive.

In this work we examine fine structures observed during type-IV solar radio events observed with the ARTEMIS-IV solar radio-spectrograph from the beginning of 1999 until the end of 2005; to these we added two well observed events with rich fine structure recorded in 2010. Some of these events were first catalogued in Caroubalos *et al.* (2004). Our study is concentrated on a statistical analysis of the fine structures and their association with the various phases of the flare/CME phenomenon, which could be useful in understanding details of the evolution of the solar energetic phenomena through their radio signatures. In developing our classification scheme we have built upon the Ondrejov catalogue (Jiřička *et al.*, 2001; Jiřička, Karlický, and Mészárosová, 2002; Mészárosová, Karlický, and Jiřička, 2005) which was based on data in the 0.8–2.0 GHz range.

In Section 2 we discuss the instrumentation and the data selection. The results of our morphological analysis and classification are given in Section 3, the relative timing of fine structures with respect to the flare evolution is discussed in Section 4 and the conclusions are presented in Section 5.

2. Observations and Data Selection

The basic data used in this study are the high and medium resolution dynamic spectra recorded by the ARTEMIS[1]–IV solar radio-spectrograph at Thermopylae (Caroubalos *et al.*, 2001, 2006; Kontogeorgos *et al.*, 2006). It consists of a 7 m parabolic antenna covering the metric range; to this a dipole aerial adapted to the decametric range was added in October 2002. Two receivers operate in parallel, a sweep frequency analyzer (ASG) covering the 650-20 MHz range in 630 channels with a cadence of 10 samples/sec and a high sensitivity multi-channel acousto-optical analyzer (SAO), which covers the 270-450 MHz range in 128 channels with a high time resolution of 100 samples/sec. The narrow band,

[1]Appareil de Routine pour le Traitement et l'Enregistrement Magnetique de l' Information Spectral

high time resolution SAO recordings are used in the analysis of the fine temporal and spectral structures and they constitute the major data set of this work. The broad band, medium time resolution data of the ASG, on the other hand, are used for the detection and analysis of radio emission from the base of the corona to $\sim 2\ R_{\odot}$.

For the study of the association of the fine structures with the flare evolution, we used:

- CME data from the LASCO coronograph (Brueckner *et al.*, 1995) on line[2] event list (Yashiro *et al.*, 2004; Gopalswamy *et al.*, 2009); the CME onset times used in this study were estimated from the LASCO movies using the linear regression by Yashiro *et al.* (2001) and are included in the on–line LASCO event list. We have supplemented this data set with information from the CACTUS[3] CME Catalogue (Robbrecht and Berghmans, 2004; Robbrecht, Berghmans, and der Linden, 2009)
- The NOAA *Solar Geophysical Data* catalogues and Soft X–Ray (SXR) on line[4] light curves from GOES. The SXR observations provide a fairly accurate estimate of the start of solar flares and a less accurate one of their end time; the corresponding source locations are also included in the NOAA catalogue and are used in this work, in addition to the EIT images, for the establishment of the spatial association of the SXR flare–CME–radio emission (see below)
- Hard X–ray (HXR) light curves were obtained from the RHESSI (Lin and The Hessi Team, 2001; Lin *et al.*, 2002) archive for the events after the beginning of 2003. For the events prior to 2003 we have used data from the MTI/HXRS (Fárník, Garcia, and Karlický, 2001) and BATSE/GRP (Fishman *et al.*, 1982, 1984) experiments.
- Microwave data from the *Radio Solar Telescope Network* (RSTN, Guidice *et al.*, 1981) at 4.995 GHz; in a few events the 2.695 GHz channel of the *Trieste Solar Radio System* (TSRS Messerotti, Zlobec, and Padovan, 2001) was used instead.
- Two-dimensional images of the Sun at five frequencies (164, 236.6, 327, 410.5, and 432 MHz) from the *Nançay Radio Heliograph* (NRH) (Kerdraon and Delouis, 1997). All five frequencies are within the spectral range of the ASG, while the last three are also within the range of the SAO; they hence, supplement the dynamic spectra with positional information on the radio emission. A detailed investigation of the positions of fine structures with respect to the bulk of the type-IV emission has not been attempted in this work, but will be the subject of subsequent publications.
- Images from the *Extreme Ultraviolet Imaging Telescope* (EIT) on-board SOHO (Delaboudinière *et al.*, 1995); they were used in order to provide information on the position of the associated flare.

[2]http://cdaw.gsfc.nasa.gov/CMElist

[3]http://sidc.oma.be/cactus/

[4]http//www.sel.noaa.gov/ftpmenu/indices

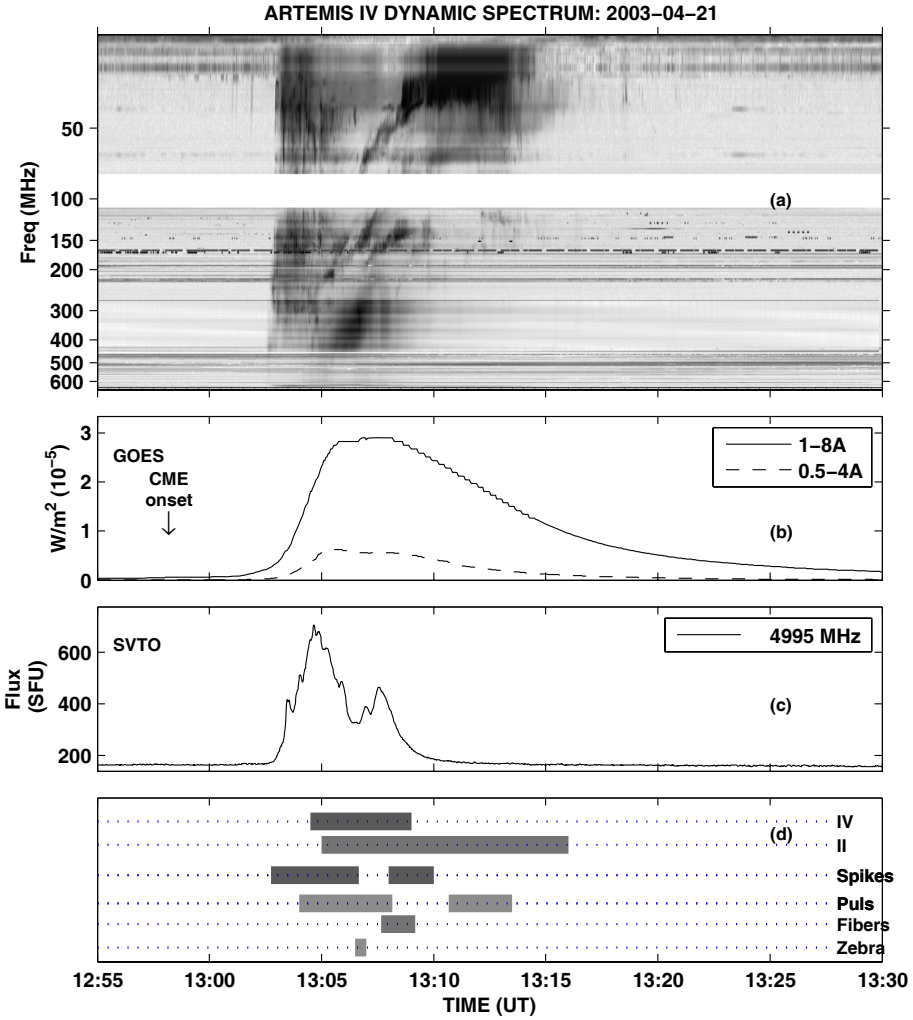

Figure 1. Example of Type-IV and fine structure–Flare–CME temporal relationship from combined data for the 21 April 2003 Event. (a): ARTEMIS-IV ASG dynamic spectrum. (b): The GOES SXR Flux; the CME onset time, from the LASCO lists is marked with arrow. (c): Microwave (4995 MHz) flux from the RSTN (SVTO). (d): Time range of the type-IV, II, spikes, fibers, pulsating and zebra structures.

The soft X-ray light curves provided the overall time evolution of the flares; the microwave and hard X-ray light curves, which are very good signatures of electron acceleration, were used to estimate the time of the first major episode of energy release. This time was used as a reference for the relative timing of fine structures. For the association of the type-IV radio events with flare emissions and CMEs we used spatial and temporal criteria as follows (see also Caroubalos *et al.*, 2004, where similar criteria were employed).:

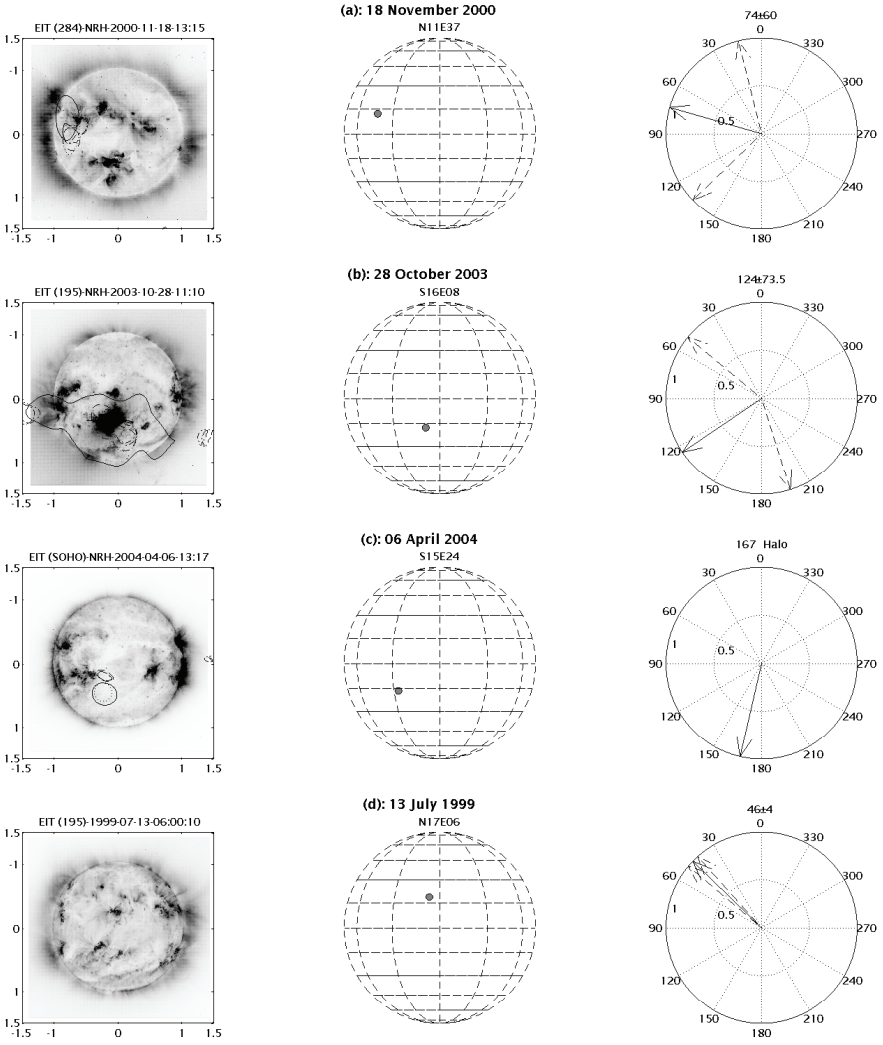

Figure 2. Examples of type-IV–flare–CME spatial association from combined data. In the left column the NRH half power contours are overlaid on EIT images. The middle and right columns show the flare position from the NOAA/SGD catalogues and the direction of the CME launch (except for halo); this is marked graphically by the CME position angle and the angular width from the LASCO lists. The events of 18 November 2000 (a) and 28 October 2003 (b) for which excellent spatial association was established among all data sets. (c): The event of 06 April 2004 accompanied by a halo CME exhibits a good association with the active region and the type-IV position (see text for details). (d): The event of 13 July 1999 at 06:00 UT, outside the NRH observation window.

- For the type-IV–flare association: for the temporal association we required the overlap, at least in part, of the total duration of the flare with the total duration of the radio emission (see Figure 1 for an example). For the spatial association we used positional data from the Nançay Radio Heliograph images and movies; we examined coincidence with flares using their position recorded in the NOAA *Solar Geophysical Data* catalogues. If both criteria were satisfied we classified the association as excellent; if we could not establish a spatial association due to lack of NRH positional data, the association was characterized good.
- Once relationship between type IV and SXR flare was established, we determined the time of the first peak of the HXR and/or the microwave bursts, which we treated as the signature of the *first impulsive energy release*. This was used as a reference for comparing the relative timing of the fine structure.
- For the CME–flare association: from the time–height diagrams in the CME lists we defined a time window of 60 minutes between the CME onset time and the peak of the accompanying SXR flare; we use the flare peak rather than the onset, since the former is more easily identifiable. To establish spatial association, we required that the flare and the CME originated in the same quadrant as schematically depicted in Figure 2. For this we compared the flare location with the CME position angle, which refers to the fastest moving segment of the CME leading edge, and the angular width; the latter was only used for non-halo CMEs.

For twelve events the spatial criterion failed to lead to the acceptance or rejection of association, due to either the lack of positional data for the radio burst or the flare or to the appearance of more than one accompanying flares as candidates for association. These events were not eliminated from the data set, but were only used in deriving the basic statistics of the fine structure parameters.

The basic characteristics of the type-IV continuum, the fine structure, the accompanying type-II and type-III bursts and the associated flare and CME of the 36 selected events are presented in Table A1. Their dynamic spectra, light curves and the relative timing of fine structures are given in Appendix B, while four examples of the CME–flare–type-IV event spatial association, of varying quality, are presented in figure 2.

3. Morphology and Classification

The 36 type-IV bursts selected as described in Section 2 were further examined for the existence of fine structures, which were classified on the basis of their morphology in the SAO dynamic spectra.

As the various types of fine structure overlapped, the use of a number of high and low pass filters on dynamic spectra became necessary. The suppression of the continuum background by high pass filtering in time resulted in enhancement of fast time-varying spectral structures such as pulsations, fibers, etc. The

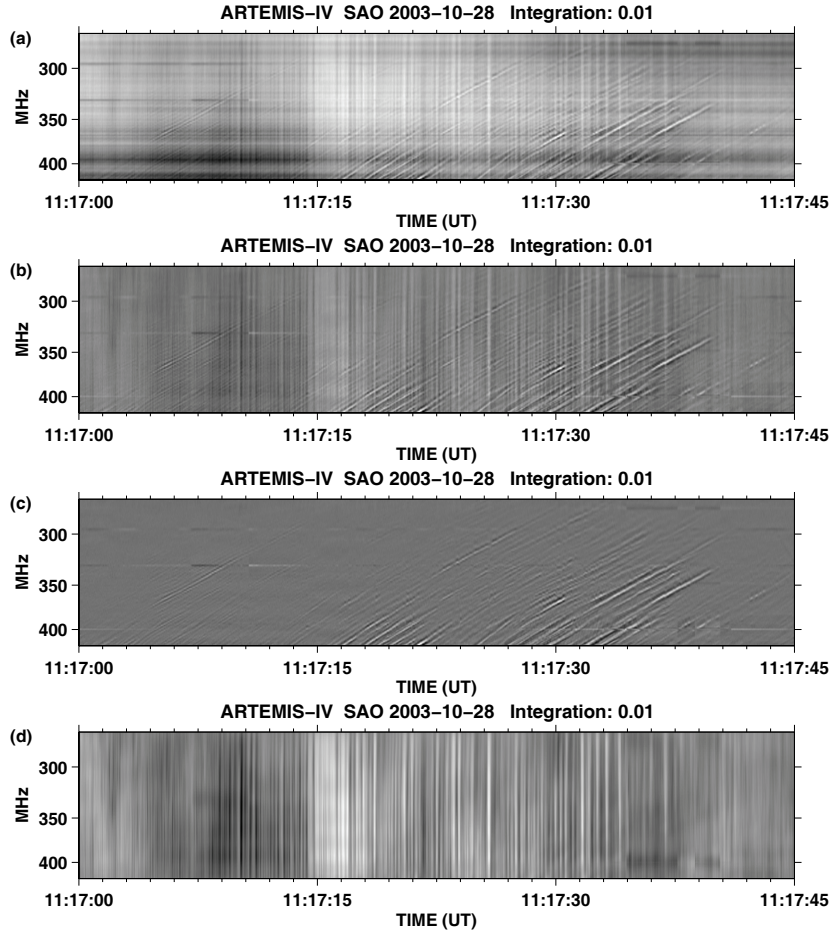

Figure 3. Example of high resolution type IV recording of the ARTEMIS-IV/SAO with fine structure enhancement by means of filtering. (a): The original dynamic spectrum of the type-IV continuum. (b): High pass filtering along the time axis reveals underlying pulsations and fibers. These are disentangled by means of high pass filtering along the frequency axis which removes pulsations (c) and low pass filtering along the frequency axis which suppresses fibers (d).

disentanglement of pulsations from other types of structures with medium to low frequency variation, such as fibers, was obtained by low–pass filtering of the dynamic spectra along the frequency axis; the opposite was obtained with the complementary high-pass filtering providing pulsation suppression and facilitating the detection of fibers and similar structures (see figure 3). Occasionally the fine structure onset appears to precede the start of the type-IV continuum on the synoptic chronological evolution diagrams (*e.g.* Figure 1); this effect results from the above-mentioned processing of the dynamic spectra which permits detection of fine-structure even if the continuum is not detectable, being too close to the background.

In all events the radio continuum was found to exhibit a combination of three or more types of fine structures embedded within longer or shorter periods of smooth continuum. The classification of fine structures was based on phenomenological characteristics, grouping these bursts by the similarity of their form in the dynamic spectra. The criteria jointly employed were: bandwidth, duration, drift rate, substructures, impulsive behavior, etc. (see the review by Benz, 2003). This work focuses mainly on basic classes of fine structures that have been identified and documented from observations by a number of radio-spectrographs during a rather extended period of time; further division into sub-classes has been known to depend on receiver sensitivity as well as on the time and frequency resolution (see Elgaroy, 1986, for example). Examples of the effect of improved resolution are zebras and fibers which, at high cadence observations, turn out to be patterns of dot-bursts (Mészárosová *et al.*, 2008) or spikes (Chernov, Yan, and Fu, 2003) in zebra-like or fiber-like chains. Most of the basic classes examined, include more than one sub-classes corresponding to the Ondrejov classification (Jiřička *et al.*, 2001) and the earlier catalog by Isliker and Benz (1994). This approach introduces a two level hierarchy of basic classes and sub-classes.

We identified the following basic classes of fine structures embedded in the type-IV continua:

3.1. Featureless Broadband Continuum

This class of structures, known also under the *diffuse continuum* label, comprises both featureless segments of type-IV bursts as well as structures of smaller frequency bandwidth and duration such as *slowly drifting bursts* and *patches*. Our data indicate long periods of broadband continuum overlapping in time with the SXR emission, with embedded intermittent periods of pulsation, fiber bursts, spike groups and zebra bands. Intensity variations within the smooth periods of the type-IV bursts, which could qualify as patches were also recorded. On the average, the smooth periods of absence of fine structure varied between 0% to 60% of the type-IV continuum duration; the relatively longest smooth periods were found to increase with the duration of the type-IV burst. We note that, although featureless periods have been recorded in the past, our high cadense data indicate that fine structure may still be revealed at adequately high resolution and sensitivity.

3.2. Pulsating Structures

This class includes drifting and stationary pulsating structures (see review by Nindos and Aurass, 2007); the shortest groups of pulsating structures with duration of the order of 10 seconds appear as Isolated Broadband Pulses in Jiřička *et al.* (2001); Jiřička, Karlický, and Mészárosová (2002); Mészárosová, Karlický, and Jiřička (2005). The pulsations are considered as the radio-signature of kinetic plasma instabilities, induced by energetic electron populations from quasi-periodic acceleration episodes in reconnecting current sheets (Aurass, 2007).

In our sample 59 periods of pulsations were detected in 33 events; an auto-correlation analysis of their intensity–time profiles indicated periodicities in the 0.6–3 sec range and individual pulse widths in the 0.35–1.3 sec range. Their bandwidth exceeds that of the SAO receiver (180 MHz).

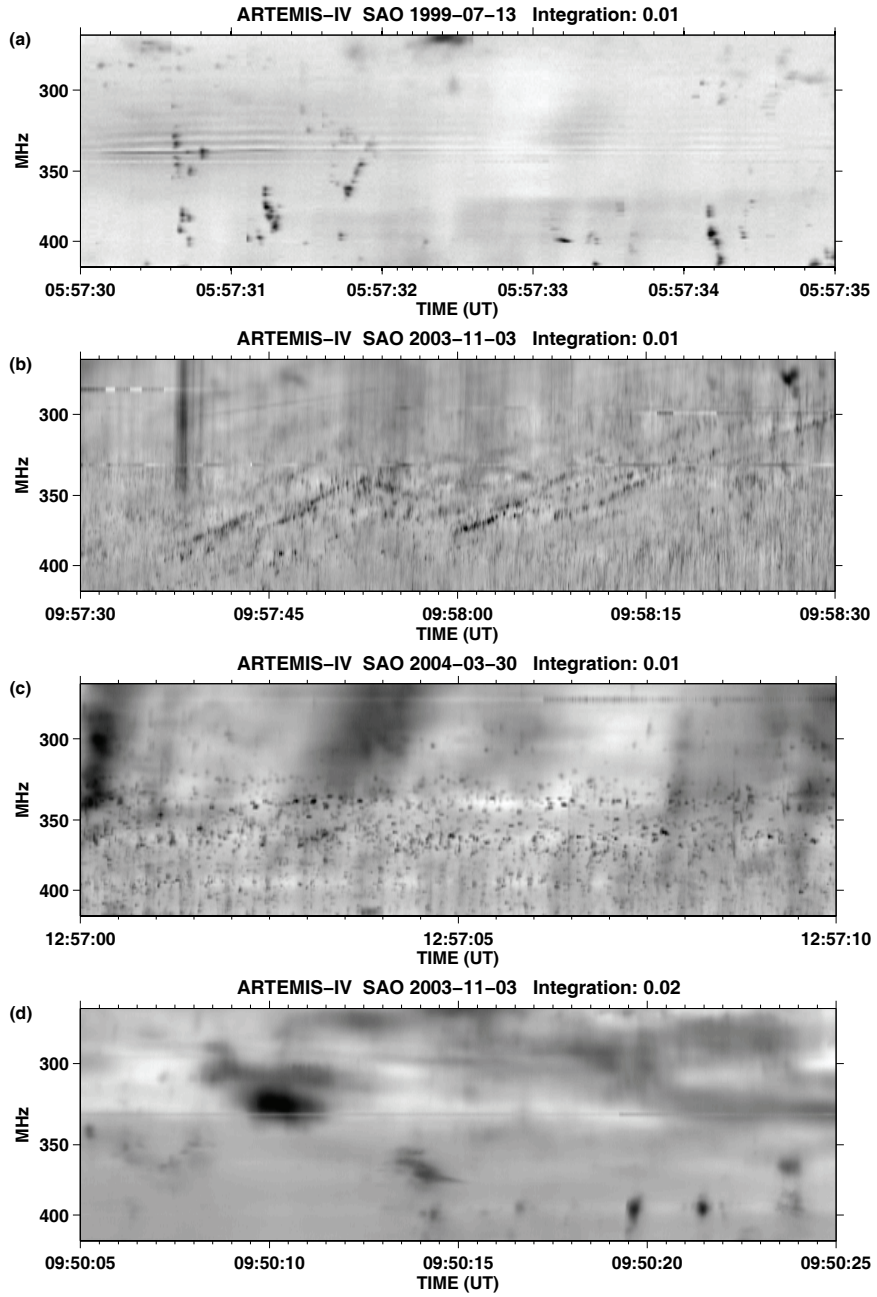

Figure 4. Examples of Narrow Band Bursts observed by ARTEMIS-IV. (a): Spike clusters on 13 July 1999 at 0.01 sec resolution. (b): Spike drifting Chains on November, 03 2003. (c): Subsecond Narrow Band Bursts. (d): Example of patch on 03 November 2003.

3.3. Narrow Band Bursts

These are reported as narrow-band bursts of the type-III family, spikes, dots and sub–second patches, depending on their shape on the dynamic spectra, (part of the same family are the III(U) and III(J) narrow-band bursts reported by Fu *et al.*, 2004; Bouratzis *et al.*, 2010). They have been interpreted as signatures of small scale acceleration episodes (Nindos and Aurass, 2007). In this basic class we might also include the *sawtooth oscillations* by (Klassen, Aurass, and Mann, 2001) although associated with type-II shocks. Figure 4 shows some examples from our data set.

In the ARTEMIS-IV/SAO data set the average duration of individual spikes was found to be $\approx$ 70 ms; the relative bandwidth on the dynamic spectra was $df/f \approx 2\%$. In a subset of the recorded spikes a positive or negative frequency drift rate was measurable; typical values were found to be $df/fdt \approx \pm(0.3 - 0.6)\, sec^{-1}$ comparable to the type-III frequency drift rate (see Table 1 of Benz, Csillaghy, and Aschwanden, 1996, where $df/fdt = 0.31\,\mathrm{sec}^{-1}$ at 328 MHz). More often than not, the bursts of this class were grouped in clusters of individual spikes close in time and/or frequency. A particular class of cluster are the spike-chains which exhibit overall frequency drift; the majority of these exhibits negative drift $df/fdt \approx$–0.021 while few drift towards higher frequencies at a rate $df/fdt \approx$-0.033 sec^{-1}. The average chain duration in our data set was within the 2–20 sec range.

3.4. Intermediate Drift Bursts

These include the typical fibers and the narrow-band *Rope-like fibers* (Mann *et al.*, 1989; Chernov, 1990, 2006, 2008); there are also variants of these subclasses such as the *broadband fibers* (Chernov *et al.*, 2007) which were observed in the wake of type-II bursts. The fiber bursts are thought to be the result of whistler–Langmuir or Alfven–Langmuir wave interaction in, mainly, postflare loops; a more recent interpretation (Karlický, Mészárosová, and Jelínek, 2013) resorts to fast magnetoacoustic wave trains. Due to their origin they qualify as, model dependent, magnetic field diagnostics (see Kuijpers, 1975; Aurass *et al.*, 2005; Rausche *et al.*, 2007).

On the average, the fiber bursts recorded by the ARTEMIS-IV/SAO (see examples in Figure 5) exhibit normalized drift rates $df/fdt \approx 0.03\,\mathrm{sec}^{-1}$. Some outliers, however, of the drift rate distribution reached $\approx 0.4\,\mathrm{sec}^{-1}$ which implies exciter speeds comparable to the type-III bursts; these were dubbed Fast Drift Bursts by Jiřička *et al.* (2001); Jiřička, Karlický, and Mészárosová (2002); Mészárosová, Karlický, and Jiřička (2005). In this work, these outliers were provisionally retained in the Intermediate Drift Bursts category.

In our data set nineteen events had multiple groups of fibers and in two events rope-like fibers were recorded; the fiber rate period was in the range 0.46–2.3 sec. The individual fibers had a duration of ≈ 0.4 sec and instantaneous bandwidth of ≈ 3.5 MHz (consistent with observations of Benz and Mann, 1998, in the 1–3 GHz range); the group extent in frequency was, on the average, ≈ 40 MHz which corresponds to $df/f \approx 0.11$. The majority of the fibers had negative drift rates $df/fdt \approx -0.023\,\mathrm{sec}^{-1}$, while those with positive drift reached

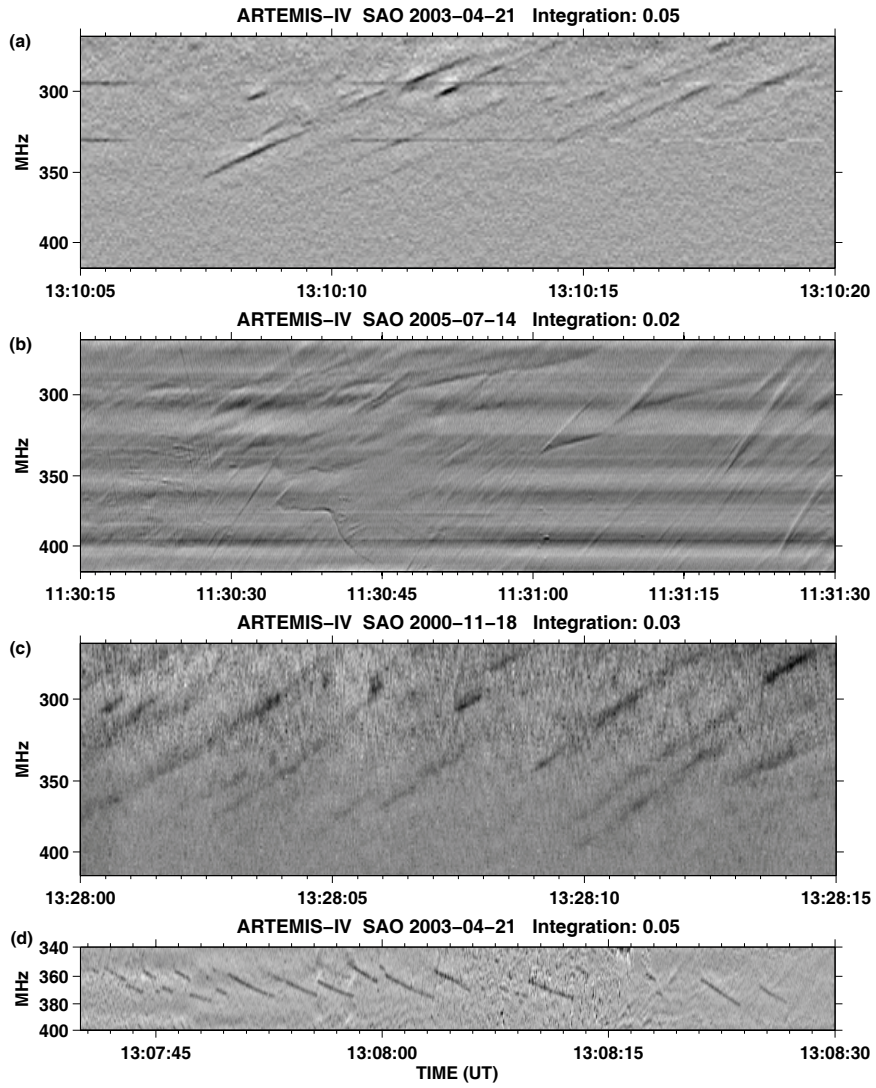

Figure 5. Example of Intermediate Drift Bursts. (a): Fiber bursts. (b): A complex group of fibers observed by ARTEMIS-IV on 14 July 2005. (c): Fast drift structures with drift rate approximately double that of the typical fiber. (d): Ropes.

rates $df/fdt \approx 0.034\,\mathrm{sec}^{-1}$; the latter always coexisted with fibers of negative drift rate. A comparison of these results with the spike-chain characteristics in subSection 3.3 indicates that the fiber frequency drift rates and instantaneous band-widths are, on the average, equal to the spike-chain frequency drift rate and the individual spike bandwidth.

Finally, groups of fibers with different drift rates were found overlapping on dynamic spectra (see Figure 5 for an example); it is not clear whether these

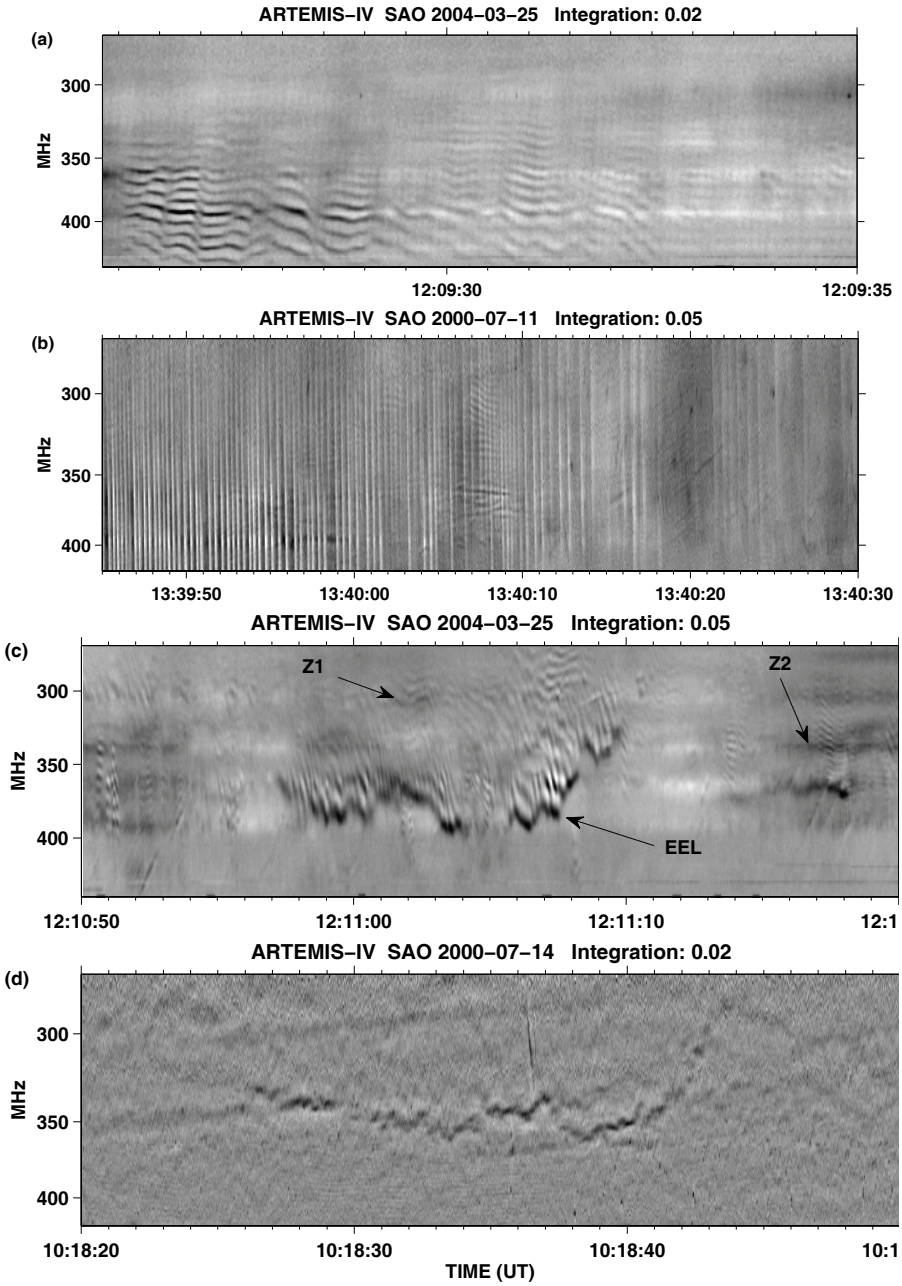

Figure 6. ARTEMIS-IV high–resolution dynamic spectra of Emission bands: (a): Zebra structure. (b): Zebra superposed on pulsations. (c): Recording of Zebra structures with possible Evolving Emission Line (EEL on the figure) at the high frequency limit of the Event; Z1 and Z2 mark typical and fiber-associated zebra patterns. (d): Lace Burst on 14 July 2000.

might constitute a separate sub-class or if they originate from different regions; further analysis employing NRH images may clarify this question.

3.5. Emission Bands

These comprise the various sub-types of the zebra family (classic or pulsation–superposed zebra patterns, fiber-associated zebras (Chernov, 2005, 2006), zebras with drifting emission envelope (Zlotnik *et al.*, 2009)), the rare lace-bursts (first reported by Karlický *et al.*, 2001, see bottom panel of Figure 6 for an example recorded by ARTEMIS-IV), the equally rare single emission band, dubbed *Evolving Emission Line (EEL)*, first reported by Chernov *et al.* (1998) in the decimetric frequency range and Fu *et al.* (2004); Ning *et al.* (2008) in the GHz range. In the same basic class we may include some unusual bursts consisting of short ($\approx$ 2–4 ms), parallel stripes with a relative delay as frequency decreases; they are characterized by an overall frequency drift (Oberoi, Evarts, and Rogers, 2009). The zebra-burst emission mechanism has been attributed to a number of different interpretations, some based on double plasma resonance (Zlotnik *et al.*, 2003; Aurass *et al.*, 2003), Bernstein modes or plasma wave trapped in resonators, to mention but a few (see Chernov, 2005; Nindos *et al.*, 2008); the double resonance interpretation has been also proposed for the lace-bursts (Fernandes *et al.*, 2003; Bárta and Karlický, 2005). Chen *et al.* (2011) have provided observational evidence in support of this interpretation.

Twenty two events of our data-set exhibited one or more patches of zebra structures; they appeared in almost equal numbers before and after the flare maximum. The examination of the energy release episodes indicated a good correspondence between these two; all *patches of zebra bands* were within 5 minutes of the time of the release episode, provided that the *frequency* of the latter, estimated from the type-III feet or the type-IV burst high frequency boundary, was within the SAO range. The majority were pulsation and fiber associated zebra (12) within overlapping pulsation and fiber activity and their association could not be resolved. Five zebra patches appear clearly pulsation-associated. Seven periods of lace-bursts were also recorded; they were found to coincide in time and frequency, mostly, with pulsations and spikes. Only one EEL was recorded. Examples of zebras, laces and the above-mentioned EEL are shown in Figure 6.

A summary of the properties of all fine structures is presented in Table 1.

Table 1. Summary of the Fine Structure Properties. The last column gives the median and the width of the distribution.

Category or Subcategory	Characteristics	Remarks	T_{md}, FWHM min
Featureless Broadband Continuum	Lack of fine structure.	Part of type-IV Burst.	–
Pulsating Structures	Periodicities 0.6–3 sec.	Embedded within the type-IV Burst Continuum (Moving or Stationary)	1.5 (8.0)
drifting	Drift rate $\|df/fdt\| \approx 0.003 sec^{-1}$	Part of moving type-IV Burst.	
stationary	Drift Rate negligible		
Isolated Broadband Pulses	Duration ≈10 seconds	Shortest pulsating structures.	
Narrow Band Bursts	Sub–second Narrow Band Bursts, near the time resolution limits of SAO.		6.5 (18.0)
Narrow–Band Type III	$df/f \approx 10\%$, $\|df/fdt\| \approx 0.4 sec^{-1}$	Including III(U)–III(J) narrow-band bursts.	
Spikes	Individual Spike: Bandwidth $df/f \approx 2\%$, duration ≈ 70 ms, $\|df/fdt\| \approx 0.45 sec^{-1}$	Often Clustered, Occasionally organized in fiber-like or type-III-like sequences.	
patches	Bandwidth $f/f \approx 3-4\%$, Drift Rate $\|df/fdt\| \lesssim 0.03 sec^{-1}$, duration ≈ 1–5 sec.		
Intermediate Drift Bursts	Drift Rate between type II–type III bursts.		–
Fibers	$\|df/fdt\| \approx 0.03 sec^{-1}$, Bandwidth $df/f \gtrsim 10\%$		
Ropes	Similar to fibers, bandwidth $df/f \lesssim 10\%$		
Fast Drift Bursts	Frequency drift rate up to $\|df/fdt\| \approx 0.4 sec^{-1}$	Drift rate comparable to type IIIs.	
Emission Bands			6.8 (10.0)
Zebra	Single band: $df/f \approx 2.5\%$, Duration 1–10 sec; Total Bandwidth df/f up to 35%.	Most of the emission bands.	
lace–bursts			
Evolving Emis. Line (EEL)		Only one was recorded.	

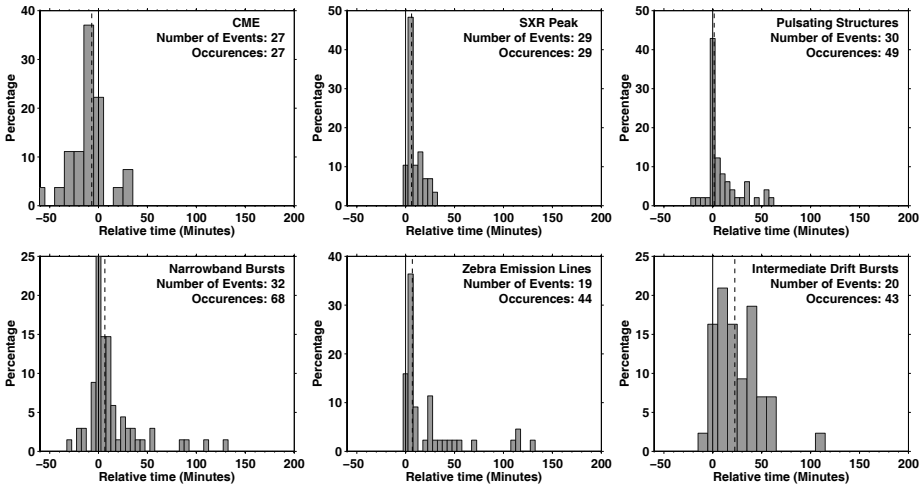

Figure 7. Histograms of the time of occurrence of the CME onset, SXR peak, pulsations, spikes (narrowband bursts), zebra patterns and fiber bursts (intermediate drift bursts) with respect to the time of the first impulsive energy release. Note that the bin size is 10 min for the CMEs and the Intermeniate Drift Bursts and 5 min for the others. Dashed vertical lines mark the median of the distributions.

4. Relative Timing of Fine Structures

As mentioned in Section 2, the time of *first impulsive energy release*, evidenced from the first HXR/microwave peak, was used as reference for timing the appearance of fine structures with respect to the evolution of the flare process. Figure 7 shows the distributions of the relative time of occurrence of various fine structures, together with those of the CME onset and SXR peaks. As each event shows multiple instances of fine structure, we used all of them for the computation of the histograms. A number of events exhibit composite structure, with clearly distinct HXR/microwave peaks or groups, within the same SXR peak and the same type-IV burst (see for example event 27, Figure B27). Some of the associated fine structures could not be identified with a particular HXR/microwave peak; these were not used for the computation of the histograms in Figure 7.

The CME onset preceeds the *first impulsive energy release*by several minutes (Figure 7) in agreement with Zhang *et al.* (2001); Webb and Howard (2012). The histogram of SXR peaks shows a sharp maximum 5 min after the first impulsive energy release, as expected. A more detailed chronological evolution is schematically depicted in figures 8, 9 and 10; in the latter we have included the times of the standard type-III bursts. We note that, in the case of the continuum, the determination of the onset is threshold dependent so the times reported in the figures as well as in Table A1 are approximate only.

Among our 36 events, small periods of broadband diffuse continuum were recorded in 8 and patches were found in 7. With very few exceptions, they started between the CME onset and the SXR peak, extending for several tens

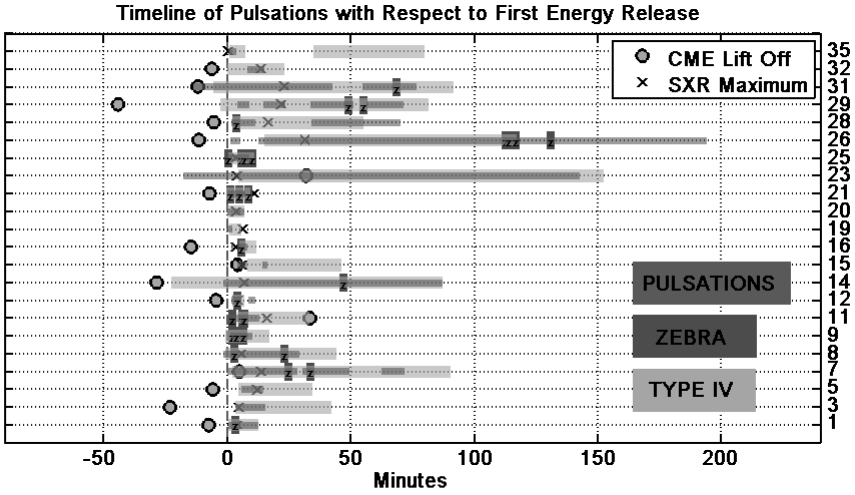

Figure 8. Relative timing of pulsations and zebra stripes associated with the Type-IV continua (gray); the **z** labels mark the short periods of zebra stripes. The circles mark the CME onset and the X symbols the SXR flux maximum. Time is in minutes from the first impulsive energy release. The event number is marked at the right (*cf.* Table A1).

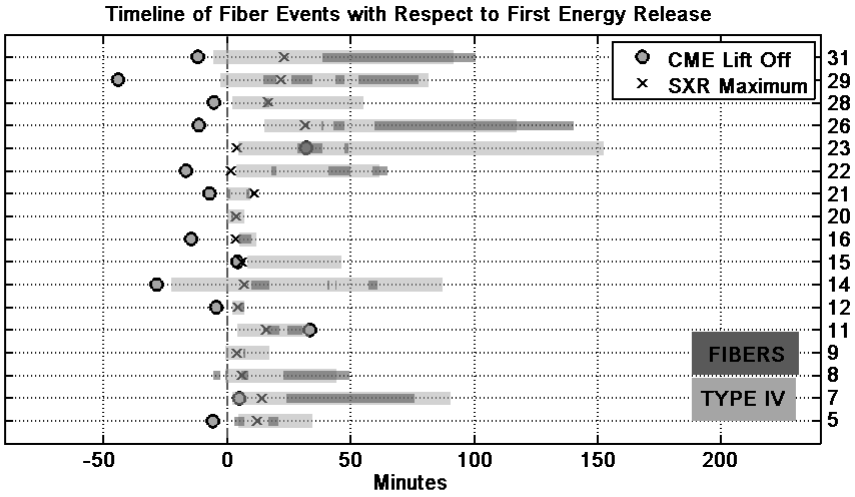

Figure 9. Same as Figure 9 for fiber bursts.

of minutes after that. This time interval of continuum emission, well past the impulsive phase, was named by Benz *et al.* (2006) *extended decimetric emission*, based on dynamic spectra obtained during the active period October–November 2003.

As shown in Figure 7, pulsations show a narrow distribution around the time of the *first impulsive energy release*, with the median of their histogram at 1.5 min

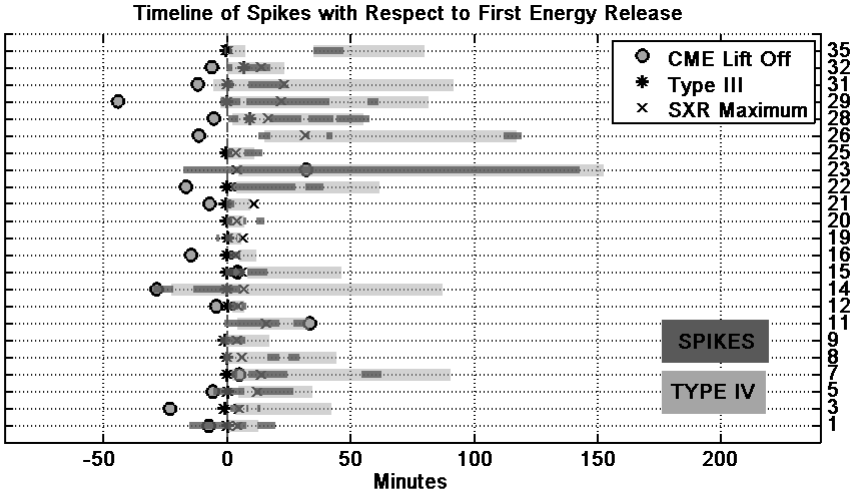

Figure 10. Same as Figure 9 for Spike groups and type-IIIs (Standard type-IIIs).

and a full width at half maximum (FWHM) of 8.0 min. Their total duration is smaller than that of the continuum, though in event 14 they extended for more than 150 min after the flare maximum (Figure 8).

Narrow band bursts also cluster around the *first impulsive energy release*; their histogram peaks at 0 min, with a median value of 6.5 min and a FWHM of 18.0 min. Although they concentrate mostly around the flare maximum, they occasionally cover longer periods within the flare decay phase, probably associated with subsequent energy releases. Furthermore, narrow band fine structures may appear before the impulsive phase of the flare (see for example Aurass, 2007).

The peak of the histogram for Zebra patterns is 5 min after the *first impulsive energy release*, with a median value of at 6.8 min and a FWHM of 10.0 min. The distribution exhibits a secondary peak around 120 min due to the contribution of the longest events which are characterized by secondary energy releases accompanied by Zebra patterns. It appears that the energy release episodes, initial and secondary, provide the energetic electrons required in triggering this type of fine structure within loops (see Zlotnik *et al.*, 2005). Characteristic examples of multiple energy release episodes are events 13 (26 October 2003) and 19 (30 March 2004 (B)) in Appendix B.

Intermediate drift bursts (fibers), which are known to appear often in postflare loops, (see Chernov, 2006), are the most dispersed of all, with their distribution showing two peaks, 10 and 40 min after the *first impulsive energy release*.

5. Discussion and Conclusions

Using the high time resolution SAO receiver, operating in the frequency range of 450–270 MHz on the ARTEMIS-IV radio-spectrograph, we observed a number of fine structure busts embedded in metric type-IV radio continua; these

were compared with the associated HXR bursts, the GOES/SXR flares and SOHO/LASCO CMEs in order to establish a relationship between this type of radio-bursts and the evolution of solar energetic phenomena. Our study started with the examination of the characteristics of each type of fine structure, such as bandwidth, duration, frequency drift rate, shape on the dynamic spectrum etc. This necessitated an appropriate taxonomy, due to the diversity of form; we introduced a two level hierarchy of basic classes and sub-classes.

At the top level, this two-level hierarchy adopted the basic classes of fine structures which have been recognized and documented from multiple observations over an long period of time. The second level division into sub-classes permits the inclusion of new and, probably, rare types of bursts alongside the well known; the ensuing subdivisions match, more or less, the Ondrejov taxonomy (Jiřička *et al.*, 2001), but include other types of fine structure as well. We note at this point, that the subdivision into types and sub-types, based solely on morphology and not the underlying radiation process, remains an artificial construct, often dependent on the resolution of observational data. Furthermore the classes thus defined, are rather broad and may, at times, include bursts morphologically similar yet originating from different radiation processes. It is, however, necessary as a background for theoretical work, as already pointed out by Elgaroy (1986) and Benz (2003), despite the fact that the classification, in particular the second level, remains more or less tentative.

The time of appearance of the type-IV fine structures with respect to the evolution of the associated CMEs and flares was subsequently examined. Our data indicate that the type-IV continua, in which the fine structures were embedded, were associated with flare eruptions exhibiting spatial scales from the active region size up to almost one solar radius, thus verifying that bursts accompanied by type-IVs are usually complex events which probably involve multiple components of smaller scale. We therefore used the time of the *first impulsive energy release*, evidenced from HXR and/or microwave time profiles, as a reference for timing the fine structures. This reference time is very near the time of the first appearance of type-III emissions, as expected.

In the vast majority of the cases studied, the onset of all classes of fine structure shows a close temporal association with the *first impulsive energy release*, which places their onset between the CME onset and the SXR peak. The closest association was found for the pulsating structures, which show a narrow distribution with a median at 1.5 min after the *first impulsive energy release*. Narrow band bursts (spikes and narrow band bursts of the type-III family) come next, with a histogram median at 6.5 min, closely followed by Zebra patterns at 6.8 min. Intermediate drift bursts (fibers) are more dispersed, with their distribution showing two peaks, 10 and 40 min after the *first impulsive energy release*.

Pulsations and zebras show the narrowest distribution with a full width at half maximum (FWHM) of 8.0 and 10.0 min respectively, followed by narrow-band bursts with FWHM=18.0 min. More dispersed are the intermediate drift bursts, with two peaks in their distribution at 10 and 40 min.

More detailed studies of the various fine structures will appear in subsequent publications.

Acknowledgements We would like to thank Gennady P. Chernov, Lidia van Driel-Gesztelyi, the anonymous first reviewer and the guest editors whose comments and suggestions have improved the quality of this work. This work was supported in part by the Special Account for Research Grants of the National and Kapodistrian University of Athens. The LASCO CME catalog is generated and maintained at the CDAW Data Center by NASA and The Catholic University of America in cooperation with the Naval Research Laboratory. SOHO is a project of international cooperation between ESA and NASA. The NRH (Nançay Radioheliograph) is operated by the Observatoire de Paris and funded by the French research agency CNRS/INSU. The Radio Solar Telescope Network (RSTN) is a network of solar observatories maintained and operated by the U.S. Air Force Weather Agency.

References

Allaart, M.A.F., van Nieuwkoop, J., Slottje, C., Sondaar, L.H.: 1990, *Solar Phys.* **130**, 183.

Aurass, H.: 2007, *Adv. Space Res.* **39**, 1407.

Aurass, H., Klein, K.L., Zlotnik, E.Y., Zaitsev, V.V.: 2003, *Astron. Astrophys.* **410**, 1001.

Aurass, H., Rausche, G., Mann, G., Hofmann, A.: 2005, *Astron. Astrophys.* **435**, 1137.

Bárta, M., Karlický, M.: 2005, *Hvar Obs. Bull.* **29**, 205.

Benz, A.O.: 2003, In: Klein, L. (ed.) *Energy Conversion and Particle Acceleration the Solar Corona, Berlin Springer Verlag, Lecture Notes Phys.* **612**, 80.

Benz, A.O., Mann, G.: 1998, *Astron. Astrophys.* **333**, 1034.

Benz, A.O., Csillaghy, A., Aschwanden, M.J.: 1996, *Astron. Astrophys.* **309**, 291.

Benz, A.O., Perret, H., Saint-Hilaire, P., Zlobec, P.: 2006, *Adv. Space Res.* **38**, 951.

Bernold, T.: 1980, *Astron. Astrophys. Suppl.* **42**, 43.

Bouratzis, C., Preka-Papadema, P., Hillaris, A., Tsitsipis, P., Kontogeorgos, A., Kurt, V., Moussas, X.: 2010, *Solar Phys.* **267**, 343.

Brueckner, G.E., Howard, R.A., Koomen, M.J., Korendyke, C.M., Michels, D.J., Moses, J.D., et al.: 1995, *Solar Phys.* **162**, 357.

Caroubalos, C., Maroulis, D., Patavalis, N., Bougeret, J.L., Dumas, G., Perche, C., et al.: 2001, *Exp. Astron.* **11**, 23.

Caroubalos, C., Hillaris, A., Bouratzis, C., Alissandrakis, C.E., Preka-Papadema, P., Polygiannakis, J., et al.: 2004, *Astron. Astrophys.* **413**, 1125.

Caroubalos, C., Alissandrakis, C.E., Hillaris, A., Preka-Papadema, P., Polygiannakis, J., Moussas, X., et al.: 2006, In: Solomos, N. (ed.) *Recent Adv. Astron. Astrophys.*, *Am. Inst. Phys. CS* **848**, 864.

Chen, B., Bastian, T.S., Gary, D.E., Jing, J.: 2011, *Astrophys. J.* **736**, 64.

Chernov, G.P.: 1990, *Solar Phys.* **130**, 75.

Chernov, G.P.: 2005, *Plasma Phys. Reports* **31**, 314.

Chernov, G.P.: 2006, *Space Sci. Rev.* **127**, 195. 10.1007/s11214-006-9141-7.

Chernov, G.P.: 2008, *Astron. Lett.* **34**, 486.

Chernov, G.P., Yan, Y.H., Fu, Q.J.: 2003, *Astron. Astrophys.* **406**, 1071.

Chernov, G.P., Markeev, A.K., Poquerusse, M., Bougeret, J.L., Klein, K.L., Mann, G., Aurass, H., Aschwanden, M.J.: 1998, *Astron. Astrophys.* **334**, 314.

Chernov, G.P., Kaiser, M.L., Bougeret, J.L., Fomichev, V.V., Gorgutsa, R.V.: 2007, *Solar Phys.* **241**, 145.

Delaboudinière, J.P., Artzner, G.E., Brunaud, J., Gabriel, A.H., Hochedez, J.F., Millier, F., et al.: 1995, *Solar Phys.* **162**, 291.

Elgaroy, O.: 1986, *Solar Phys.* **104**, 41.

Fárník, F., Garcia, H., Karlický, M.: 2001, *Solar Phys.* **201**, 357.

Fernandes, F.C.R., Krishan, V., Andrade, M.C., Cecatto, J.R., Freitas, D.C., Sawant, H.S.: 2003, *Adv. Space Res.* **32**, 2545.

Fishman, G.J., Meegan, C.A., Parnell, T.A., Wilson, R.B.: 1982, In: Lingenfelter, R.E., Hudson, H.S., Worrall, D.M. (eds.) *Gamma Ray Transients and Related Astrophys. Phenomena*, *Am. Inst. Phys. CS* **77**, 443.

Fishman, G.J., Meegan, C.A., Parnell, T.A., Wilson, R.B., Paciesas, W.: 1984, In: Woosley, S.E. (ed.) *Am. Inst. Phys. CS* **115**, 651.

Fu, Q.J., Yan, Y.H., Liu, Y.Y., Wang, M., Wang, S.J.: 2004, *Chinese J. Astron. Astrophys.* **4**, 176.

Gopalswamy, N., Yashiro, S., Michalek, G., Stenborg, G., Vourlidas, A., Freeland, S., Howard, R.: 2009, *Earth Moon and Planets* **104**, 295.

Guedel, M., Benz, A.O.: 1988, *Astron. Astrophys. Suppl.* **75**, 243.

Guidice, D.A., Cliver, E.W., Barron, W.R., Kahler, S.: 1981, In: *Bull. Amer. Astron. Soc.* **13**, 553.

Hillaris, A., Malandraki, O., Klein, K.L., Preka-Papadema, P., Moussas, X., Bouratzis, C., Mitsakou, E., Tsitsipis, P., Kontogeorgos, A.: 2011, *Solar Phys.* **273**, 493.

Isliker, H., Benz, A.O.: 1994, *Astron. Astrophys. Suppl.* **104**, 145.

Jiřička, K., Karlický, M., Mészárosová, H.: 2002, In: Sawaya-Lacoste, H. (ed.) *Solspa 2001, Proc. Second Solar Cycle and Space Weather Euroconference*, *ESA–SP* **477**, 351.

Jiřička, K., Karlický, M., Mészárosová, H., Snížek, V.: 2001, *Astron. Astrophys.* **375**, 243.

Karlický, M., Mészárosová, H., Jelínek, P.: 2013, *Astron. Astrophys.* **550**, A1.

Karlický, M., Bárta, M., Jiřička, K., Mészárosová, H., Sawant, H.S., Fernandes, F.C.R., Cecatto, J.R.: 2001, *Astron. Astrophys.* **375**, 638.

Kerdraon, A., Delouis, J.M.: 1997, In: Trottet, G. (ed.) *Coronal Phys. from Radio and Space Observations, Berlin Springer Verlag*, *Lecture Notes Phys.* **483**, 192.

Klassen, A., Aurass, H., Mann, G.: 2001, *Astron. Astrophys.* **370**, L41.

Kontogeorgos, A., Tsitsipis, P., Moussas, X., Preka-Papadema, G., Hillaris, A., Caroubalos, C., et al.: 2006, *Space Sci. Rev.* **122**, 169.

Kuijpers, J.: 1975, *Solar Phys.* **44**, 173.

Lin, R.P., The Hessi Team: 2001, In: Gladysheva, O.G., Kocharov, G.E., Kovaltsov, G.A., Usoskin, I.G. (eds.) *Internat. Cosmic Ray Conf.* **27**, 209.

Lin, R.P., Dennis, B.R., Hurford, G.J., Smith, D.M., Zehnder, A., Harvey, P.R., et al.: 2002, *Solar Phys.* **210**, 3.

Mann, G., Baumgaertel, K., Chernov, G.P., Karlicky, M.: 1989, *Solar Phys.* **120**, 383.

Messerotti, M., Zlobec, P., Padovan, S.: 2001, *Mem.S.A.It.* **72**, 633.

Mészárosová, H., Karlický, M., Jiřička, K.: 2005, *Hvar Obs. Bull.* **29**, 309.

Mészárosová, H., Karlický, M., Sawant, H.S., Fernandes, F.C.R., Cecatto, J.R., de Andrade, M.C.: 2008, *Astron. Astrophys.* **491**, 555.

Nindos, A., Aurass, H.: 2007, In: K.-L. Klein & A. L. MacKinnon (ed.) *The High Energy Solar Corona: Waves, Eruptions, Particles, Berlin Springer Verlag*, *Lecture Notes Phys.* **725**, 251.

Nindos, A., Aurass, H., Klein, K.L., Trottet, G.: 2008, *Solar Phys.* **253**, 3.

Ning, Z., Wu, H., Xu, F., Meng, X.: 2008, *Solar Phys.* **250**, 107.

Oberoi, D., Evarts, E.R., Rogers, A.E.E.: 2009, *Solar Phys.* **260**, 389.

Pick, M., Vilmer, N.: 2008, *Astron. Astrophys. Rev.* **16**, 1.

Rausche, G., Aurass, H., Mann, G., Karlický, M., Vocks, C.: 2007, *Solar Phys.* **245**, 327.

Robbrecht, E., Berghmans, D.: 2004, *Astron. Astrophys.* **425**, 1097.

Robbrecht, E., Berghmans, D., der Linden, R.A.M.V.: 2009, *The Astrophys. J.* **691**(2), 1222.

Slottje, C.: 1981, *Dissertation, Utrecht Obs.*.

Webb, D.F., Howard, T.A.: 2012, *Living Rev. Solar Phys.* **9**(3).

Yashiro, S., Gopalswamy, N., St. Cyr, O.C., Lawrence, G., Michalek, G., Young, C.A., Plunkett, S.P., Howard, R.A.: 2001, *AGU Spring Meeting Abstracts*, 31.

Yashiro, S., Gopalswamy, N., Michalek, G., St. Cyr, O.C., Plunkett, S.P., Rich, N.B., Howard, R.A.: 2004, *J. Geophys. Res.* **109**(18), 7105.

Zhang, J., Dere, K.P., Howard, R.A., Kundu, M.R., White, S.M.: 2001, *Astrophys. J.* **559**, 452.

Zlotnik, E.Y., Zaitsev, V.V., Aurass, H., Mann, G., Hofmann, A.: 2003, *Astron. Astrophys.* **410**, 1011.

Zlotnik, E., Zaitsev, V., Aurass, H., Mann, G.: 2005, *Adv. Space Res.* **35**, 1774.

Zlotnik, E., Zaitsev, V., Aurass, H., Mann, G.: 2009, *Solar Phys.* **255**, 273.

Appendix

A. Comprehensive Catalogue of the ARTEMIS-IV Recordings

In Table A1 we provide a summary of the metric type-IV bursts with fine structure recorded by the ARTEMIS-IV/SAO receiver; accompanying metric busts and explosive events are included for comparison. Column 3 gives the type of activity (for SXR flares we give the flare class, IV corresponds to type-IV continuum). Column 4 gives the extrapolated launch time of CMEs, as specified in section 3. The location of the flare on the disk and the NOAA active region number are given in column 8. In the same column we give the Measurement Position Angle (MPA) of the CMEs with their angular width in parenthesis as explained in section 2. Comments and remarks, when necessary, have been added below the appropriate entries. A collection of observational data, including dynamic spectra, is given in Appendix B.

Table A1.: ARTEMIS-IV Observations: Metric Radio Bursts and Associated LASCO CMEs and GOES SXR Flares.

#	Date	Activity	Start	Max	End	Position of
			Universal Time			AR–CME
1	30.06.1999	M1.9	11:24	11:30	11:45	S15E00–8603
		CME	11:18			03 (halo)
		SVTO 4995 MHz	11:26	11:28	11:29	
		IV	11:26		11:38	
		II	11:26		11:28	
		III	11:26			
		Spikes	11:10		11:27	
		Puls.	11:26		11:38	
		Zebra	11:29		11:29	
		Spikes	11:29		11:33	
		Spikes	11:37		11:45	
Note: In the 11:10–11:22 UT Interval there are intermittent spike bursts; these become chains and clusters after 11:22 UT by the time of the energy release episode marked by the SVTO peak.						
2	13.07.1999	C2.9	05:22	05:46	07:00	8628
		CME	05:43			46 (8)
		IV	05:57		05:59	
		II	06:02		06:05	
		SVTO 4995 MHz	05:57	05:58	06:00	
		III	05:57			
		Spikes	05:55		6:05	
		Puls.	05:57		05:59	
		Zebra	05:57		05:58	
Note: The event started before the ARTEMIS-IV Observations. Outside NRH Daily Observations.						

Table A1.: ARTEMIS-IV Observations – Continued

#	Date	Activity	Start	Max	End	Position of AR–CME
			Universal Time			
3	15.04.2000	M4.3	10:09	10:18	10:35	S22E29–8955
		CME	10:04			93 (176)
		IV	10:16		10:55	
		III	10:12			
		III	10:17			
		Spikes	10:14		10:18	
		Puls.	10:16		10:27	
		Ropes	10:17		10:17	
		Spikes	10:20		10:22	
Note: No HXR or Microwave Data.						
4	15.04.2000	C1.0	12:13	12:17	12:23	–
		C3.0	13:38	13:43	13:50	S22E29–8955
		M2.2	14:37	14:48	15:00	S23E28–8955
		CME	14:18			165 (43)
		HXRS 45 KeV	14:31	14:34	14:37	
		IV	12:13		14:44	
		III	13:41			
		III	14:40			
		III	15:10			
		HXRS 45 KeV	14:40	14:42	14:44	
		Spikes	11:50		15:10	
		Puls.	14:39		14:43	
Note: Spikes started during the previous flare at 10:14 UT and lasted till the end of the day. There are also several type-III bursts during this time interval. Propably a type-IV burst was still present from the previous flare (event 03), but it is too faint on dynamic spectrum. NRH Data GAP.						
5	30.04.2000	C7.7	07:53	08:08	09:30	S11W18–8976
		CME	08:10			186 (104)
		IV	08:00		08:30	
		SVTO 4995 MHz	07:54	08:01	08:09	
		II	07:55		08:02	
		III	07:56			
		Spikes	07:50		08:01	
		Fiber	07:58		08:02	
		Puls.	08:01		08:10	
		Spikes	08:08		08:22	
		Fiber	08:12		08:16	
		Ropes	08:20		08:20	
Note: Weak flux enhancement at 4995 MHz, peak uncertain. The type-IV burst in two parts; a drifting type-IV 07:59-08:07 UT from 500–200 MHz and a stationary continuum in the 600–250 MHz range; NRH Data GAP.						

Table A1.: ARTEMIS-IV Observations – Continued

#	Date	Activity	Start	Max	End	Position of AR–CME
			Universal Time			
6	11.07.2000	X1.0	12:12	13:10	14:30	N18E42–9077
		CME	12:33			62 (halo)
		IV	12:36		15:20	
		HXRS 45 KeV		12:58		
		Spikes	12:38		13:16	
		Puls.	12:47		12:48	
		Fiber	12:55		12:56	
		Puls.	12:56		13:29	
		Fiber	13:03		13:04	
		Fiber	13:19		13:26	
		Spikes	13:22		13:29	
		Zebra	13:29		13:29	
		Fiber	13:31		13:40	
		Puls.	13:32		13:40	
		Zebra	13:35		13:35	
		Puls.	13:43		13:53	
		Fiber	13:48		13:54	
Note: Double peak in HXR						
7	14.07.2000	X5.7	10:03	10:24	11:30	N22W07–9077
		CME	10:15			273 (halo)
		IV	10:12		11:41	
		II	10:11		10:37	
		III	10:10			
		HXRS 45 KeV	10:08		10:15	
		TSRS 2695 MHz	10:10	10:29	10:45	
		III	10:28			
		Puls.	10:10		10:38	
		Spikes	10:11		10:14	
		Spikes	10:18		10:34	
		Lace	10:18		10:19	
		Fiber	10:33		11:25	
		Zebra	10:35		10:35	
		Puls.	10:40		10:59	
		Zebra	10:43		10:44	
		Spikes	11:04		11:12	
		Puls.	11:12		11:21	
Note: The type-IV burst appears in two parts: a structureless drifting continuum starting at 10:12 and a stationary type-IV starting at 10:10, becoming quite pronounced at 10:27 continuing up to 10:41. The TSRS 2695 MHz flux exhibits a number of peaks between 10:10–10:45 UT						

Table A1.: ARTEMIS-IV Observations – Continued

#	Date	Activity	Start	Max	End	Position of AR–CME
			Universal Time			
8	14.07.2000	M1.7	12:50	12:57	13:10	S09W01–9002
		TSRS 2695 MHz	12:50	12:52	12:56	No CME
		IV	12:50		13:35	
		Fiber	12:45		12:48	
		Puls.	12:49		13:20	
		Fiber	12:50		12:51	
		Zebra	12:54		12:54	
		Fiber	12:56		12:59	
		Fiber	13:13		13:40	
		Spikes	12:49		12:51	
		Spikes	13:07		13:12	
		Zebra	13:14		13:14	
		Spikes	13:15		13:20	
9	14.07.2000	M3.7	13:44	14:00	14:30	N22W07–9077
		III	13:47			No CME
		TSRS 2695 MHz	13:46	13:50	13:51	
		Spikes	13:45		13:55	
		Puls.	13:49		13:58	
		III	13:55			
		TSRS 2695 MHz	13:53	13:54	13:56	
		IV	13:47		14:05	
		Zebra	13:50		13:50	
		Zebra	13:51		13:52	
		Zebra	13:54		13:54	
		Fiber	13:54		13:55	
Note: Double peak of TSRS 2695 MHz flux.						
10	19.09.2000	M5.1	08:06	08:26	08:42	N14 W46–9165
		CME	08:08			283 (76)
		IV	08:11		08:27	
		II	08:13		08:20	
		III	08:13			
		Spikes	08:10		08:12	
		Puls.	08:11		08:12	
Note: No HXR or Microwave Data.						

Table A1.: ARTEMIS-IV Observations – Continued

#	Date	Activity	Start	Max	End	Position of
			Universal Time			AR–CME
11	18.11.2000	M1.5	13:02	13:25	15:00	N11E37–9235
		CME	13:42			74 (120)
		HXRS 45 KeV	13:09	13:11	13:12	
		IV	13:13		13:42	
		II	13:12		13:17	
		Spikes	13:07		13:30	
		Puls.	13:09		13:21	
		Zebra	13:11		13:11	
		Zebra	13:15		13:15	
		Zebra	13:16		13:16	
		Lace	13:22		13:22	
		Spikes	13:35		13:40	
12	21.04.2003	M2.8	12:54	13:07	13:30	N18E02–10338
		CME	12:58			355 (163)
		IV	13:04		13:09	
		II	13:05		13:16	
		SVTO 4995 MHz	13:03	13:04	13:10	
		III	13:03			
		Spikes	13:03		13:07	
		Puls.	13:04		13:08	
		Lace	13:05		13:05	
		Zebra	13:06		13:07	
		Fiber	13:07		13:09	
		Spikes	13:08		13:10	
		Puls.	13:11		13:13	
Note: Position Angle from CACTUS Catalogue. SVTO 4995 MHz double peak. AR Localization from MDI.						
13	26.10.2003	X1.2	05:57	06:54	09:00	S15E44–10486
		CME	06:13			108 (207)
		IV	07:06		09:10	
		II	06:16		06:30	
		SVTO 4995 MHz	06:12		08:00	
		RHESSI 50–100 KeV	06:09	06:12	06:18	
		Puls.	07:07		07:45	
		Spikes	07:11		07:12	
		Lace	07:19		07:19	
		Zebra	07:22		07:23	
		RHESSI 50–100 KeV	08:30	08:32	08:34	
		Puls.	08:35		08:40	
		RHESSI 50–100 KeV	08:40	08:41	08:42	
Note: Probably Multiple Event which began before start time of ARTEMIS-IV; SVTO 4995 MHz flux exhibits multiple peaks. NRH Data GAP.						

Table A1.: ARTEMIS-IV Observations – Continued

#	Date	Activity	Start	Max	End	Position of AR–CME
			Universal Time			
14	28.10.2003	X17.2	09:51	11:10	12:40	S16E08–10486
		CME	10:34			124 (147)
		IV	10:40		15:00	
		II	11:03		11:11	
		SVTO 4995 MHz	11:03		11:25	
		III	11:03			
		Spikes	10:33		11:41	
		Spikes	10:49		11:08	
		Puls.	11:01		12:26	
		RHESSI 50–100 KeV	11:06	11:14	11:25	
		Lace	11:07		11:09	
		Fiber	11:12		11:20	
		Fiber	11:43		11:44	
		Fiber	11:46		11:47	
		Zebra	11:50		11:50	
		Fiber	12:00		12:03	
		Spikes	14:14		14:22	
Note: SVTO 4995 MHz flux exhibits multiple peaks.						
15	03.11.2003	X3.9	09:43	09:55	11:00	N08W77–10488
		CME	09:53			293 (103)
		IV	09:57		10:35	
		II	09:51		10:10	
		III	09:49			
		III	09:51			
		RHESSI 100–300 KeV	09:48	09:49	09:55	
		SVTO 4995 MHz	09:49		10:20	
		Spikes	09:48		09:48	
		Puls.	09:48		09:49	
		Fiber	09:48		09:48	
		Puls.	09:53		09:57	
		Lace	09:57		09:57	
Note: SVTO flux exhibits multiple peaks.						

Table A1.: ARTEMIS-IV Observations – Continued

#	Date	Activity	Start	Max	End	Position of
			Universal Time			AR–CME
16	04.02.2004	C9.9	11:12	11:18	12:15	S07W49–10547
		CME	11:19			274 (33)
		IV	11:19		11:26	
		II	11:16		11:17	
		III	11:14			
		SVTO 4995 MHz	11:14	11:16	11:19	
		Puls.	11:16		11:17	
		Fiber	11:19		11:24	
		Puls.	11:19		11:23	
		Lace	11:19		11:19	
		Zebra	11:20		11:20	
		Spikes	11:15		11:20	
Note: NRH Data GAP.						
17	25.03.2004	C3.7	12:01	12:12	12:20	N01W19–10577
		IV	12:08		12:14	LASCO Data GAP.
		SVTO 4995 MHz	12:05	12:06	12:07	
		SVTO 4995 MHz	12:08	12:10	12:12	
		Zebra	12:07		12:08	
		Puls.	12:08		12:13	
		Zebra	12:09		12:09	
		Zebra	12:11		12:11	
		Zebra	12:12		12:12	
		Spikes	12:13		12:15	
Note: NRH Data GAP; No EIT Data, MDI is used for spatial localization of the active region. Double SVTO 4995 MHz peak						
18	30.03.2004	C1.7	05:37	05:41	05:46	N15E05–10582
		IV	05:43		05:49	LASCO Data GAP.
		III	05:45			
		RHESSI 12–25 KeV	05:36	05:40	05:47	
		RHESSI 12–25 KeV	06:00	06:05	06:10	
		Puls.	05:43		05:45	
		Puls.	05:47		05:49	
		Spikes	05:48		05:50	
Note: Outside NRH Daily Observations; No EIT Data, MDI is used for spatial localization of the active region. Multiple HXR peaks in two main groups indicating, probably, a double event.						

Table A1.: ARTEMIS-IV Observations – Continued

#	Date	Activity	Start	Max	End	Position of AR–CME
			Universal Time			
19	30.03.2004	C5.9	09:41	09:51	09:54	N15E06–10582
		IV	09:45		09:55	LASCO Data GAP.
		SVTO 4995 MHz	09:44	09:45	09:46	
		SVTO 4995 MHz	09:51	09:52	09:55	
		III	09:45			
		III	09:51			
		Puls.	09:44		09:47	
		Puls.	09:51		09:55	
		Spikes	09:40		09:41	
		Spikes	09:43		09:46	
		Spikes	09:48		09:49	
		Spikes	09:51		09:55	
		Zebra	09:54		09:55	
Note: No EIT Data, MDI is used for spatial localization of the active region. Multiple SVTO 4995 MHz peaks in two main groups indicating, probably, a double event from the same AR; the second part starts at ≈09:50 UT.						
20	30.03.2004	C4.7	12:54	13:00	13:06	N15E05–10582
		CME	GAP			LASCO Data GAP.
		IV	12:56		13:03	
		III	12:56		13:03	
		SVTO 4995 MHz	12:56	12:57	12:58	
		SVTO 4995 MHz	13:00	13:01	13:03	
		Puls.	12:56		13:03	
		Fiber	12:57		12:58	
		Spikes	12:55		12:58	
		Spikes	13:02		13:04	
		Spikes	13:08		13:11	
Note: Following type-III group at 12:56, there is intermittent type-III activity up to 13:03 UT. No EIT Data, MDI is used for spatial localization of the active region. Multiple SVTO 4995 MHz peaks.						
21	06.04.2004	M2.4	12:30	13:28	14:30	S18E15–10588
		CME	13:17			167 (halo)
		IV	13:16		13:26	
		III	13:16			
		SVTO 4995 MHz	13:16	13:23	13:30	
		RHESSI 50–100 KeV	13:19	13:23	13:28	
		Puls.	13:16		13:24	
		Zebra	13:22		13:22	
		Fiber	13:25		13:26	
		Zebra	13:22		13:22	
Note: Multiple SVTO 4995 MHz peaks.						

Table A1.: ARTEMIS-IV Observations – Continued

#	Date	Activity	Start	Max	End	Position of AR–CME
			Universal Time			
22	13.07.2004	M5.4	08:40	08:48	10:15	N12W52–10646
		CME	08:45			326 (halo)
		IV	08:50		09:48	
		II	08:48		08:57	
		III	08:46			
		SVTO 4995 MHz	08:44	08:47	08:51	
		RHESSI 12–25 KeV	08:39	08:44	08:46	
		Spikes	08:48		09:14	
		Fiber	09:04		09:06	
		Fiber	09:27		09:36	
		Fiber	09:45		09:51	
Note: Position Angle from CACTUS. Multiple SVTO 4995 MHz peaks in a single group.						
23	20.07.2004	M8.6	12:22	12:32	13:00	N11E34–10652
		CME	13:17			334 (halo)
		IV	07:00		15:00	
		SVTO 4995 MHz	12:25	12:29	12:36	
		II	12:33		12:40	
		Spikes	12:10		14:50	
		Puls.	12:10		14:50	
		Fiber	12:56		13:06	
		Fiber	13:15		13:16	
Note: The CME onset appears on the 195 Å movies at AR 10652 bound to North West across the disk. Due to this, non radial, propagation the onset time is somewhat uncertain.						
24	21.07.2004	C8.9	05:05	05:21	06:35	N05E24–10652
		CME	05:11			165 (66)
		IV	05:41		10:55	
		III	07:49			
		III	07:58			
		III	08:15			
		SVTO 4995 MHz	05:15	05:16	05:30	
		RHESSI 12–25 KeV	05:10	05:16	05:30	
		Puls.	05:42		09:18	
		Spikes	05:30		06:30	
		Spikes	06:44		06:56	
		Spikes	07:17		07:28	
		Spikes	07:34		07:45	
		Spikes	07:55		08:22	

Table A1.: ARTEMIS-IV Observations – Continued

#	Date	Activity	Start	Max	End	Position of AR–CME
			Universal Time			
25	14.01.2005	C4.6	12:33	12:41	13:00	S07E05–10718
		IV	12:37		12:48	No CME
		II	12:47		12:50	
		III	12:37			
		SVTO 4995 MHz	12:37	12:38	12:40	
		III	12:46			
		RHESSI 25–50 KeV	12:35	12:39	12:42	
		Puls.	12:37		12:46	
		Zebra	12:37		12:37	
		RHESSI 25–50 KeV	12:42	12:43	12:55	
		Zebra	12:43		12:43	
		Zebra	12:44		12:44	
		SVTO 4995 MHz	12:45	12:46	12:47	
		Zebra	12:47		12:48	
		Spikes	12:47		12:52	
Note: Multiple HXR peaks.						
26	15.01.2005	M8.6	05:54	06:38	8:30	N16E04–10720
		CME	06:03			359 (halo)
		IV	06:21		8:40	
		SVTO 4995 MHz	05:56	06:29	07:10	
		Puls.	06:07		06:11	
		Spikes	06:18		06:24	
		Puls.	06:18		09:20	
		Spikes	06:38		06:40	
		Fiber	06:44		06:45	
		Spikes	06:46		06:49	
		Fiber	06:49		06:53	
		Fiber	07:05		08:26	
		Spikes	07:58		08:05	
		Zebra	07:59		07:59	
		Zebra	08:00		08:00	
		Zebra	08:03		08:03	
		Zebra	08:17		08:17	
Note: Multiple SVTO 4995 MHz peaks.						

Table A1.: ARTEMIS-IV Observations – Continued

#	Date	Activity	Start	Max	End	Position of AR–CME
			Universal Time			
27	17.01.2005	X3.8	6:59	09:52	11:00	N15W25–10720
		CME	09:06			334 (halo)
		IV	08:40		10:46	
		II	09:44		9:48	
		III	09:44			
		RHESSI 100–300 KeV	09:36	09:50	10:30	
		SVTO 4995 MHz	09:02	09:29	10:30	
		Spikes	09:02		09:09	
		Puls.	09:02		10:27	
		Spikes	09:13		09:22	
		Fiber	09:15		09:54	
		Spikes	09:32		09:34	
		CME	09:43			309 (halo)
		Fiber	09:59		10:49	
		Spikes	10:12		10:38	
		Puls.	10:34		11:20	
		Fiber	11:09		12:02	
		Puls.	11:33		12:02	
		Zebra	09:20		09:20	
		Zebra	10:45		10:45	
		Spikes	10:56		11:40	
		Zebra	10:58		11:00	
		Spikes	11:51		12:01	

Note: Two CMEs in close succession with SXR flux rising in two stages (see Hillaris *et al.*, 2011).

Table A1.: ARTEMIS-IV Observations – Continued

#	Date	Activity	Start	Max	End	Position of AR–CME
			Universal Time			
28	19.01.2005	X1.3	08:03	08:22	9:00	N15W51–10720
		CME	08:08			320 (halo)
		IV	08:07		9:00	
		II	08:11		8:18	
		III	08:14			
		RHESSI 100–300 KeV	08:12	08:26	08:38	
		SVTO 4995 MHz	08:12	08:26	09:20	
		Spikes	08:05		08:10	
		Puls.	08:06		08:16	
		Zebra	08:09		08:09	
		Spikes	08:12		08:15	
		Fiber	08:20		08:22	
		Spikes	08:22		09:03	
		Puls.	08:39		09:38	
		Spikes	09:22		09:35	
		Fiber	09:53		09:54	
		III	10:24			
		Puls.	10:23		10:25	
		Spikes	10:23		10:28	

Note: Multiple SVTO 4995 MHz peaks and probably double event with second part starting at ≈ 09:15 UT.

Table A1.: ARTEMIS-IV Observations – Continued

#	Date	Activity	Start	Max	End	Position of AR–CME
			Universal Time			
29	20.01.2005	X7.1	06:36	07:01	07:45	N15W51–10720
		CME	06:08			288 (halo)
		IV	06:36		08:00	
		III	06:39			
		II	06:44		06:49	
		III	06:44			
		III	06:57			
		III	07:07			
		RHESSI 25–50 KeV	06:38	06:45	07:27	
		SVTO 4995 MHz	06:38	06:49	07:30	
		Spikes	06:36		06:44	
		II	06:56		06:58	
		Puls.	06:42		06:47	
		Spikes	06:46		07:20	
		Puls.	06:53		07:02	
		Fiber	06:53		06:59	
		Fiber	07:05		07:13	
		Puls.	07:12		07:30	
		Fiber	07:22		07:26	
		Zebra	07:28		07:28	
		Fiber	07:32		07:56	
		Zebra	07:34		07:34	
		Puls.	07:35		07:50	
		Spikes	07:35		07:40	
Note: Double SVTO 4995 MHz peak.						
30	13.07.2005	M5.0	14:01	14:49	18:15	N11W90–10786
		CME	14:12			303 (halo)
		IV	13:56		14:23	
		RHESSI 25–50 KeV	14:12			
		SVTO 4995 MHz	14:02	14:18	14:34	
		Puls.	13:52		14:12	
		Zebra	13:58		13:59	
		Fiber	14:03		14:06	
		Zebra	14:08		14:08	
		Spikes	14:09		14:11	
		Puls.	14:16		14:22	
		Zebra	14:18		14:18	
		Zebra	14:19		14:19	
		Zebra	14:21		14:21	
		Zebra	14:22		14:22	
Note: No EIT Data, MDI is used for spatial localization of the active region. Activity Extends beyond ARTEMIS-IV Observation Period.						

Table A1.: ARTEMIS-IV Observations – Continued

#	Date	Activity	Start	Max	End	Position of AR–CME
			Universal Time			
31	14.07.2005	X1.2	10:16	10:55	12:00	N11W90–10786
		CME	10:27			296 (halo)
		IV	10:26		12:03	
		III	10:32			
		III	10:38			
		RHESSI 25–50 KeV	10:25	10:27	10:29	
		SVTO 4995 MHz	10:30	10:35	11:25	
		RHESSI 25–50 KeV	11:00	11:04	11:25	
		Puls.	10:18		11:14	
		Spikes	10:32		10:34	
		Spikes	10:40		10:55	
		Fiber	11:10		12:12	
		Puls.	11:26		11:48	
Note: NRH Data GAP. Multiple SVTO 4995 MHz peaks.						
32	30.07.2005	X1.3	06:17	06:35	07:30	N12E60–10792
		CME	06:21			050 (halo)
		IV	06:21		06:44	
		II	06:26		06:32	
		III	06:28			
		SVTO 4995 MHz	06:20	06:32	06:45	
		RHESSI 100–300 KeV	06:27	06:32	06:45	
		Spikes	06:20		06:23	
		Spikes	06:26		06:39	
		Puls.	06:29		06:36	
Note: Outside NRH Daily Observations. Multiple SVTO 4995 MHz peaks						
33	22.8.2005	M2.6	00:44	01:33	09:00	S11W65–10798
		CME	05:09			222 (56)
		IV	05:43		6:30	
		RHESSI 6–12 KeV	05:50	06:01	06:30	
		Spikes	05:40		05:46	
		Puls.	05:52		05:54	
		Zebra	05:53		05:54	
		Zebra	05:59		06:03	
		Spikes	06:14		06:14	
Note: Partial Observation of the end of a type-IV Continuum starting at about 00:44 UT,as reported by the Culgoora Radio–Spectrograph. Outside NRH Daily Observations.						

Table A1.: ARTEMIS-IV Observations – Continued

#	Date	Activity	Start	Max	End	Position of AR–CME
			Universal Time			
34	23.8.2005	M2.7	14:19	14:44	16:08	S11W65–10798
		CME	14:45			230 (halo)
		IV	14:26		15:02	
		SVTO 4995 MHz	14:23	14:49	15:20	
		RHESSI 50–100 KeV	14:23	14:38	15:10	
		Spikes	14:26		15:00	
Note: Activity Extends beyond ARTEMIS-IV Observation Period. Multiple HXR and SVTO 4995 MHz peaks						
35	12.02.2010	M8.3	11:19	11:26	11:28	N26E11–11046
		CME	11:18			044 (halo)
		IV	11:26		11:32	
		IV	12:00		12:45	
		II	11:26		11:31	
		III	11:25			
		III	11:29			
		RHESSI 50–100 KeV	11:21	11:26	11:36	
		Spikes	11:24		11:25	
		Spikes	12:00		12:12	
		Puls.	11:25		11:28	
36	01.08.2010	C3.2	07:55	08:26	09:35	N20E36–11092
		CME	08:27			084 (halo)
		IV	08:06		10:00	
		RHESSI 100–300 KeV	08:00	08:33	08:48	
		Puls.	08:00		08:03	
		Spikes	08:08		08:09	
		Spikes	08:18		08:22	
		Puls.	08:16		09:26	
		Fiber	08:26		09:36	
		Spikes	09:30		09:50	
		Fiber	09:47		09:48	
		Spikes	10:12		10:20	
Note: NRH Data GAP.						

B. Details on the ARTEMIS-IV Recordings and Accompanying Data

In the following figures we present dynamic spectra and other observational data for the 36 events used in the compilation of table A1 and figures 9, 8 and 10. They are intended to show the temporal and spatial association of type IV continua and their fine structure with flares, microwave and HXR bursts and CMEs, as detailed in section 2. In each Figure we give:

- The upper panel shows medium resolution dynamic spectra recorded by the ARTEMIS-IV/ASG in the 650–20 MHz range (cadence of 10 samples/sec); in the 270-450 MHz range the ARTEMIS-IV/SAO high sensitivity–high time resolution spectrum is overlaid (sampling rate 100 samples/sec).
- Soft X–Ray (SXR) light curves, obtained from the Geostationary Operational Environmental Satellites (GOES). The CME Onset times are marked with arrows; they were estimated from the LASCO movies using the linear regression and are included in the on–line LASCO event lists.
- Hard X–Ray (HXR) light curves from the Reuven Ramaty High Energy Solar Spectroscopic Imager (RHESSI) archive for events after the beginning of 2003; prior to 2003, HXR data are from the MTI/HXRS and BATSE/GRP experiments.
- Centimetric Radio Flux; 4.995 GHz radio flux profiles from the Radio Solar Telescope Network (RSTN) or, in a few events, from the 2.695 GHz channel of the Trieste solar Radio System (TSTS).
- Timeline plot; relative timing of Pulsations, fiber bursts, zebra stripes and Spike groups associated with type-IV continuum.
- Type IV–flare–CME positions; these include, from left to the right: Nançay Radioheliograph (NRH) half power contours at 164, 236, 327 MHz, 410 and 432 MHz (when available), overlaid on Extreme Ultraviolet Imaging Telescope (EIT) images. When EIT data were not available, MDI images were used to identify the associated active region. The flare position from the NOAA/SGD catalogs is schematically shown in the middle panel, for comparison with the direction of the CME launch to the right panel. This is marked graphically in the right panel, which shows the CME measurement position angle (MPA) and, for non-halo CMEs, the angular width, both from the LASCO coronograph event lists and the CACTUS CME catalogue.

A concise list of the dates and event start and end times is given in Table B1

Table B1. List of Event Dates and Start–End Times.

#	Date	Start	End	#	Date	Start	End
		Universal Time				Universal Time	
1	30.06.1999	11:24	11:45	2	13.07.1999	05:22	07:00
3	15.04.2000	10:04	10:55	4	15.04.2000	12:13	14:43
5	30.04.2000	07:53	09:30	6	11.07.2000	12:12	15:20
7	14.07.2000	10:03	11:30	8	14.07.2000	12:50	13:40
9	14.07.2000	13:44	14:30	10	19.09.2000	08:06	08:42
11	18.11.2000	13:02	15:00	12	21.04.2003	12:54	13:30
13	26.10.2003	05:57	09:10	14	28.10.2003	09:51	15:00
15	03.11.2003	09:43	11:00	16	04.02.2004	11:12	12:15
17	25.03.2004	12:01	12:20	18	30.03.2004	05:37	06:10
19	30.03.2004	09:41	09:55	20	30.03.2004	12:54	13:11
21	06.04.2004	12:30	14:30	22	13.07.2004	08:39	10:15
23	20.07.2004	12:10	15:00	24	21.07.2004	05:05	10:55
25	14.01.2005	12:33	13:00	26	15.01.2005	05:54	08:40
27	17.01.2005	06:59	12:00	28	19.01.2005	08:03	10:28
29	20.01.2005	06:36	07:56	30	13.07.2005	14:01	18:15
31	14.07.2005	10:16	12:12	32	30.07.2005	06:17	07:30
33	22.08.2005	00:44	09:00	34	23.08.2005	14:19	16:08
35	12.02.2010	11:18	12:45	36	01.08.2010	07:55	10:20

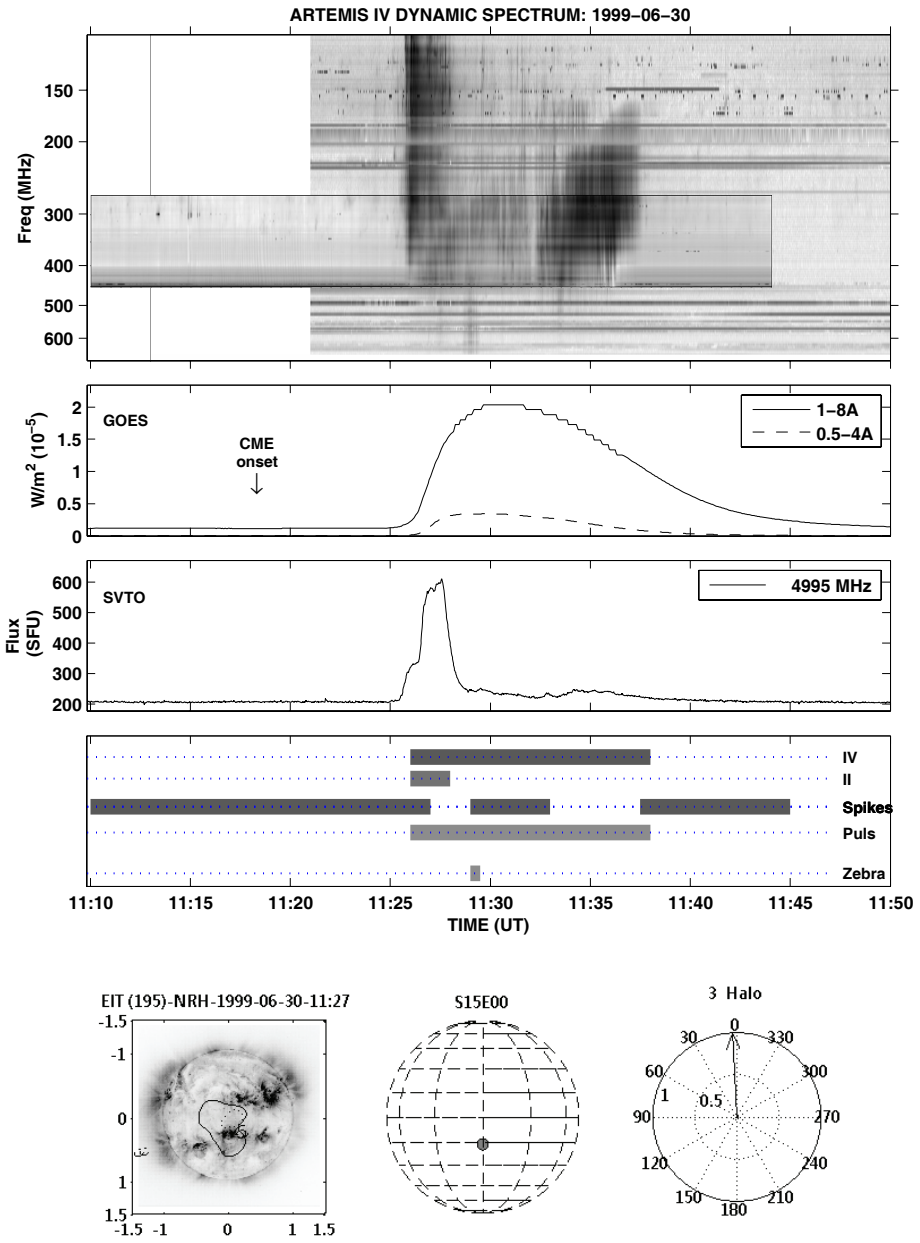

Figure B1. 30 June 1999

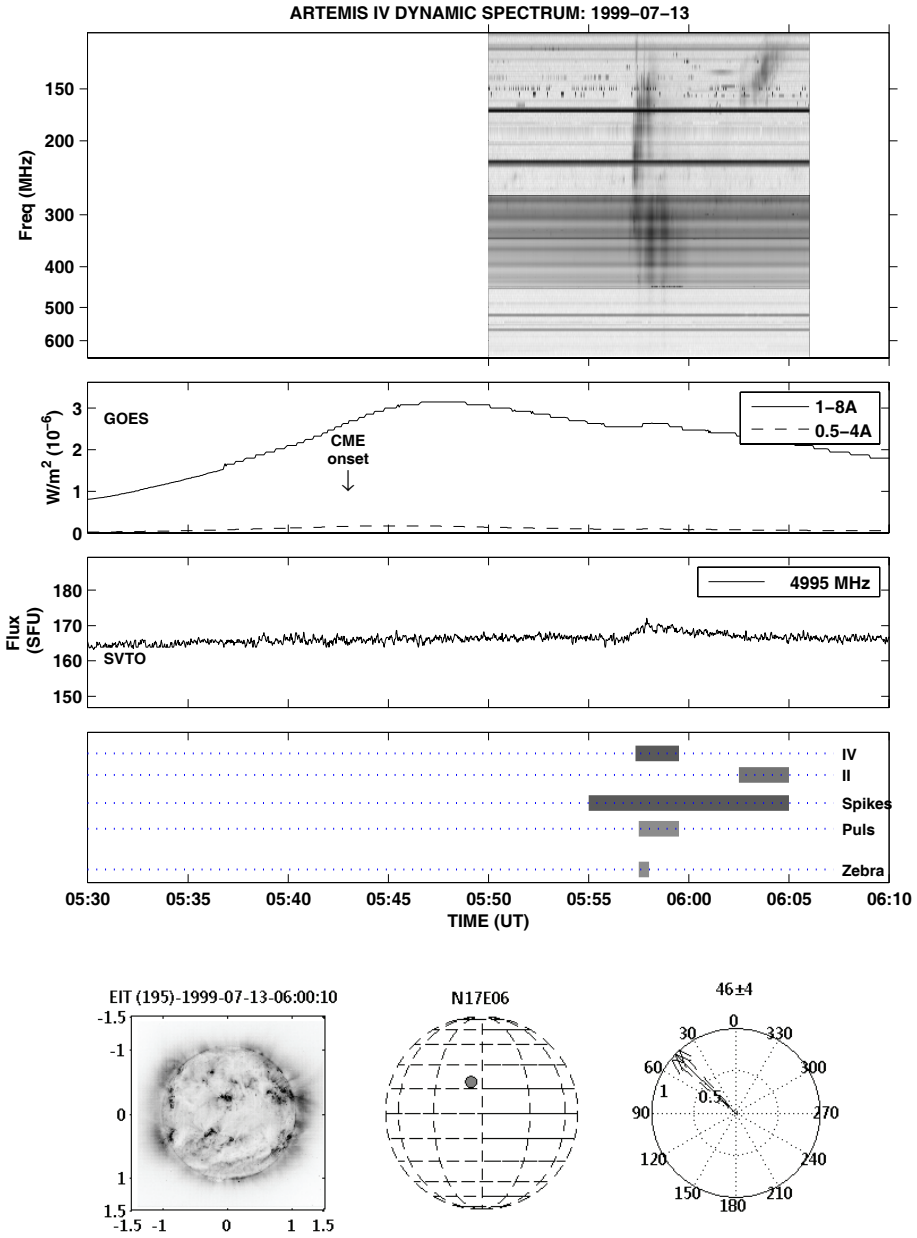

Figure B2. 13 July 1999

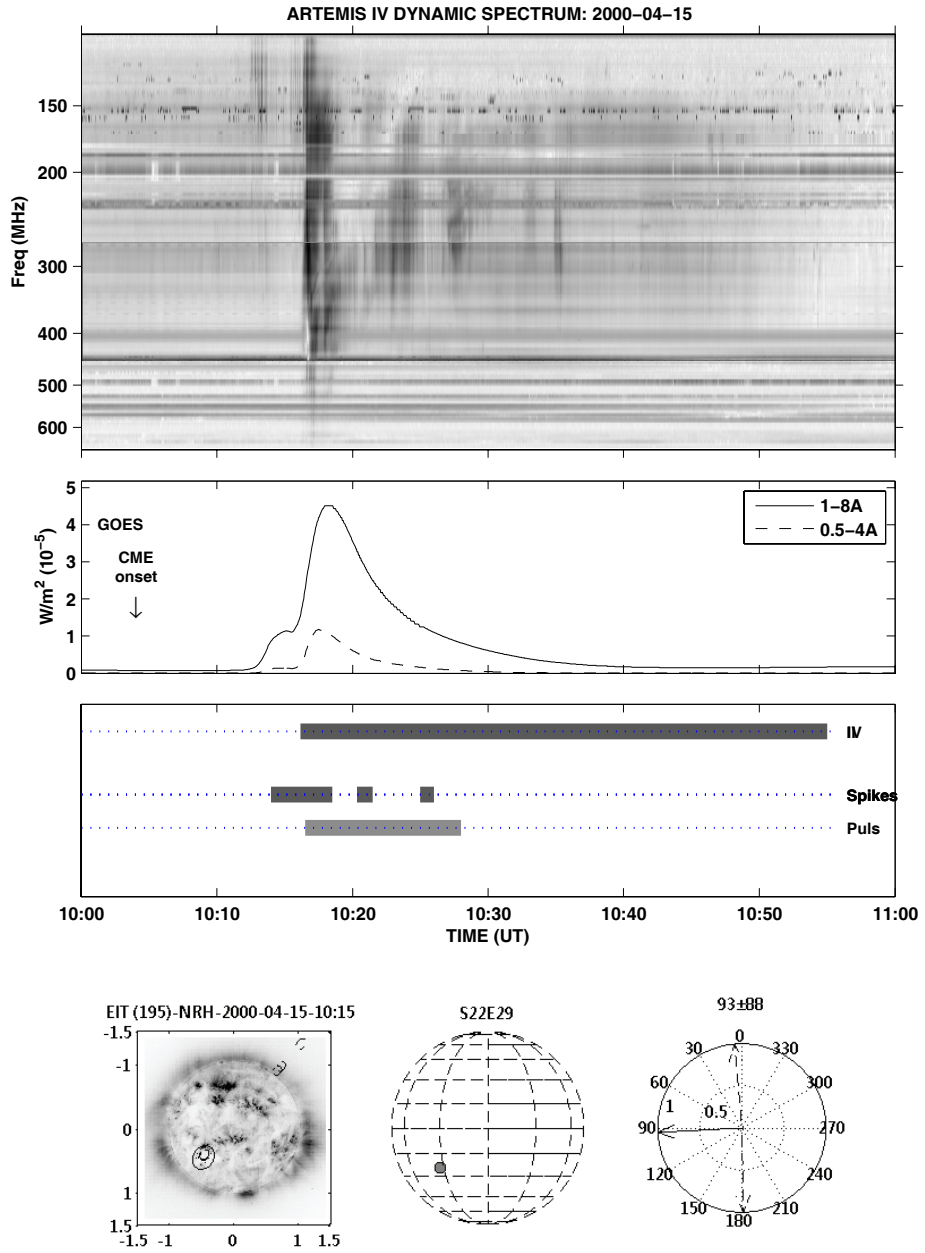

Figure B3. 15 April 2000 Event(A)

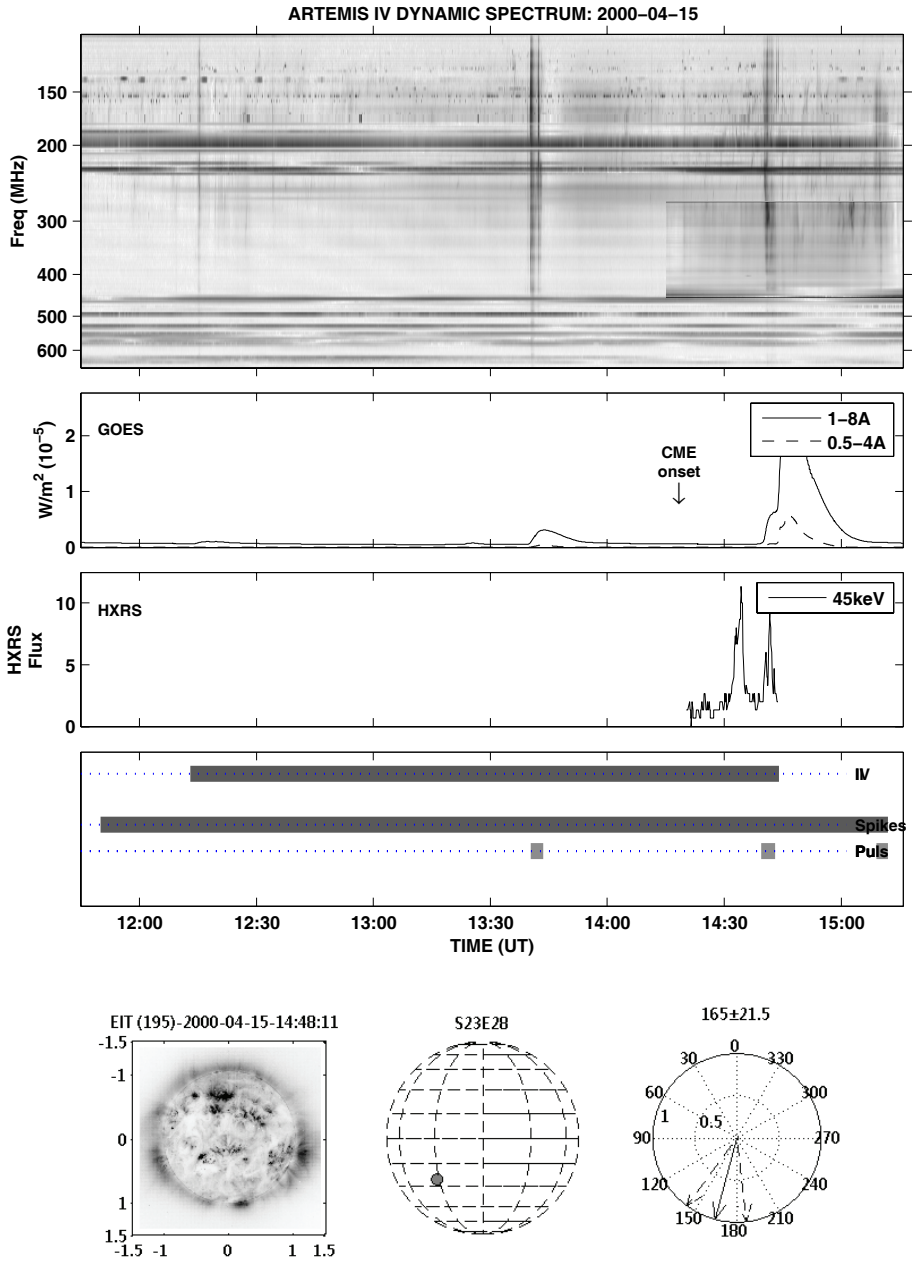

Figure B4. 15 April 2000 Event(B)

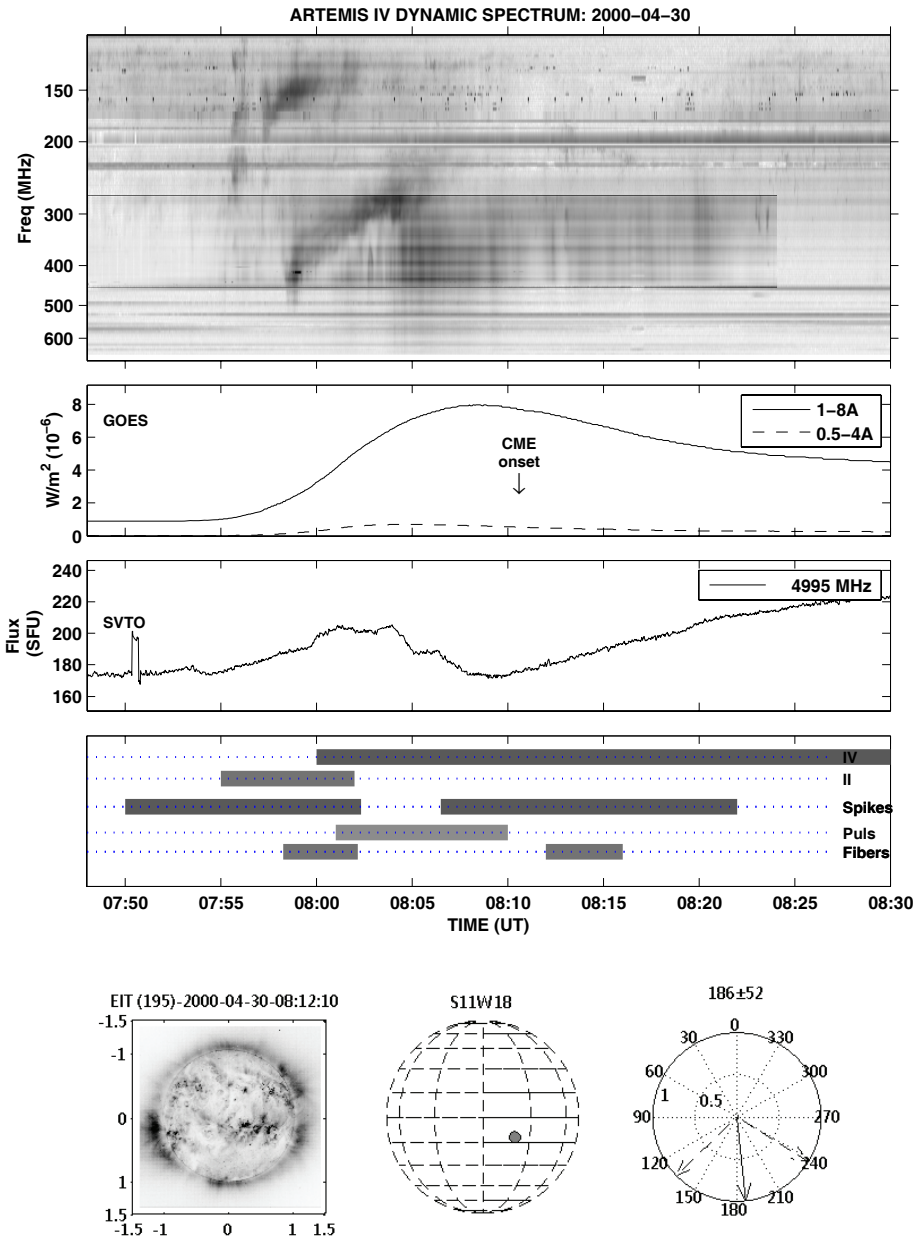

Figure B5. 30 April 2000

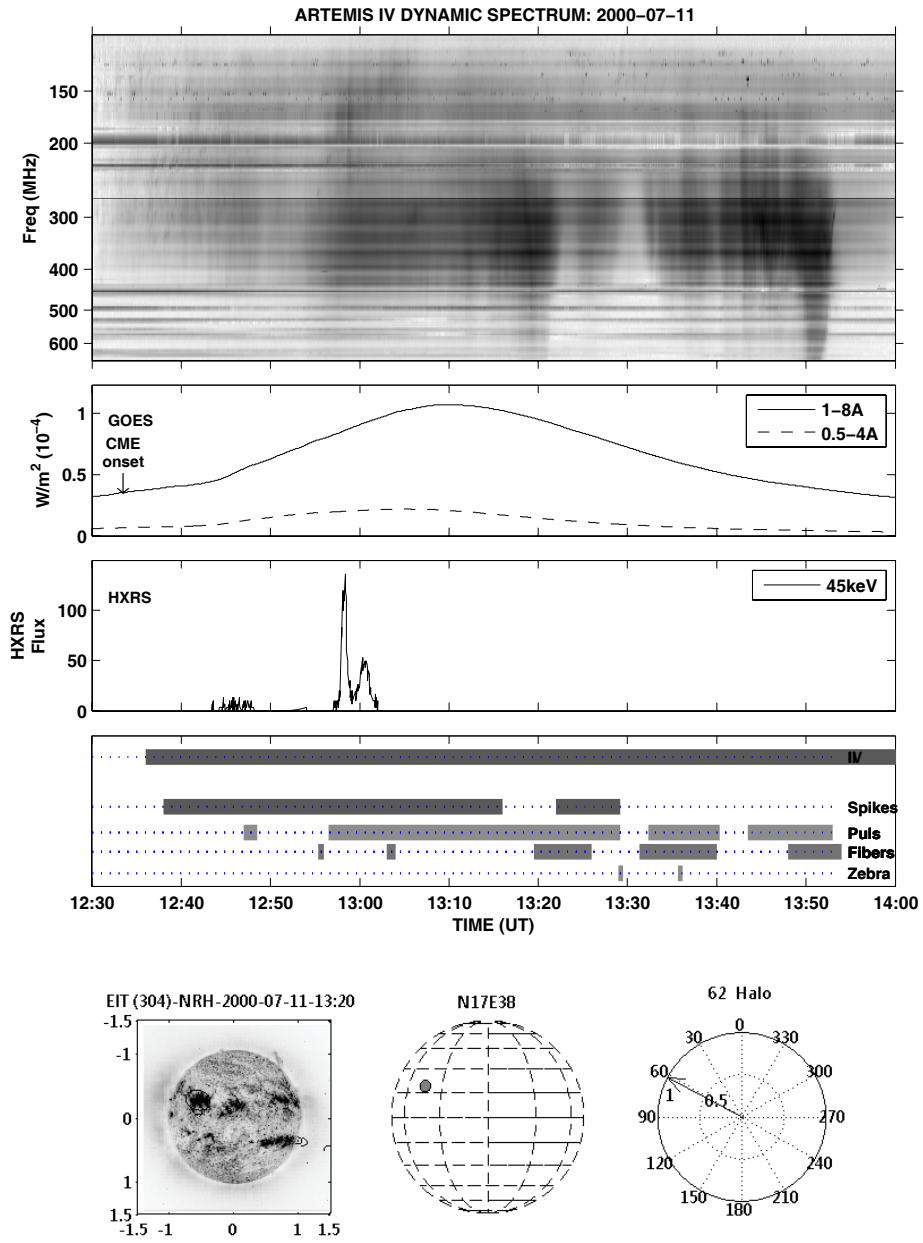

Figure B6. 11 July 2000

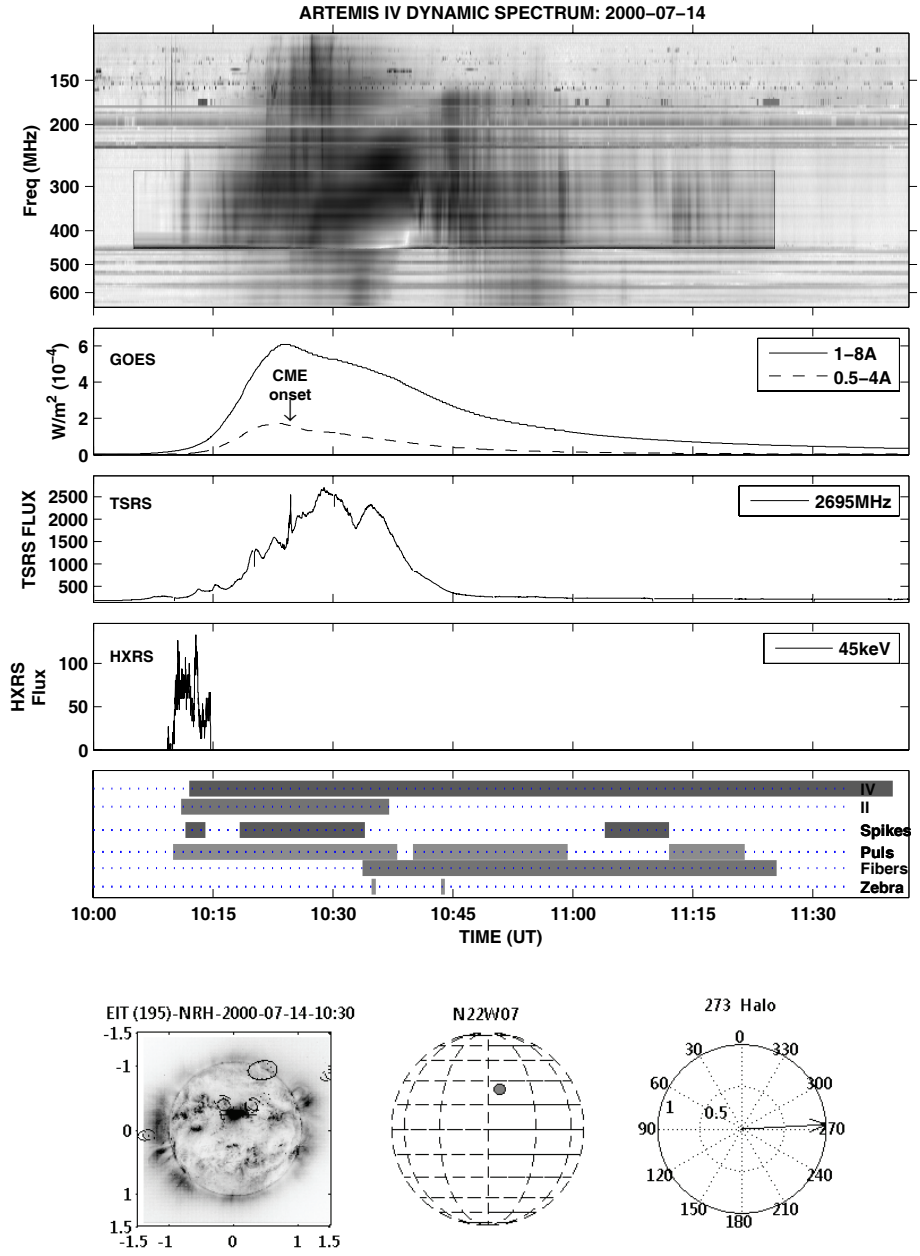

Figure B7. 14 July 2000 Event(A)

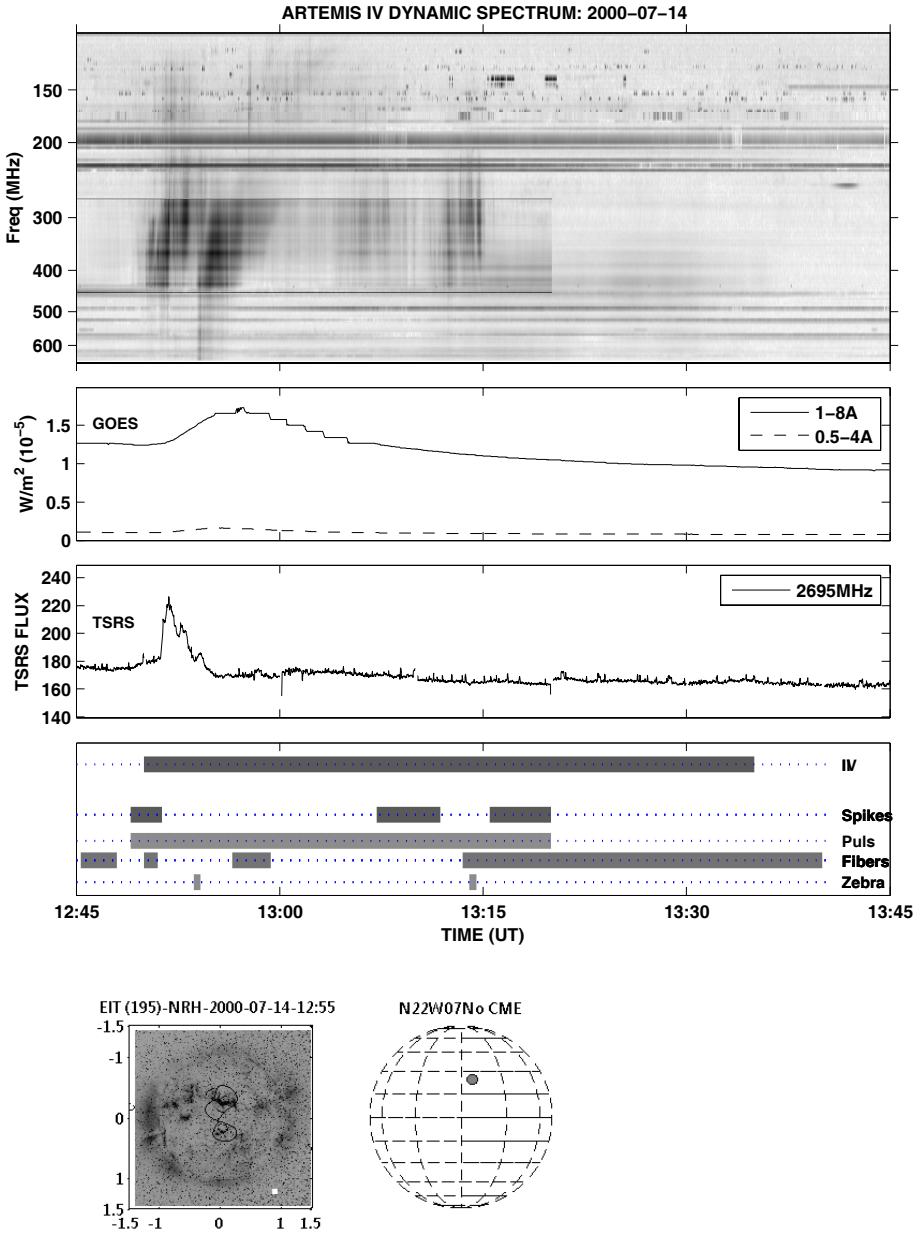

Figure B8. 14 July 2000 Event(B)

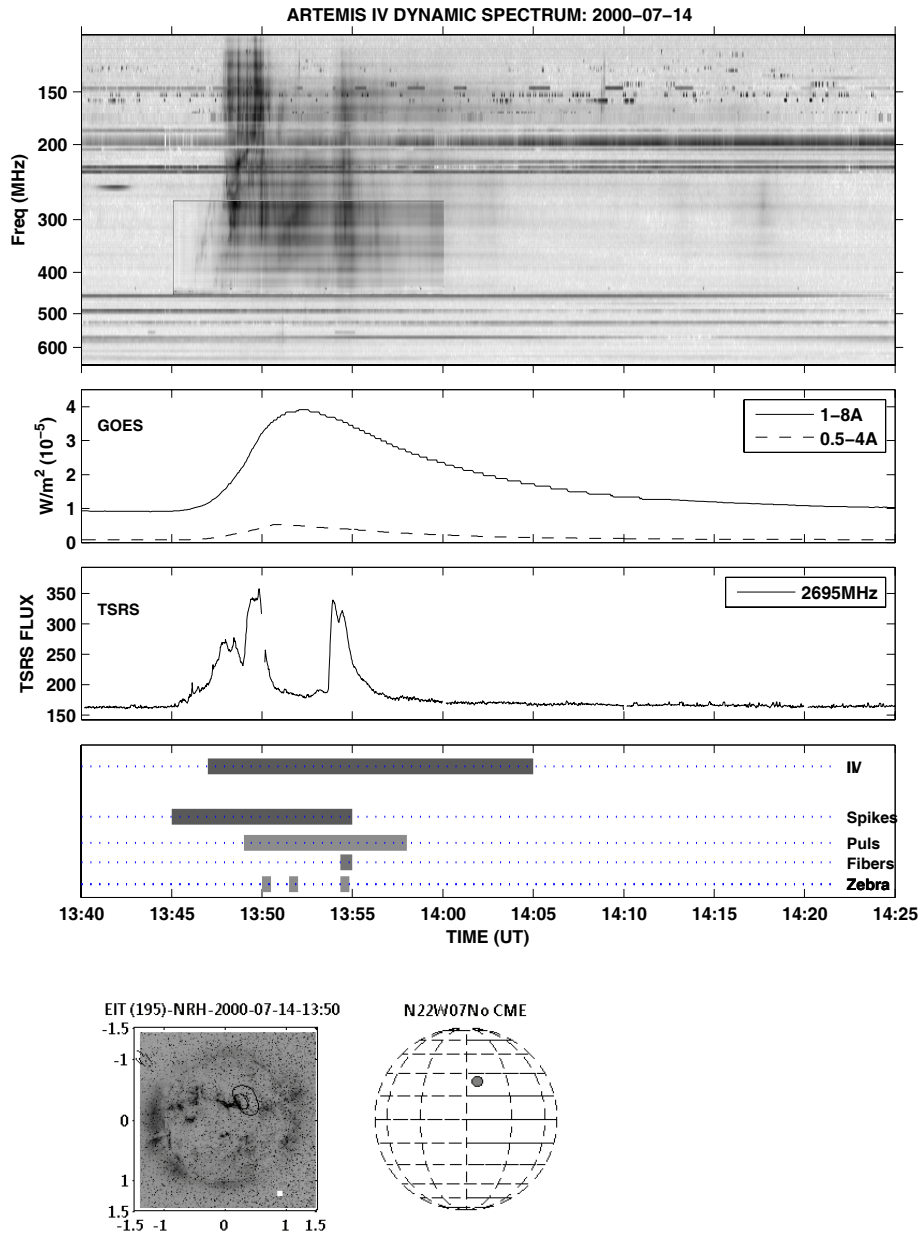

Figure B9. 14 July 2000 Event(C)

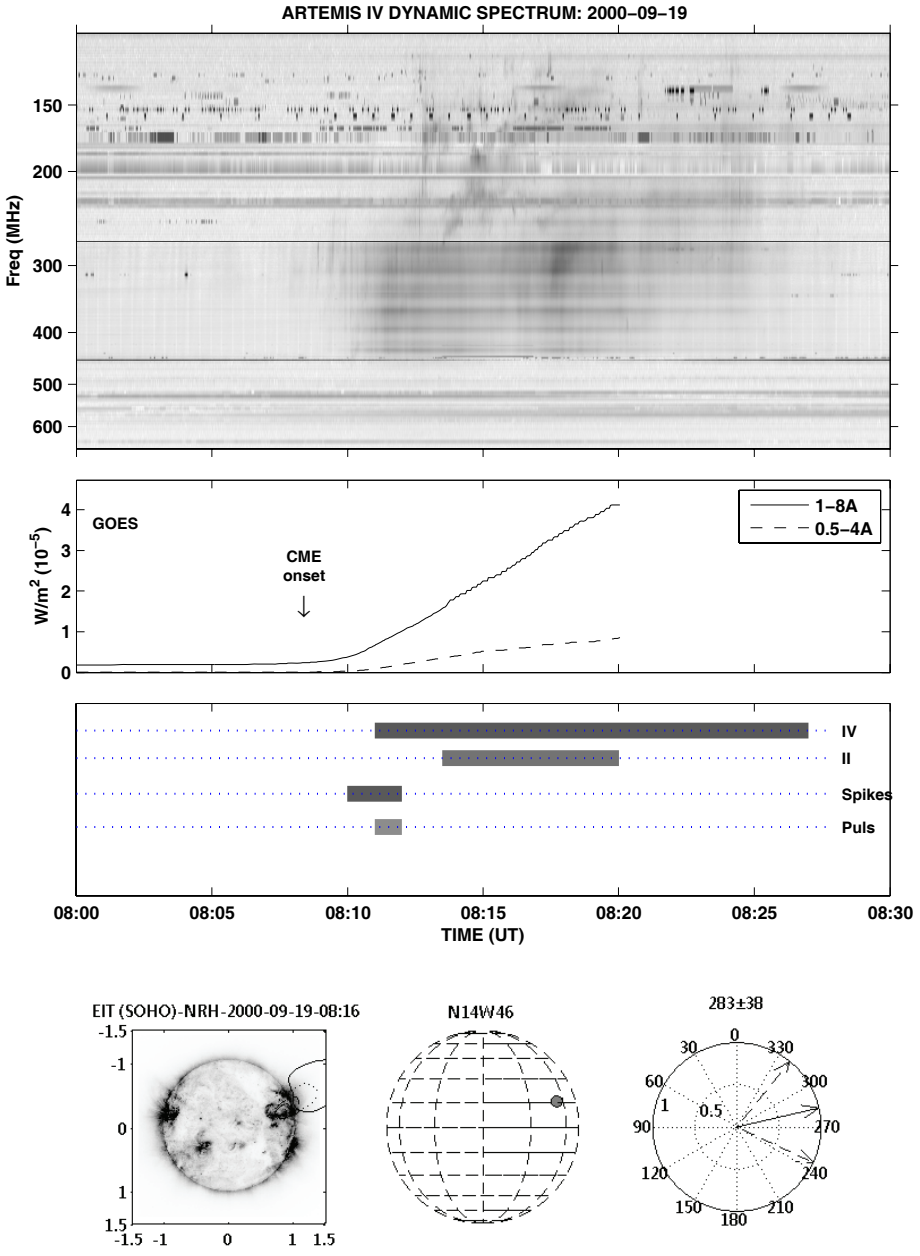

Figure B10. 19 September 2000

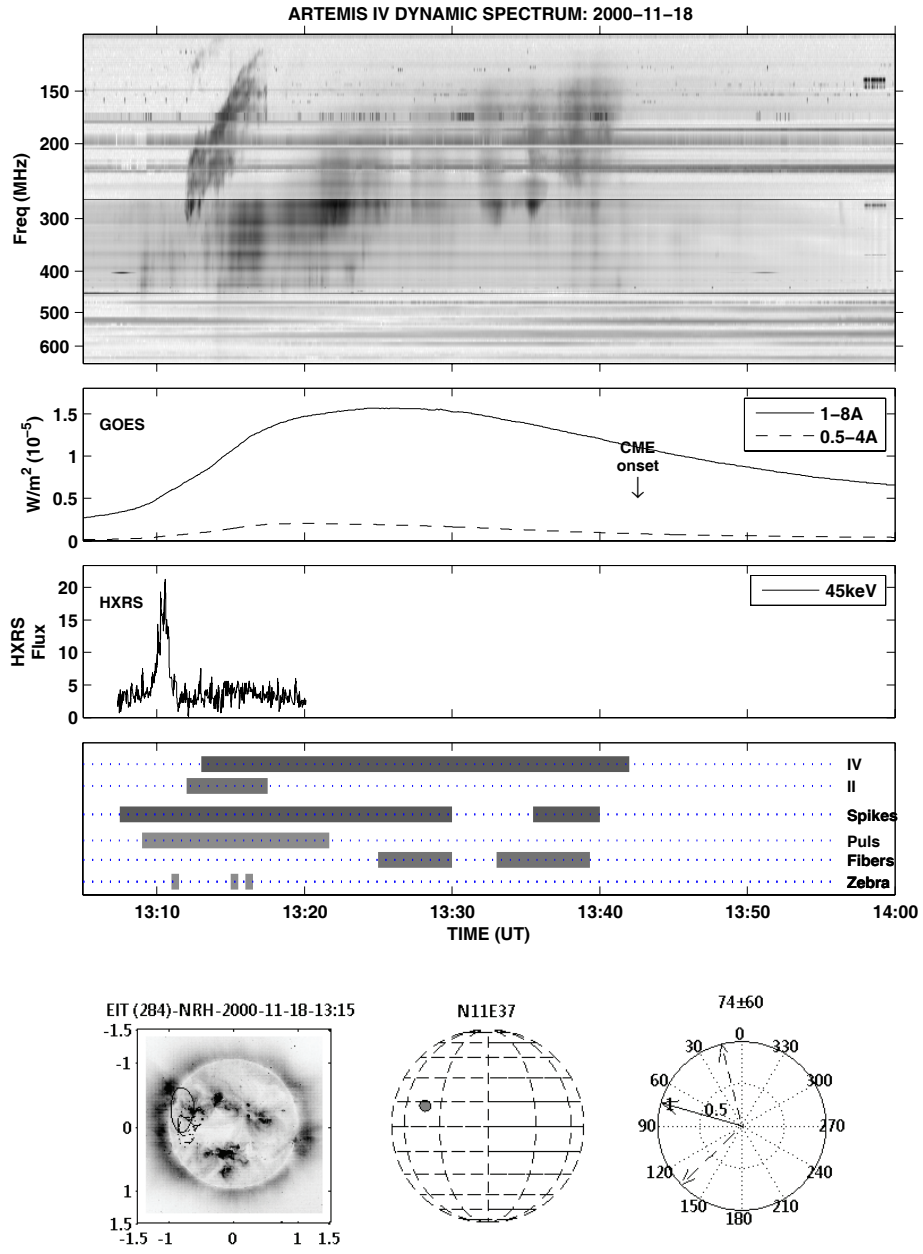

Figure B11. 18 November 2000

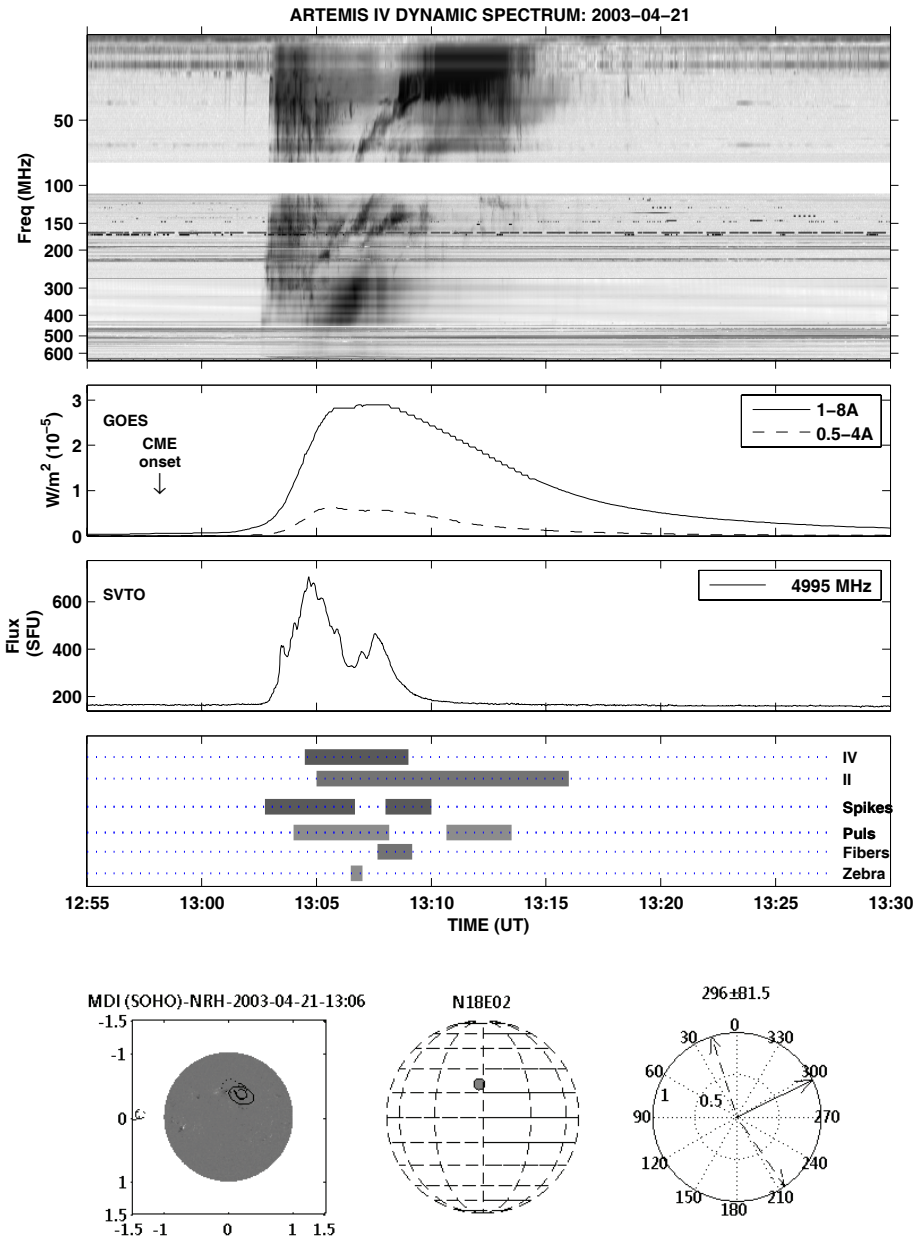

Figure B12. 21 April 2003

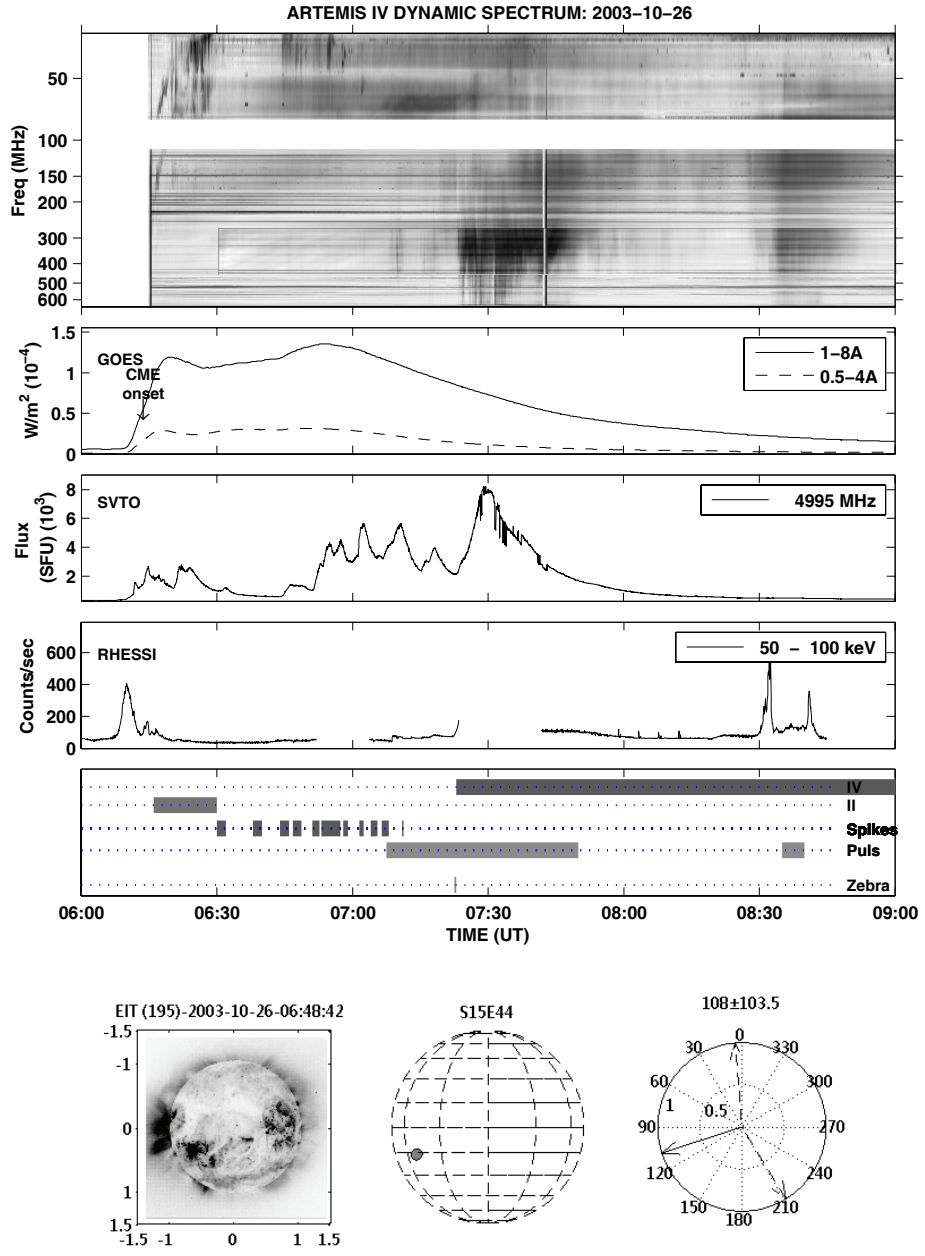

Figure B13. 26 October 2003

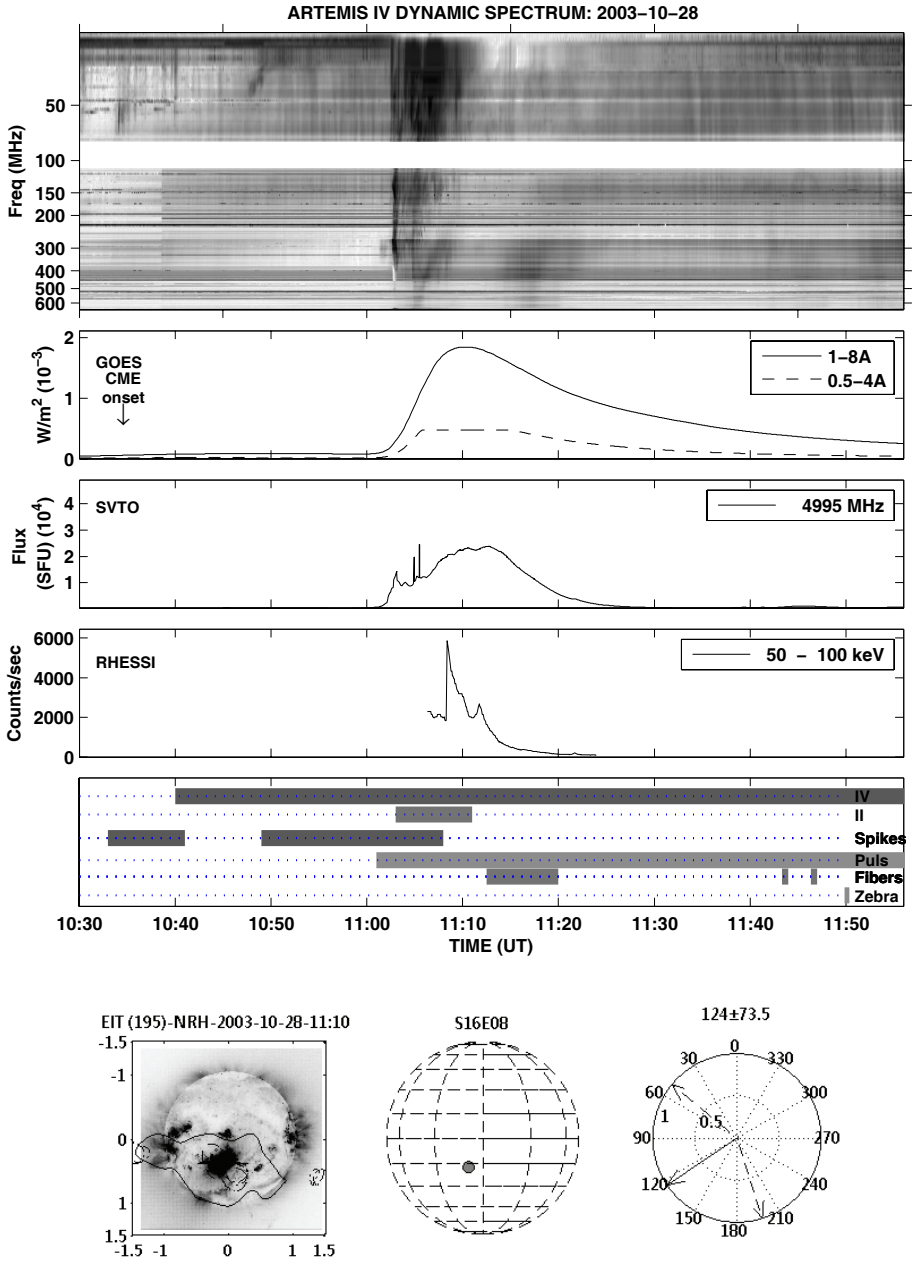

Figure B14. 28 October 2003

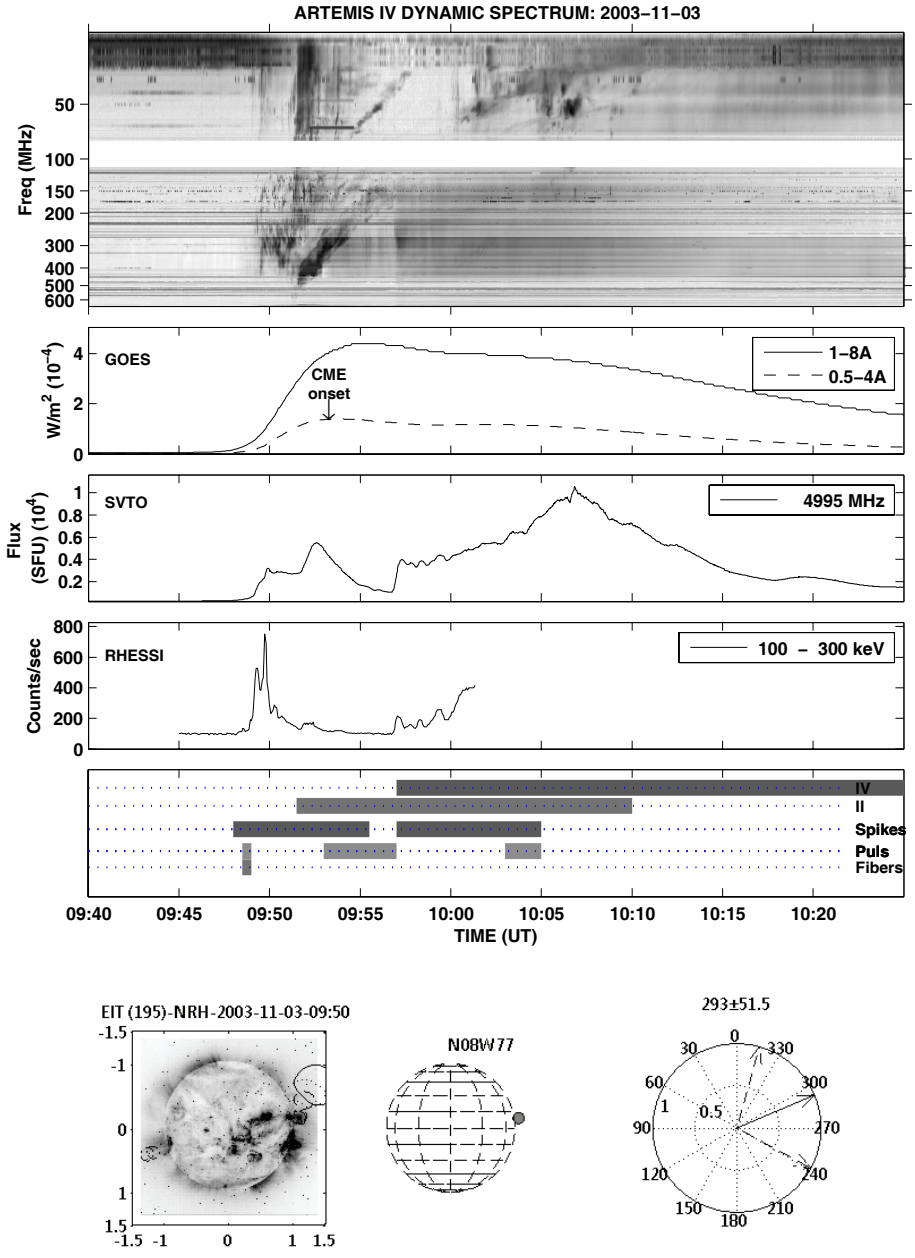

Figure B15. 03 November 2003

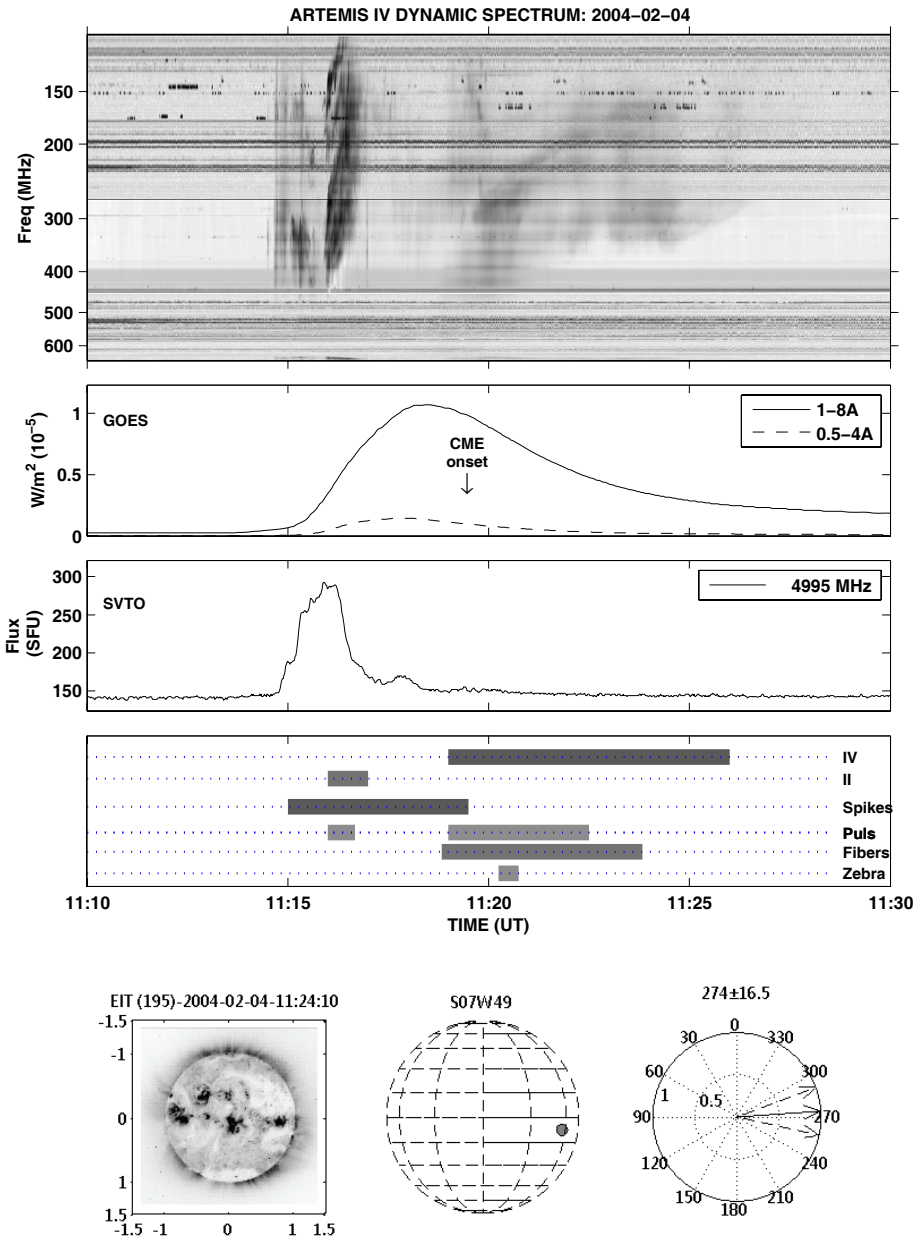

Figure B16. 04 February 2004

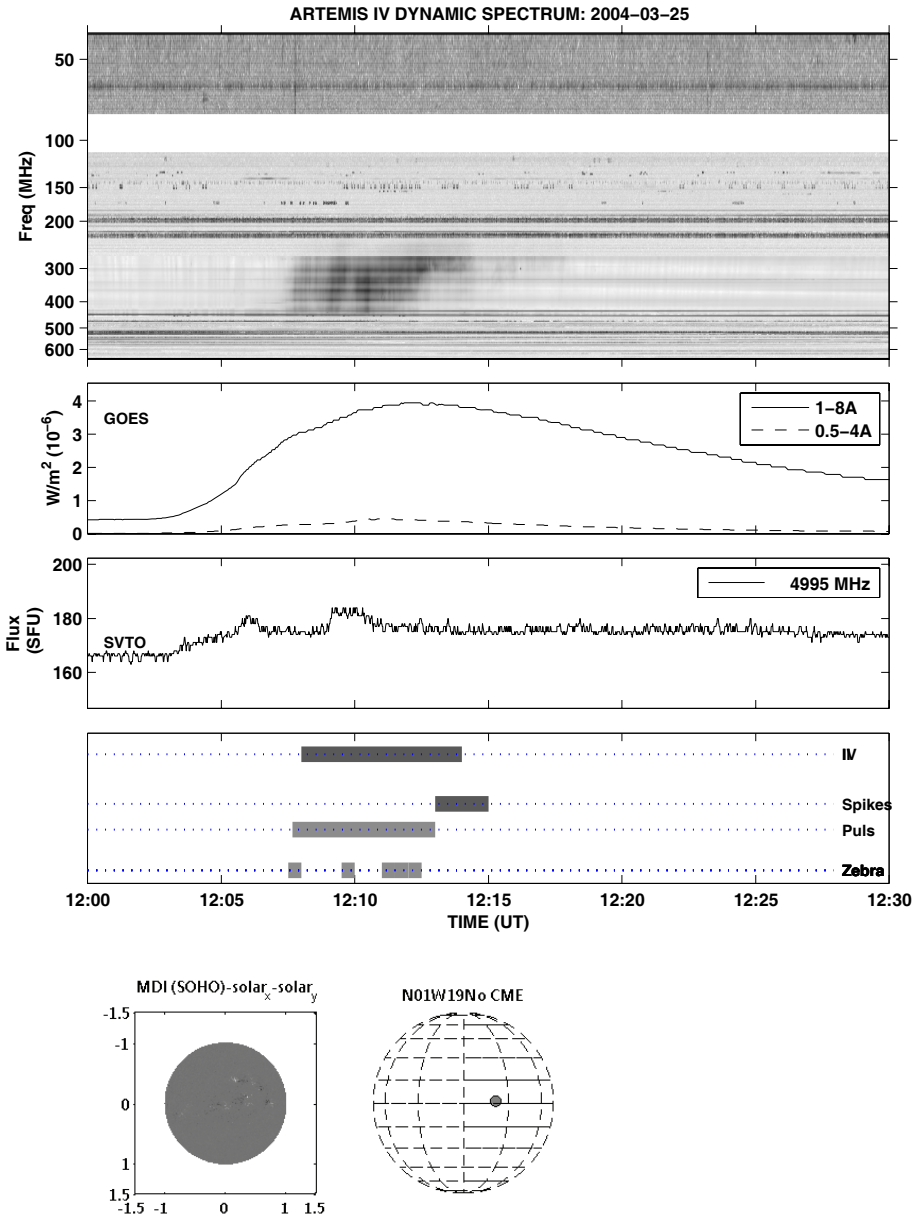

Figure B17. 25 March 2004

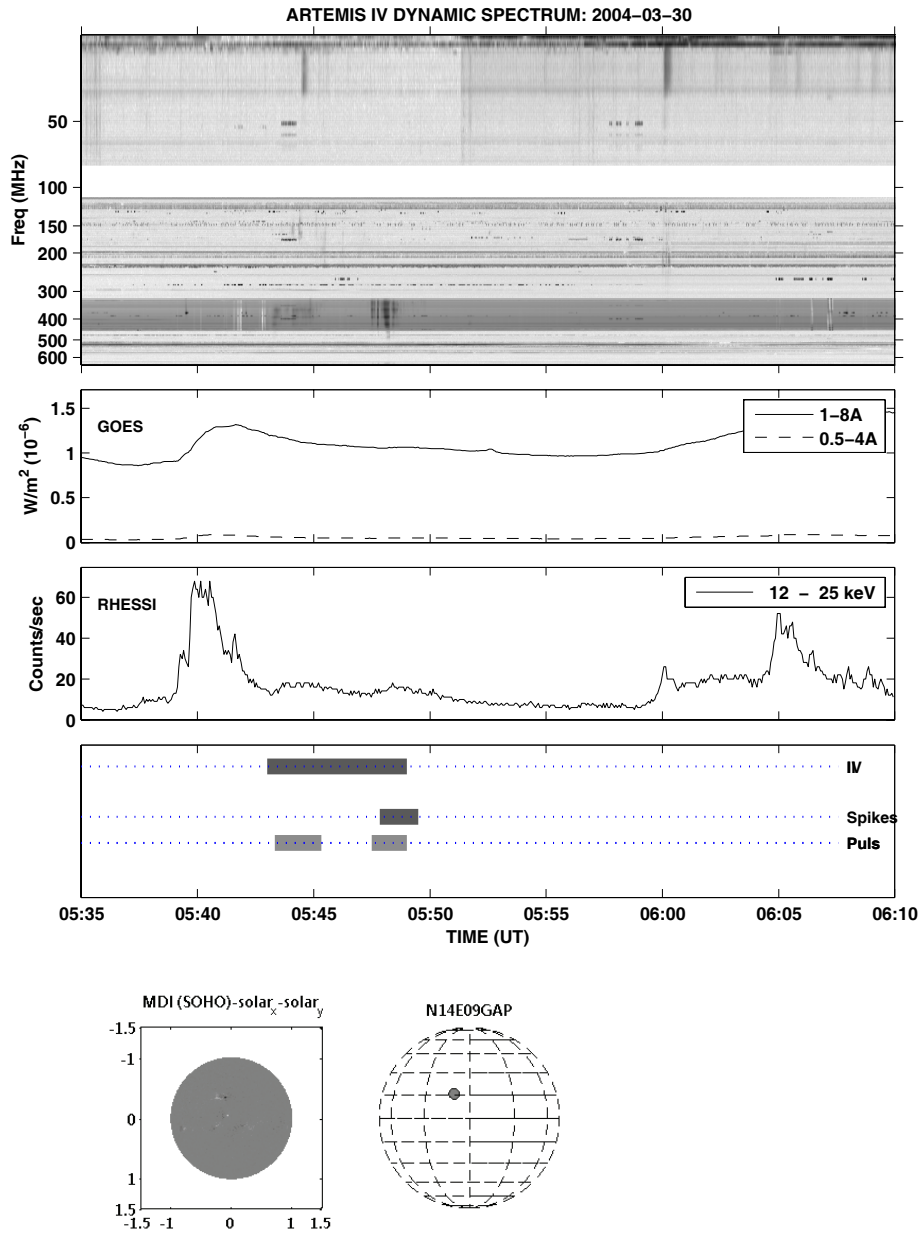

Figure B18. 30 March 2004 Event(A)

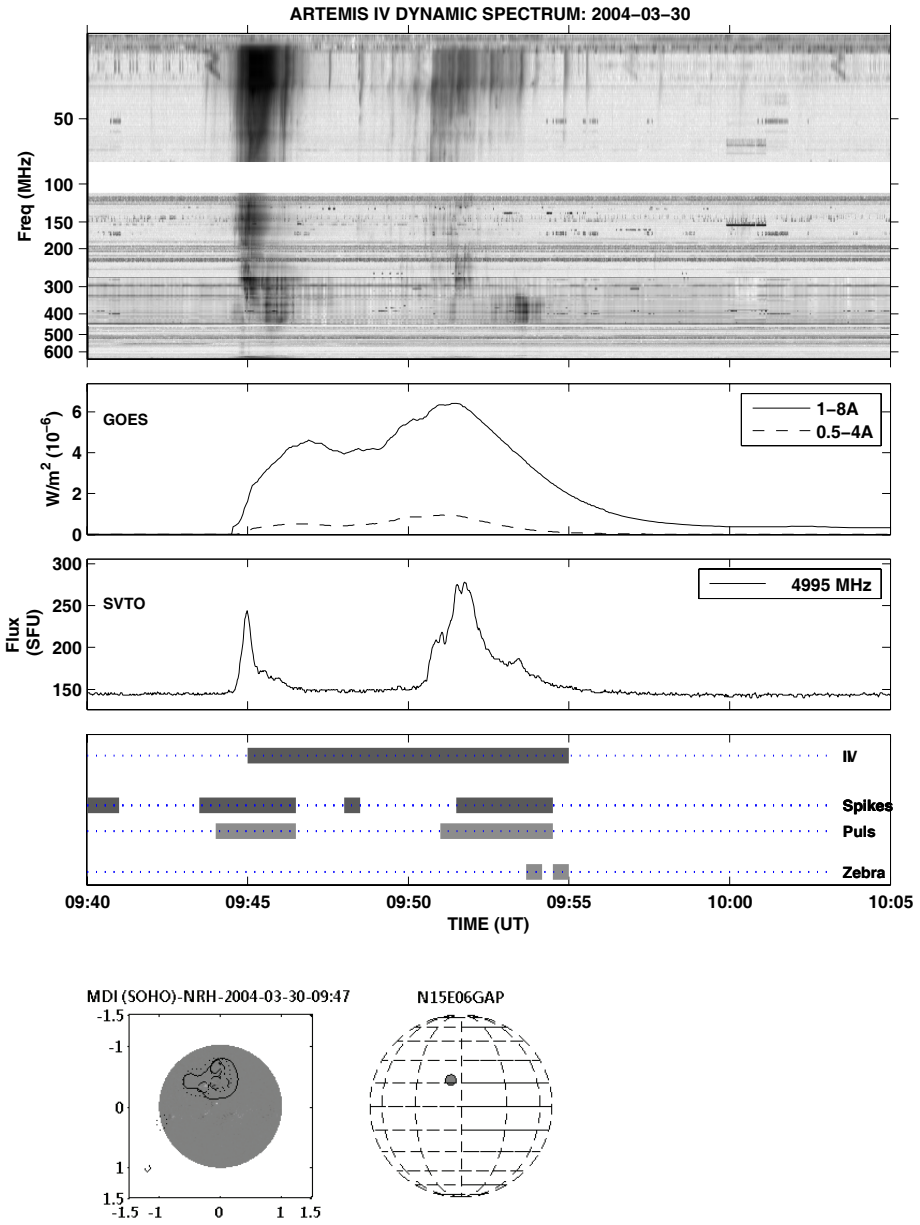

Figure B19. 30 March 2004 Event(B)

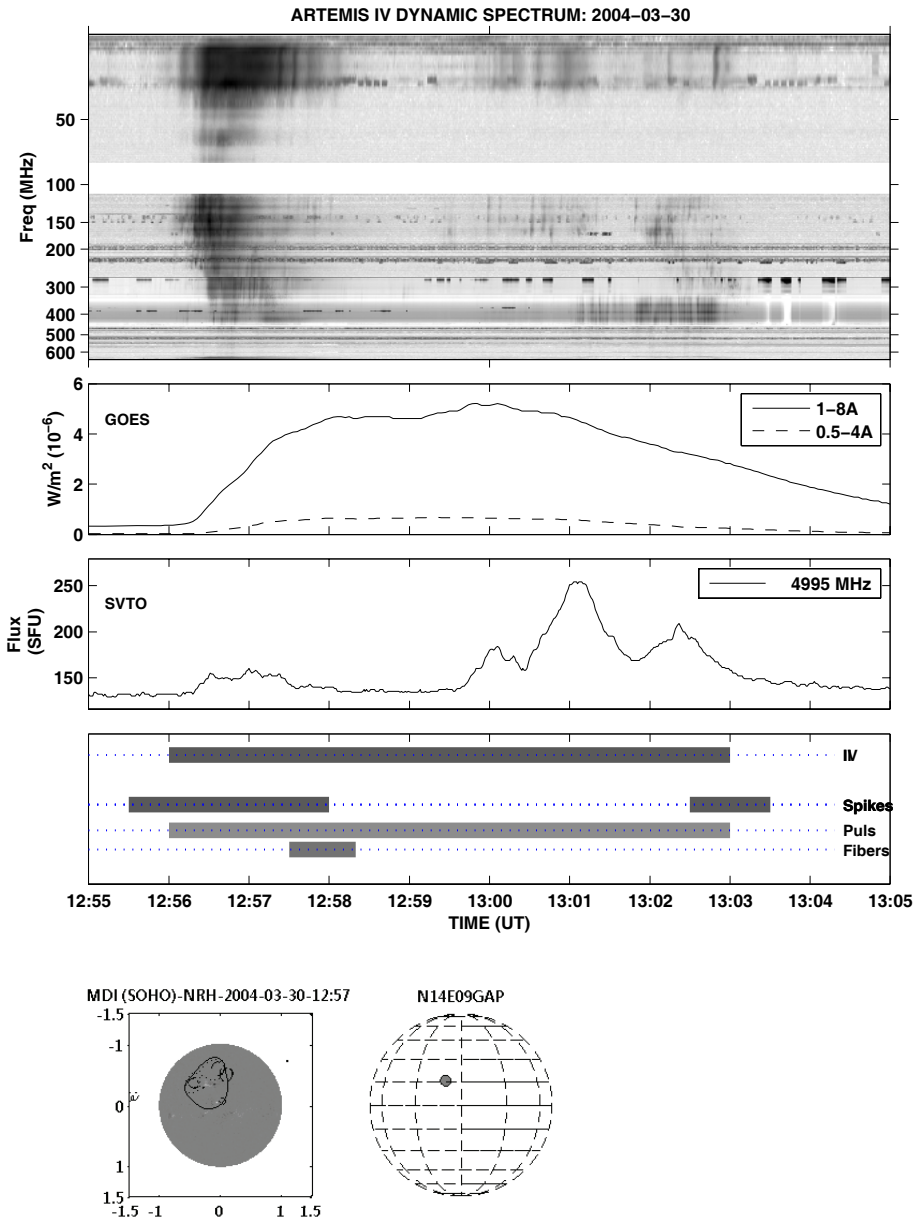

Figure B20. 30 March 2004 Event(C)

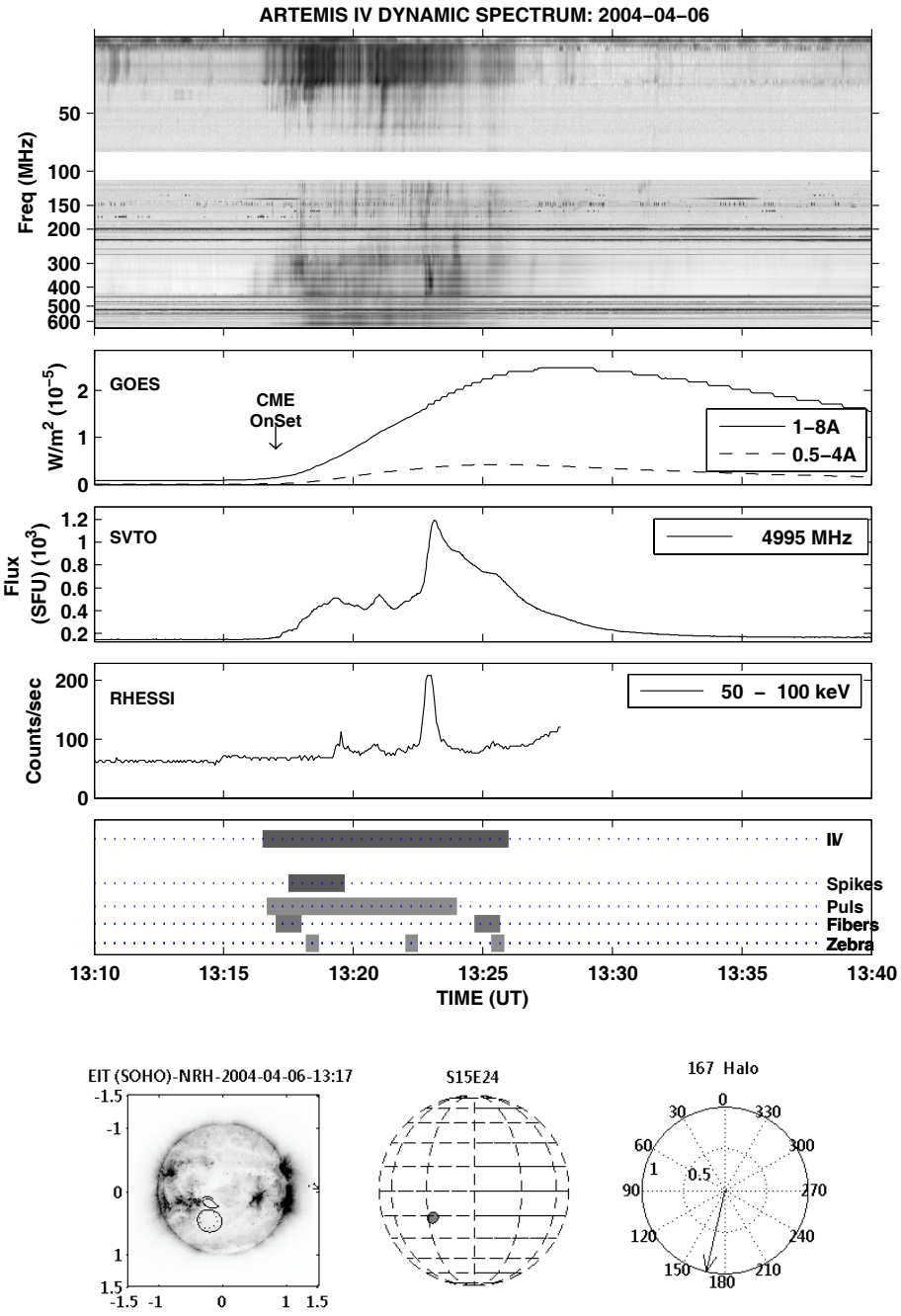

Figure B21. 06 April 2004

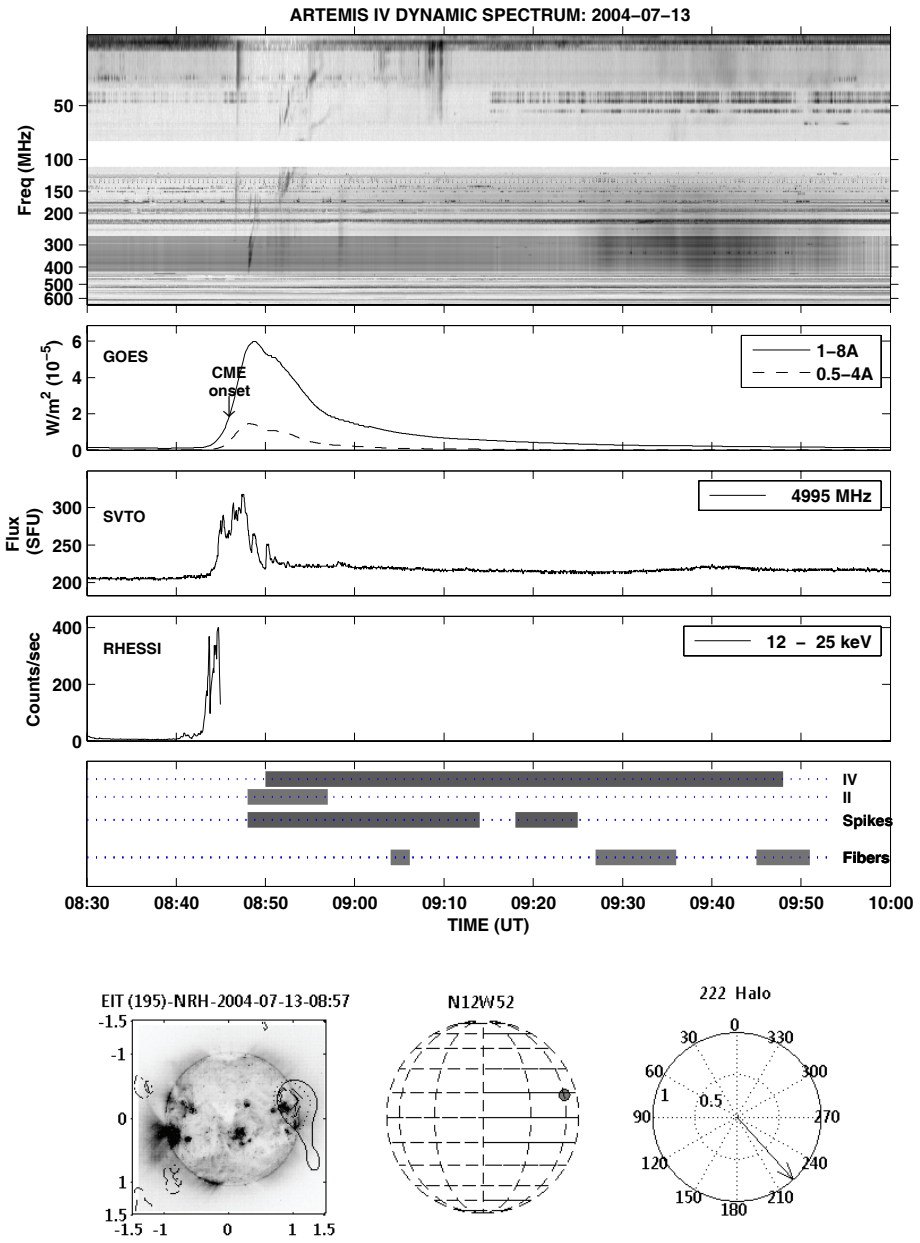

Figure B22. 13 July 2004

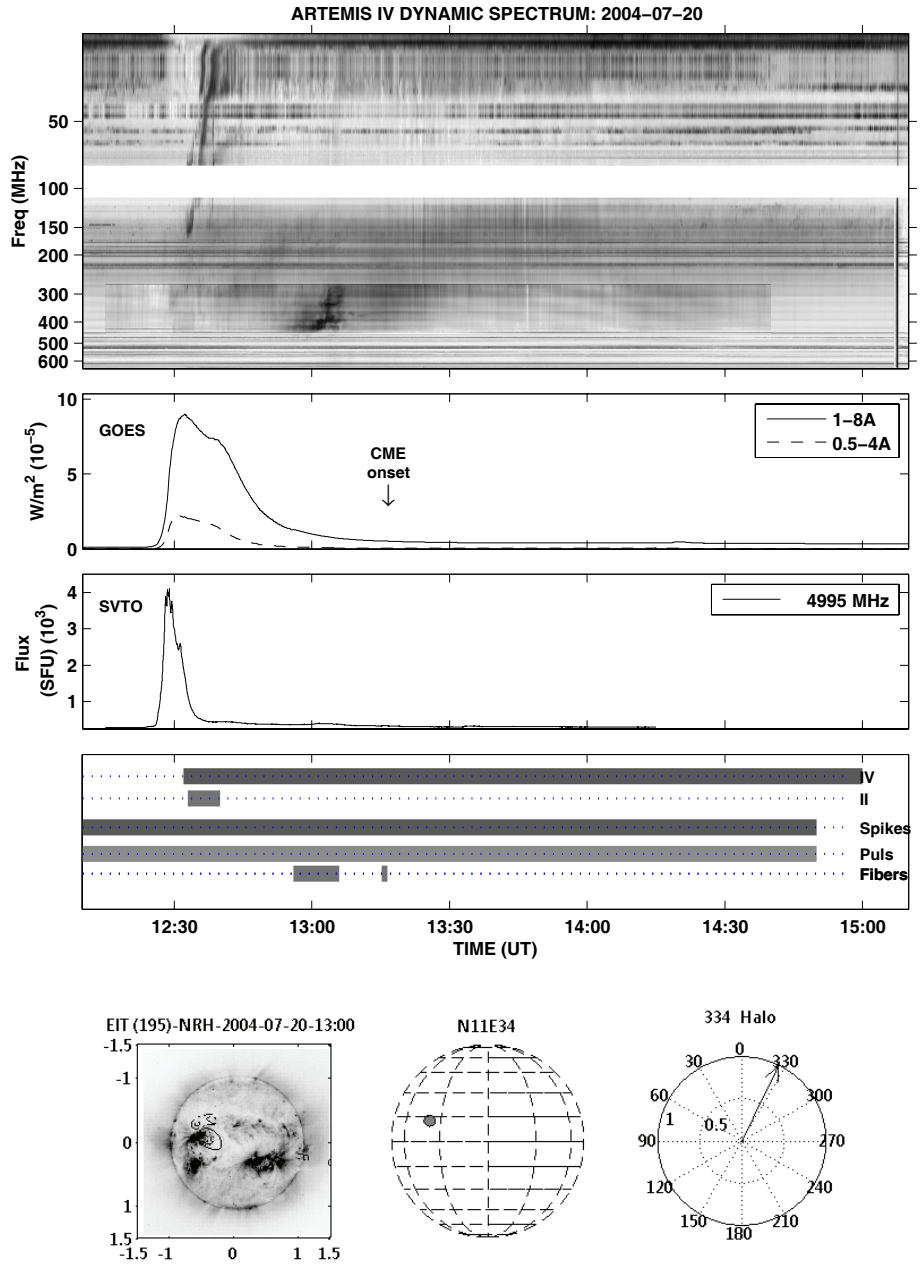

Figure B23. 20 July 2004

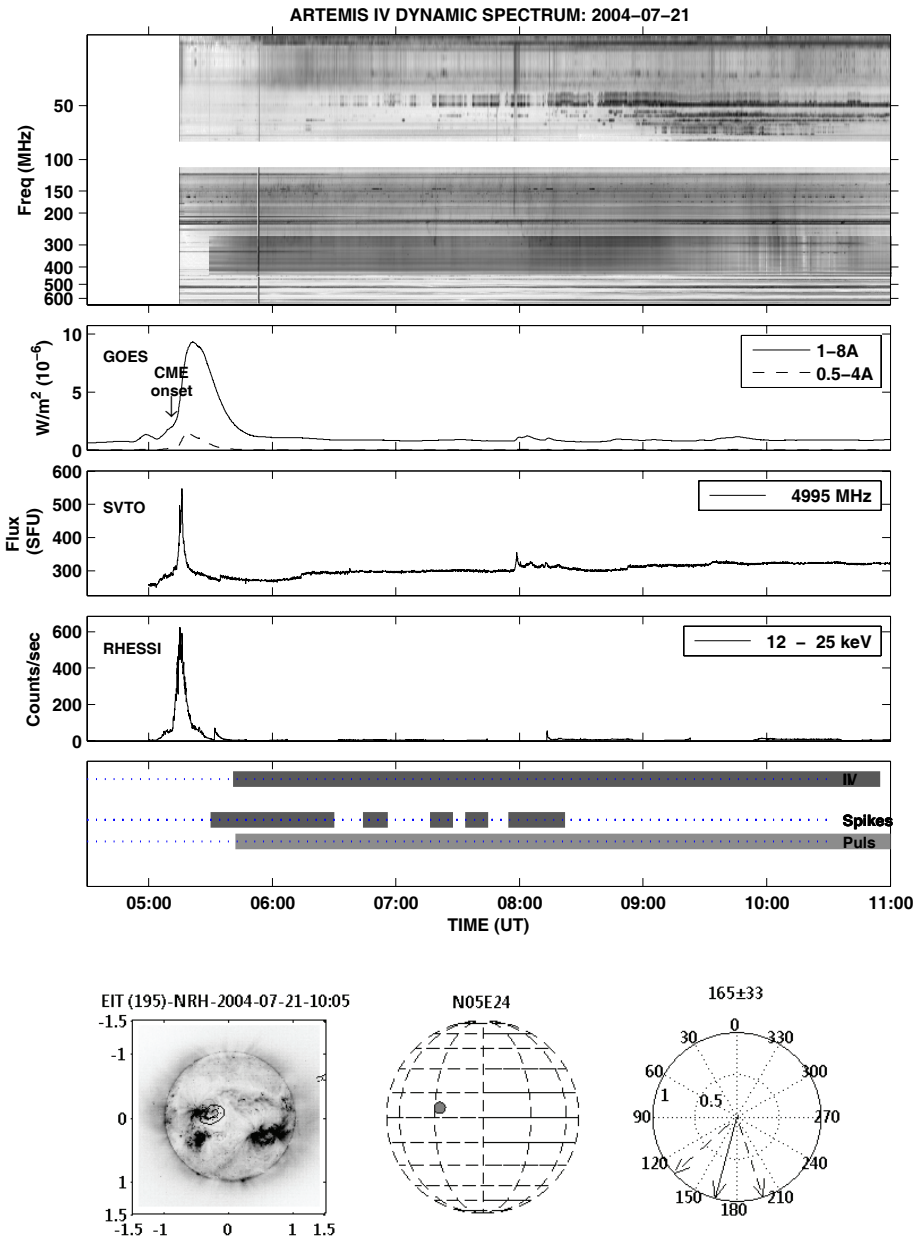

Figure B24. 21 July 2004

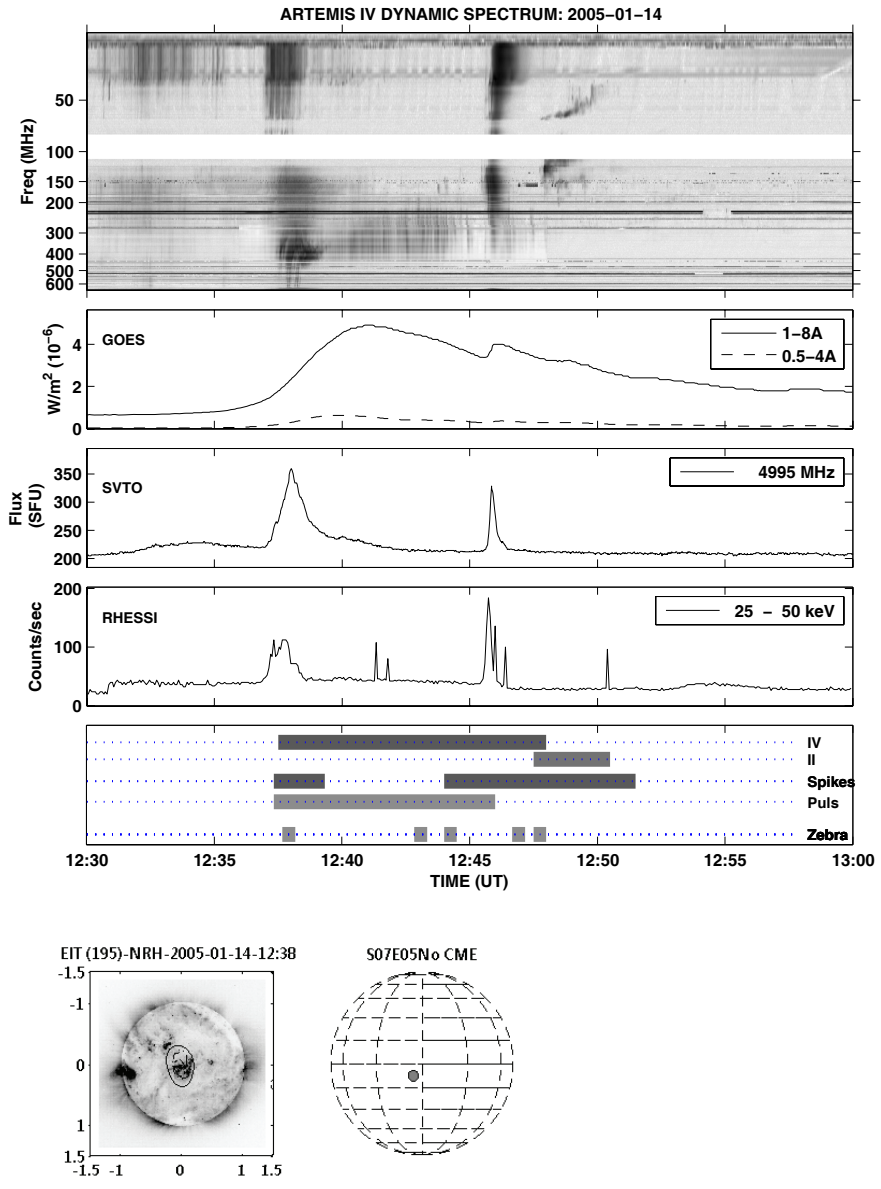

Figure B25. 14 January 2005

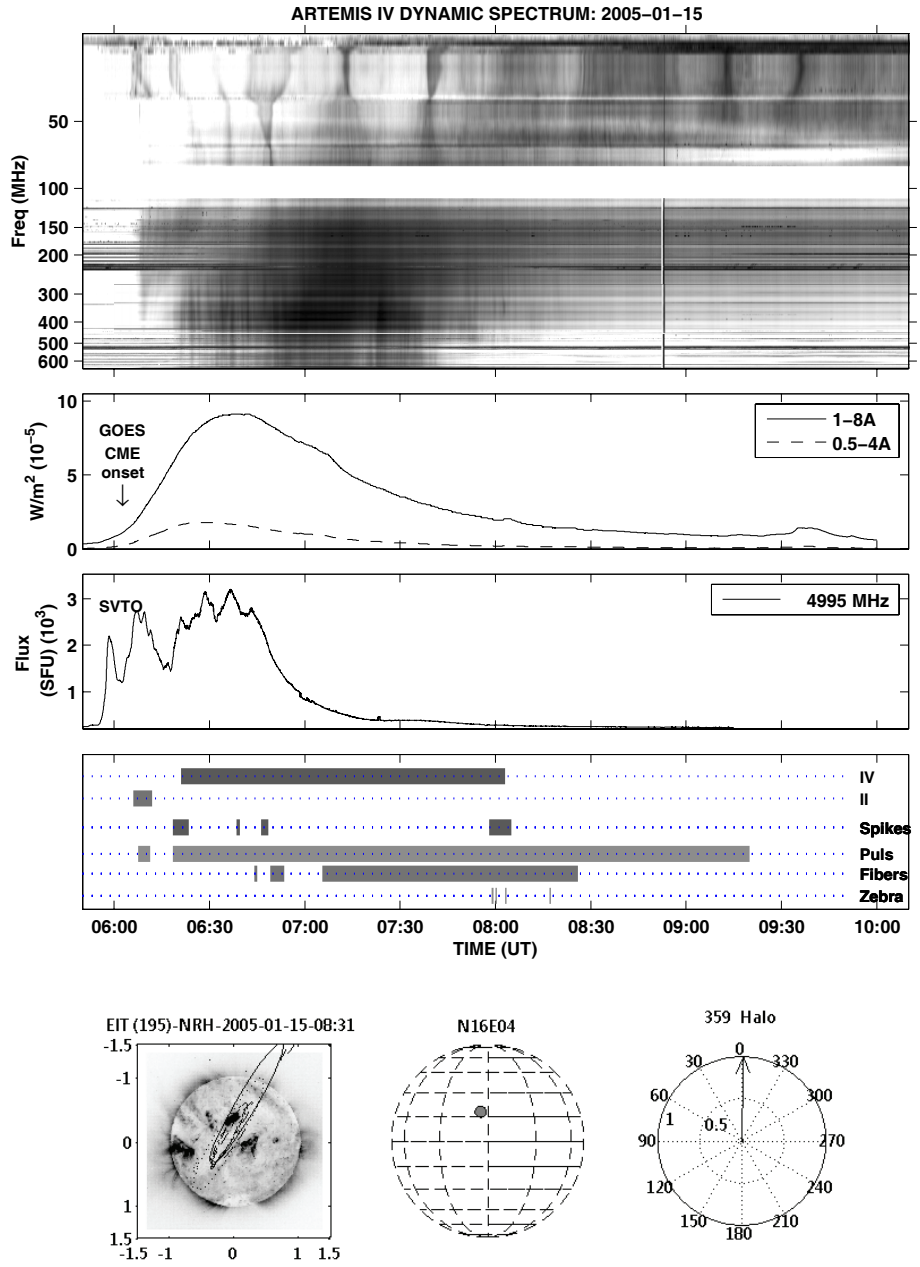

Figure B26. 15 January 2005

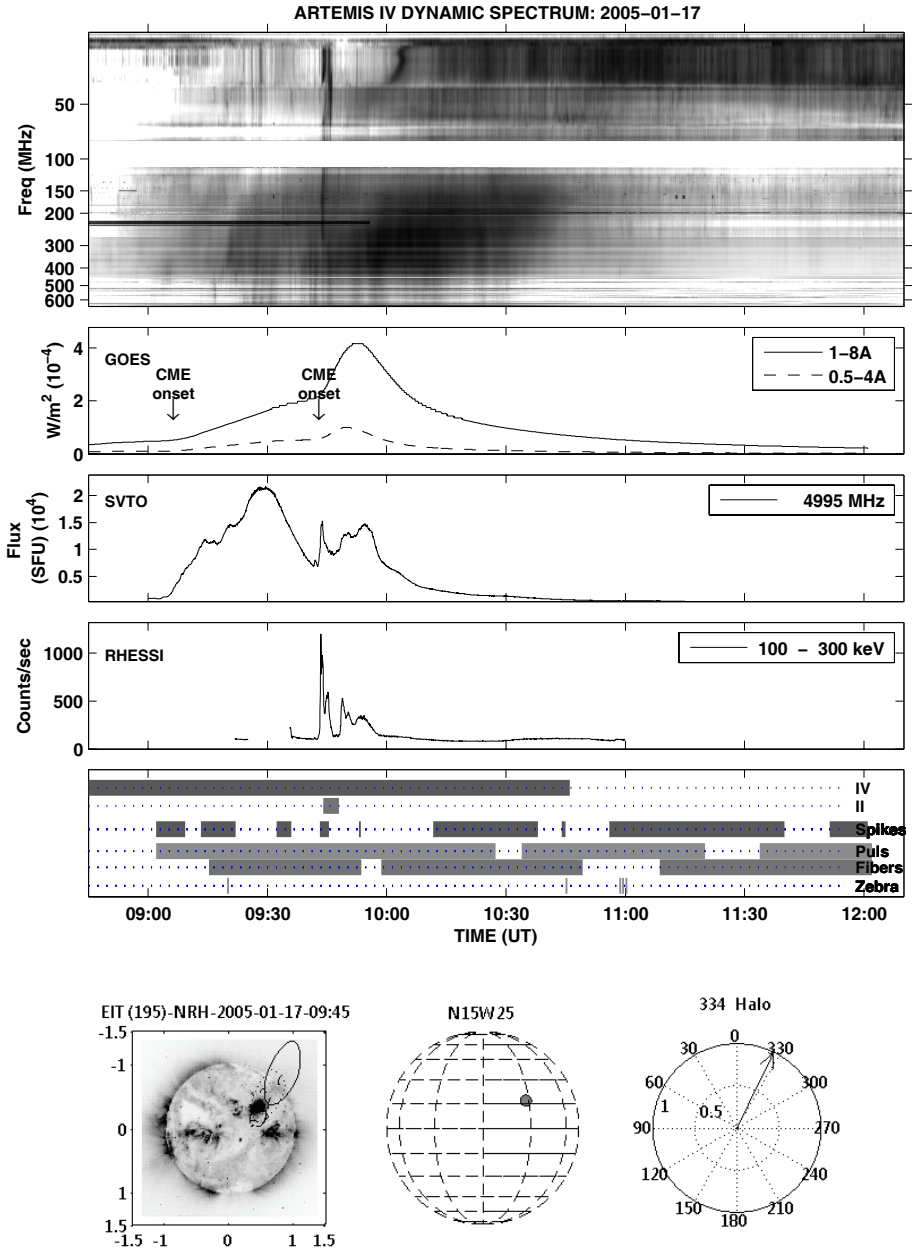

Figure B27. 17 January 2005

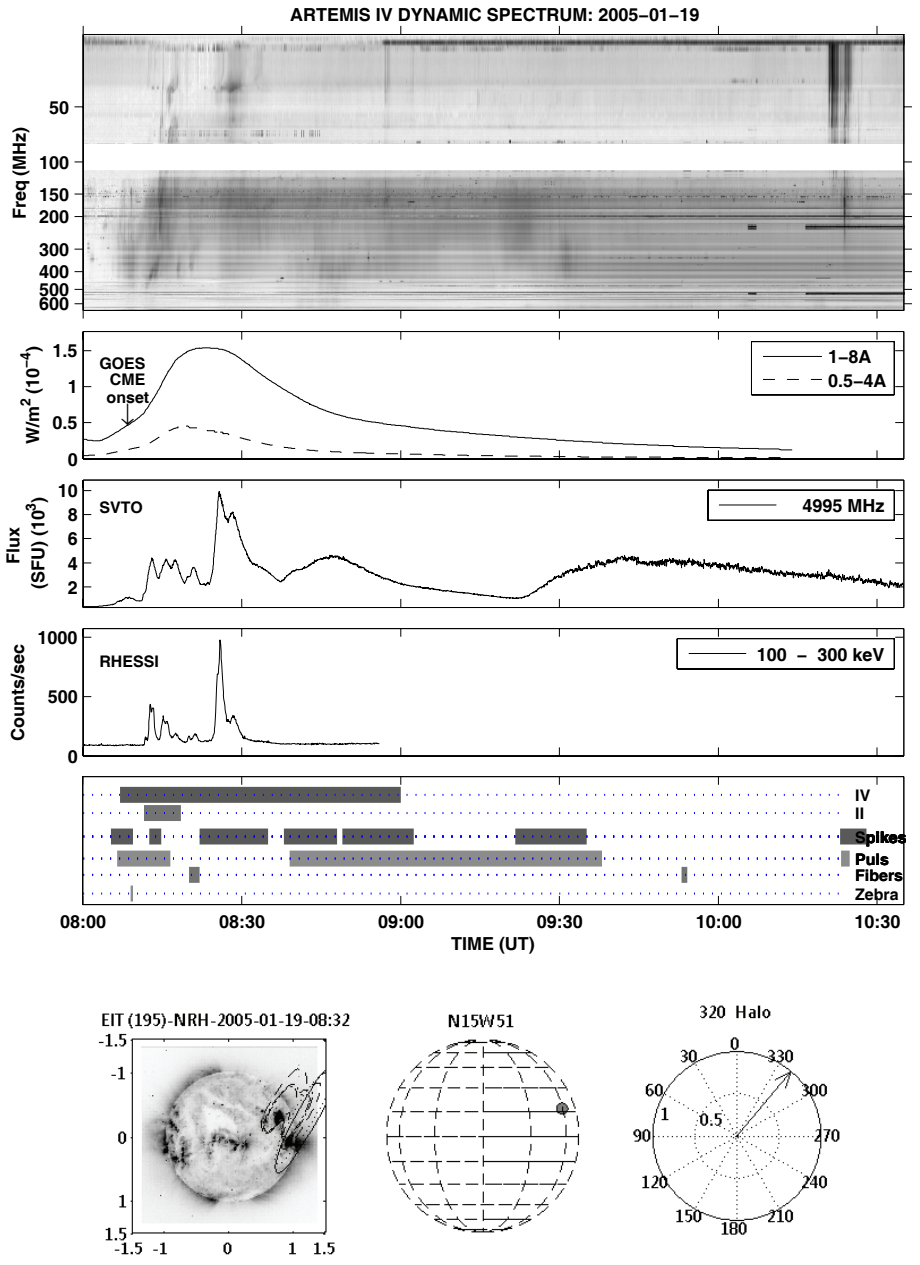

Figure B28. 19 January 2005

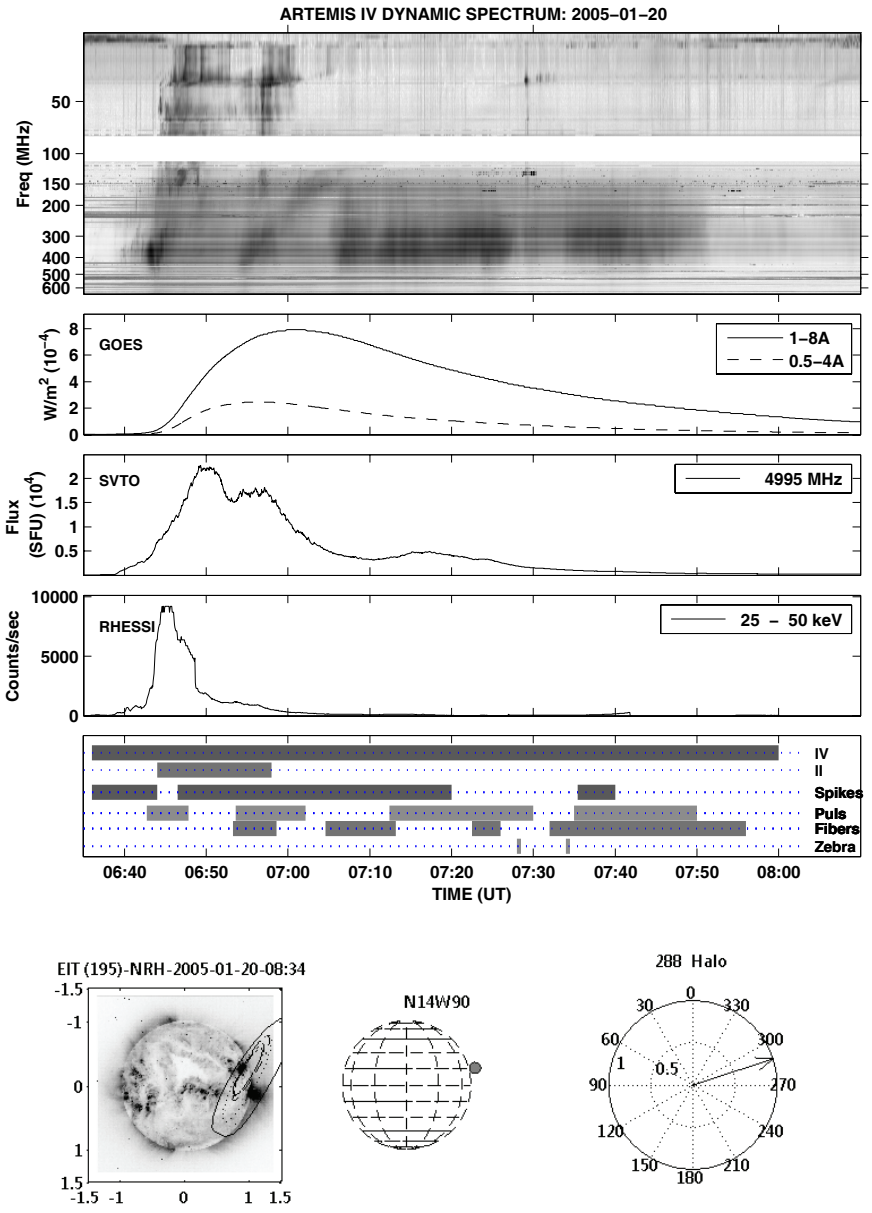

Figure B29. 20 January 2005

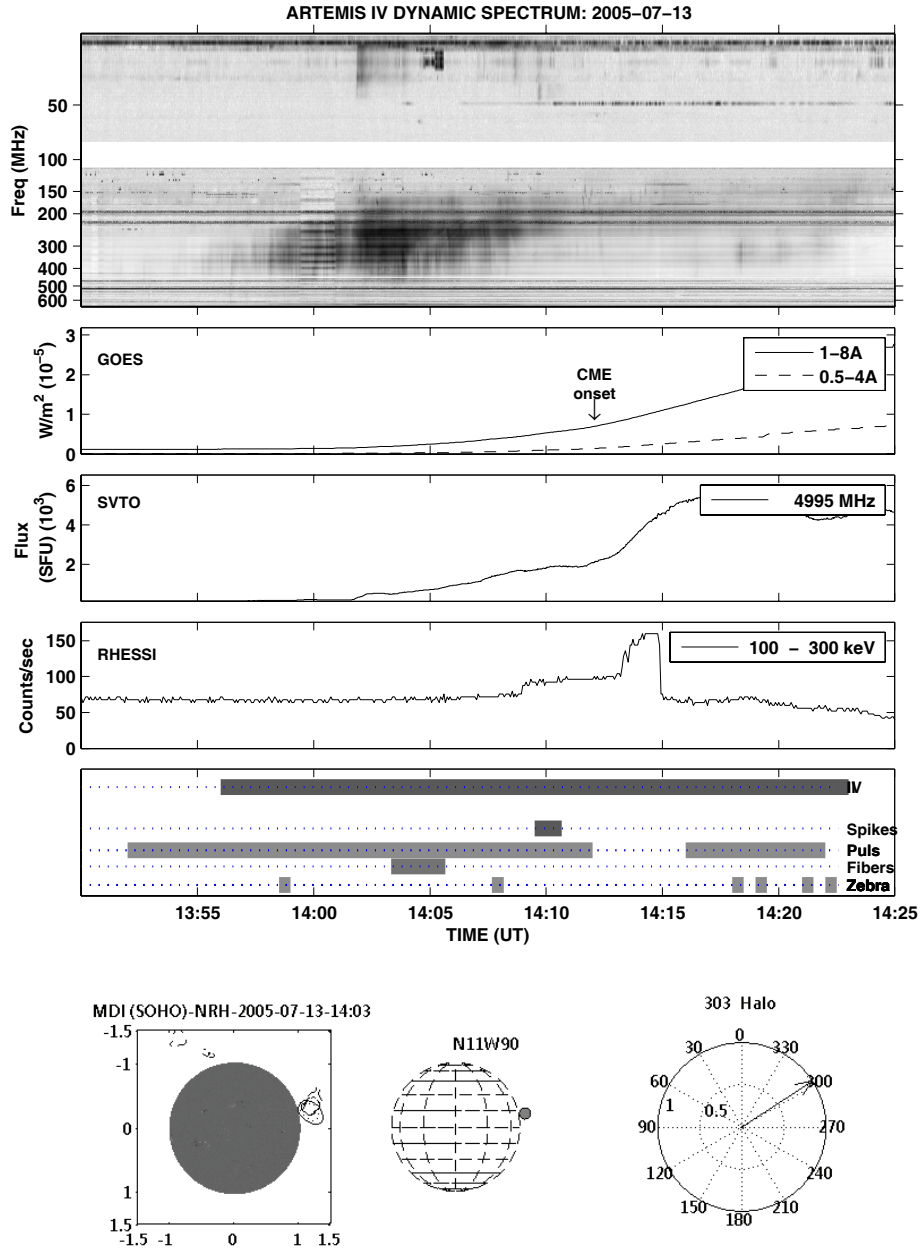

Figure B30. 13 July 2005

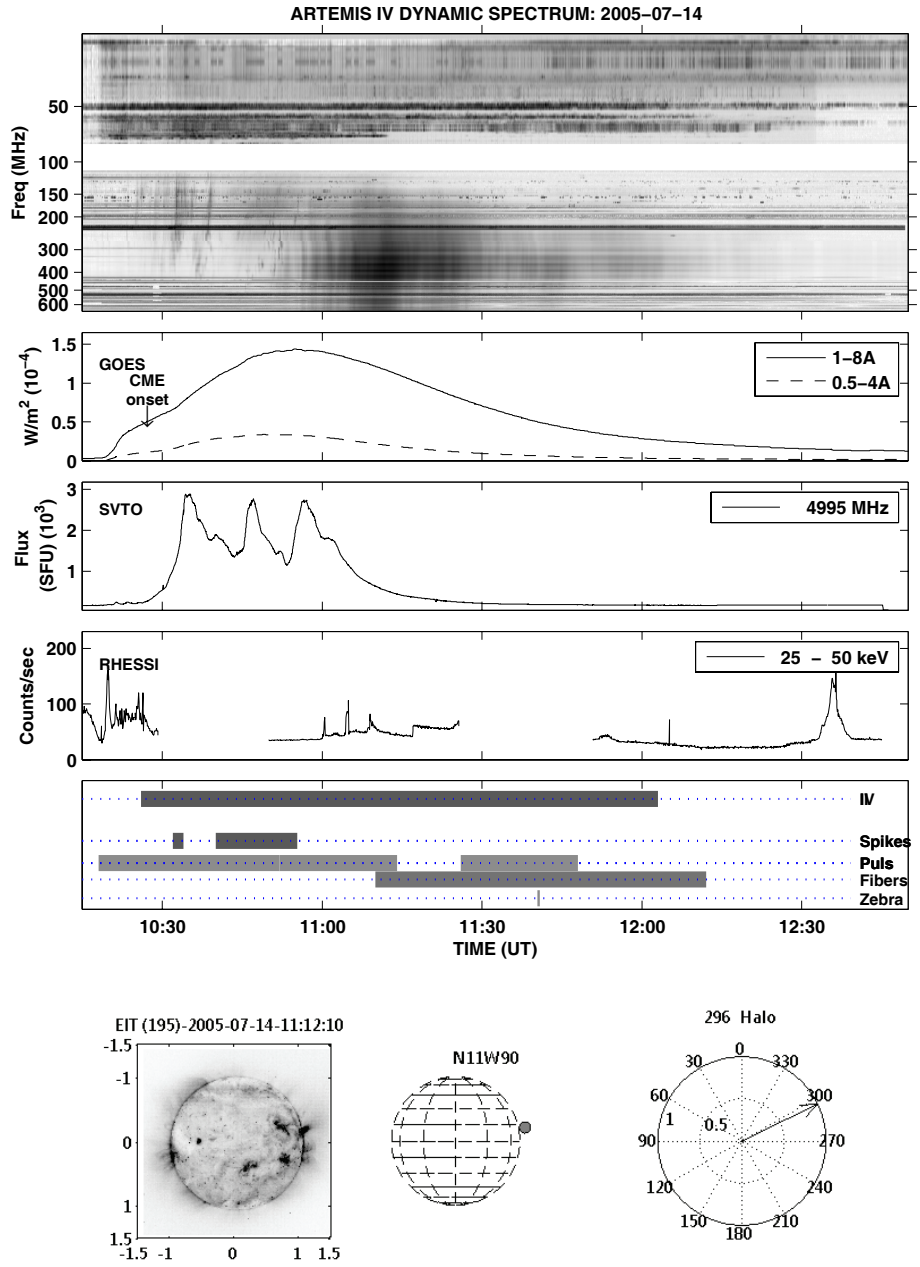

Figure B31. 14 July 2005

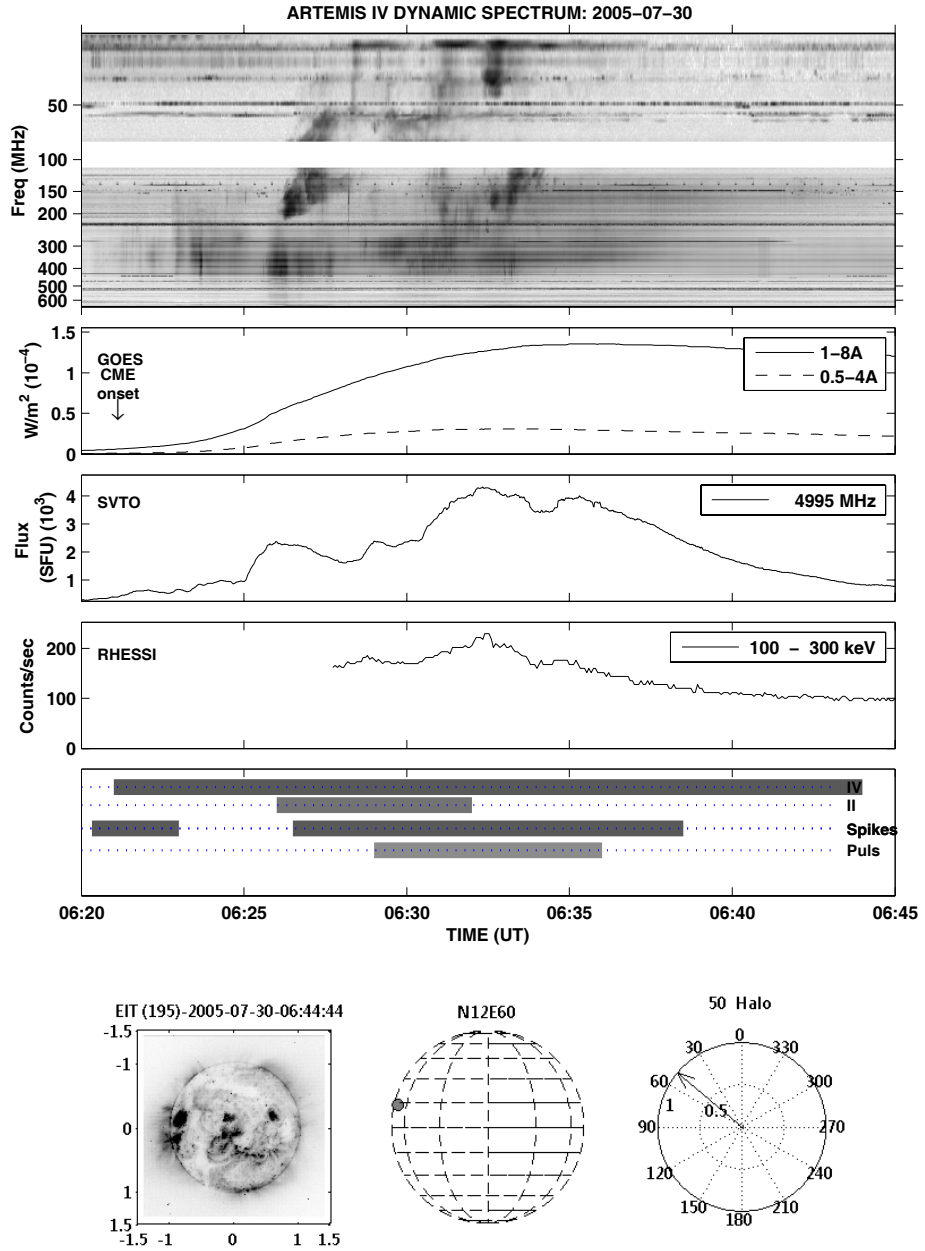

Figure B32. 30 July 2005

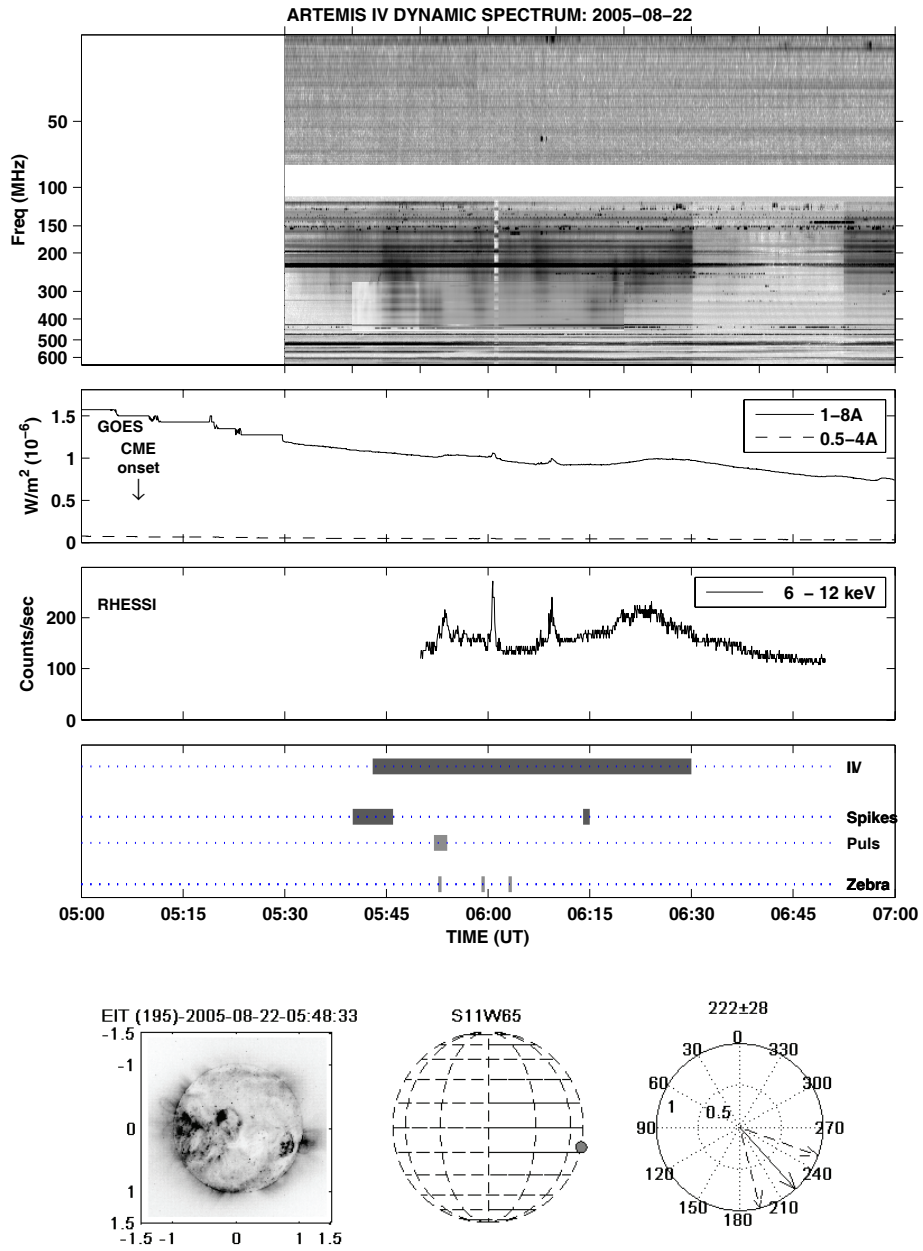

Figure B33. 22 August 2005

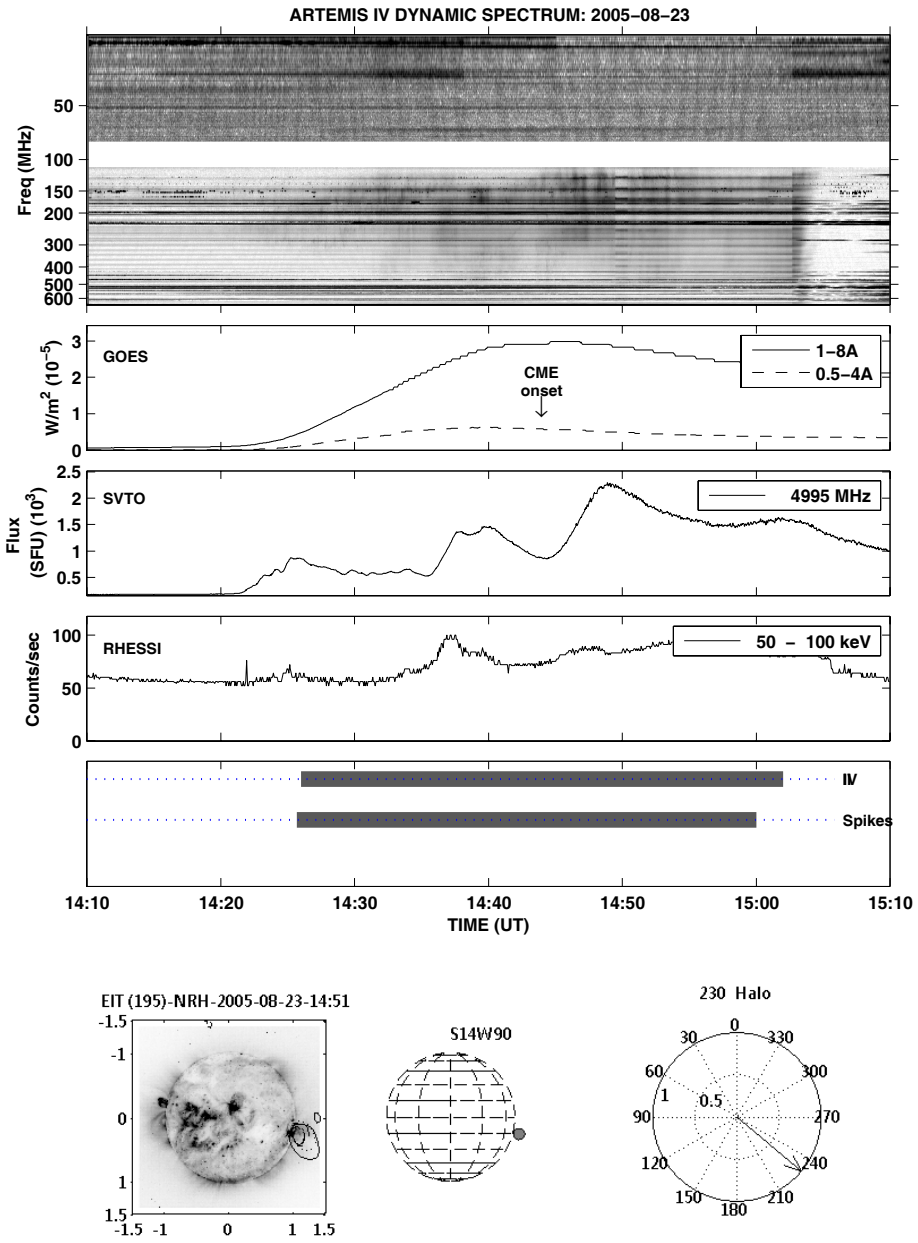

Figure B34. 23 August 2005

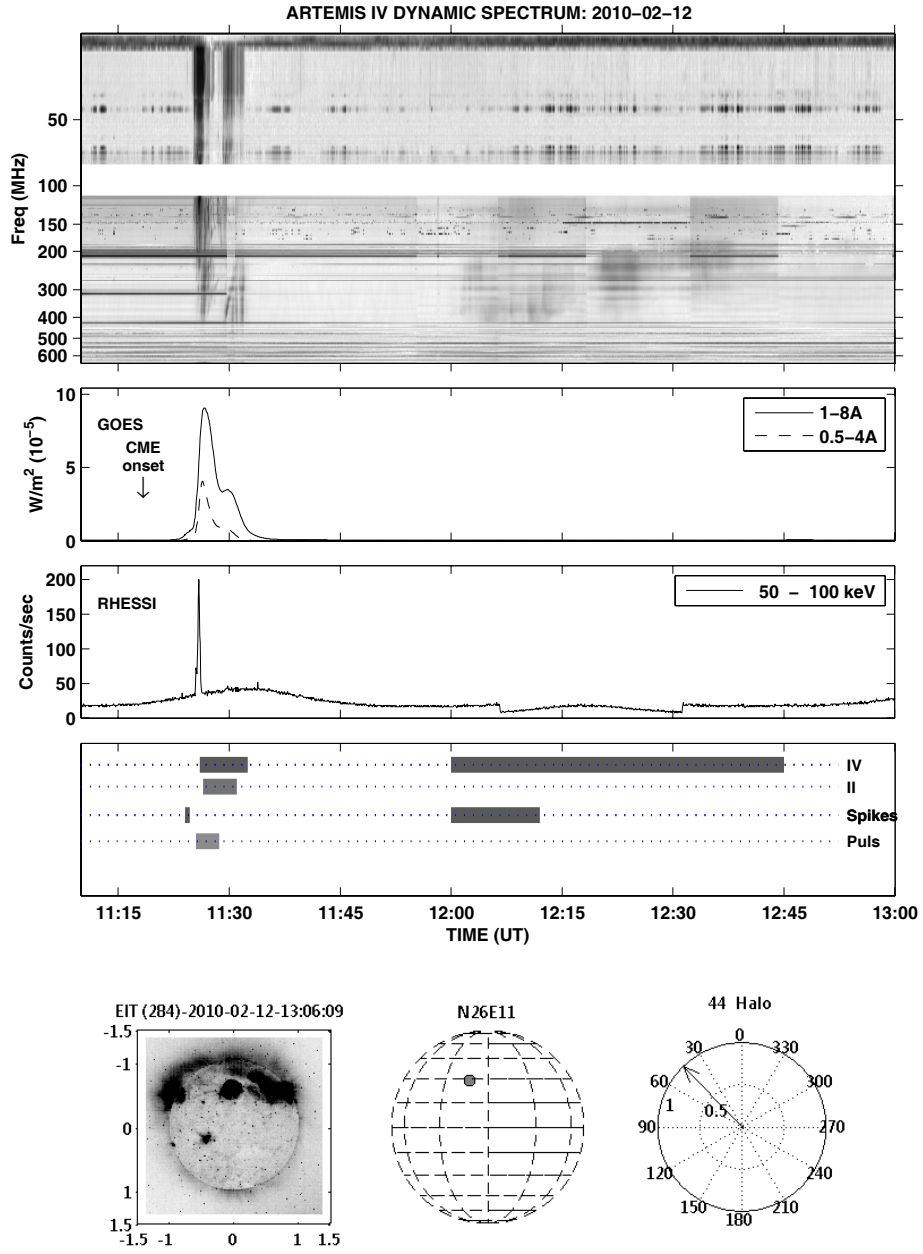

Figure B35. 12 February 2010

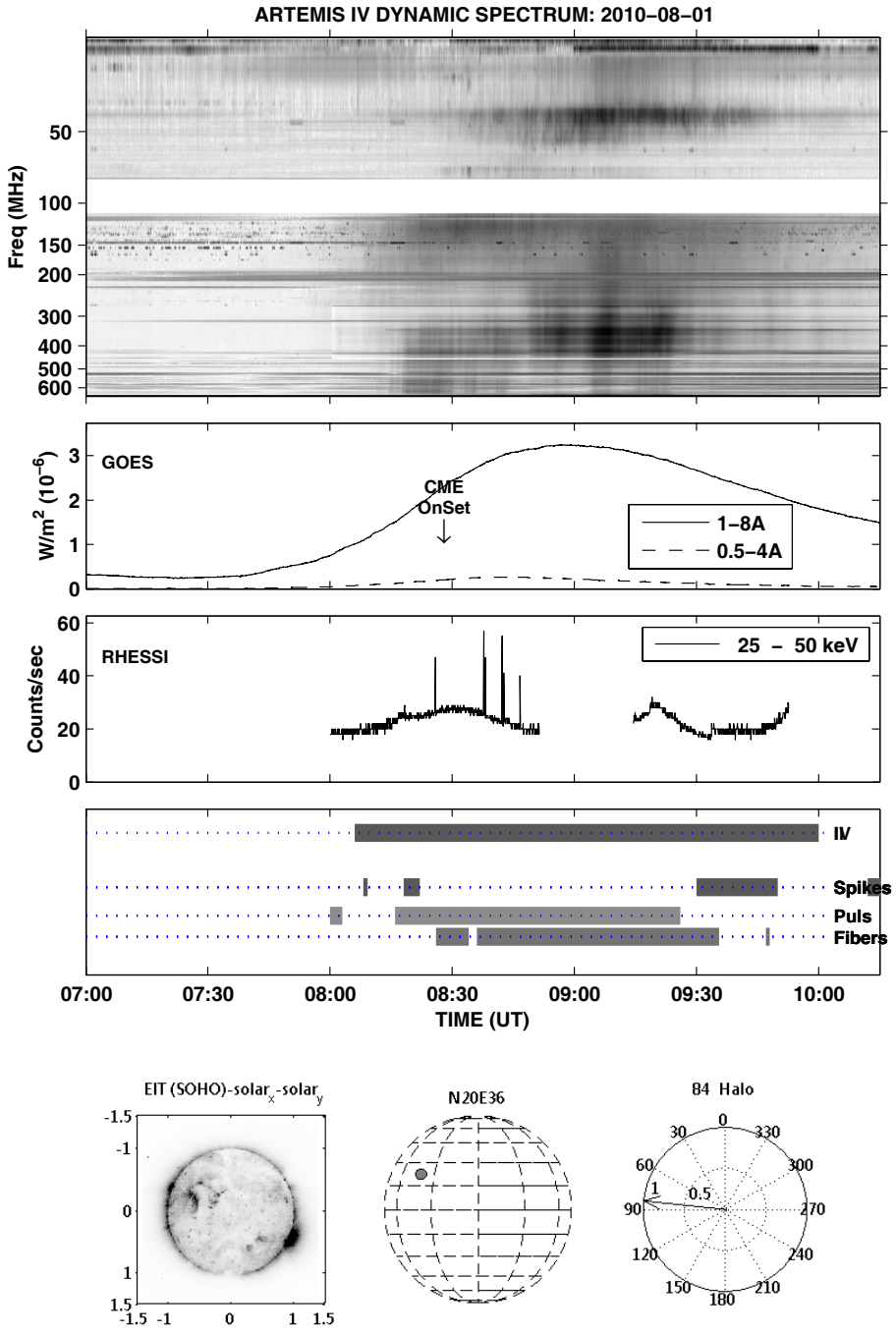

Figure B36. 01 August 2010